Final Report
COVER PAGE

Federal Agency to which Report is submitted: DOE EERE – Wind & Water Power Program

Recipient: The Pennsylvania State University, DUNS number: 003403953
Award Number: DE-EE0002667
Project Title: DOE/PSU Graduate Student Fellowship Program for Hydropower
Project Period: Jan 1, 2010 to December 31, 2013

Principle Investigator: John M. Cimbala, Professor Mech. Engr., jmc6@psu.edu, 814-863-2739
Report Submitted by: Same as above

Date of Report: March 30, 2013
Covering Period: Jan 1, 2010 to December 31, 2013 [Final Report]

Working Partners: John M. Cimbala, Professor Mech. Engr., 814-863-2739, jmc6@psu.edu
Cost-Sharing Partners: Weir American Hydro / Weir Power and Industrial
Contacts: Robert Rittase, Chief Hydraulic Engineer, 717-801-3859,
Robert.Rittase@weirgroup.com, www.weirpowerindustrial.com

DOE Project Team: DOE HQ Program Manager – Jose Zayas
DOE Field Contract Officer – Pamela Brodie
DOE Field Grants Management Specialist – Laura Merrick
DOE Field Project Officer – Brad Ring
DOE/CNJV Project Monitor – Erik Mauer

Signature of Submitting Official: ___**Electronic – John M. Cimbala**_____
(electronic signature is acceptable)

ACCOMPLISHMENTS

Project Objective: The primary objective of this project is to stimulate academic interest in the conventional hydropower field by supplying research support for at least eight individual Master of Science (MS) or Doctoral (PhD) level research projects, each consisting of a graduate student supervised by a faculty member.

Project Goals: To train and graduate at least eight MS and/or PhD students who will be experts in some aspect of hydropower, and will publish papers that enhance our knowledge of hydropower. Hopefully, these students will work in the hydropower field after graduation.

Goal Status:
Overall Summary: We have completed many of the individual student research projects: 2 PhD students have finished, and 4 are still working towards their PhD degree. 4 MS students have finished, and 2 are still working towards their MS degree, one of which is due to finish this April. In addition, 4 undergraduate student projects have been completed, and one is to be completed this April. These projects were supervised by 7 faculty members and an Advisory/Review Panel. Our students and faculty have presented their work at national or international conferences and have submitted several journal publications. Three of our graduate students (Keith Martin, Dan Leonard and Hosein Foroutan) have received HRF Fellowships during the course of this project. All of the remaining students are anticipated to be graduated by the end of Fall Semester 2014. All of the tasks for this project will have been completed once all the students have been graduated, although it will be another year or two until all the journal publications have been finalized based on the work performed as part of this DOE Hydropower project.

Individual Student Project Reports:
Each individual student project is summarized separately in the pages that follow. The Principal Investigator (John Cimbala) had asked each student to write up a few pages summarizing his/her work, and the write-ups were edited by the student's faculty advisor. These summaries give a good feel for the kind of work that we have done over the past four years.

The papers are arranged alphabetically by the student's last name.

DE-EE0002667
DOE/PSU Graduate Student Fellowship Program for Hydropower
The Pennsylvania State University
Final Report, March 2014

David Beevers, PhD Candidate. Advisor: Horacio Perez-Blanco

Hydropower System Optimization through Dynamic Programming and Gradient Analysis

The growing need for power production has inspired a great deal of research into increasing the efficiency of the physical components involved in hydropower production, and the development of new hydropower technologies. The resulting improvements are of limited benefit, however, if they are not optimally utilized on a daily basis. Optimal utilization involves the determination of when dispatch schedule in a hydropower facility, and of the power output of each unit , when active. The optimization problem is highly complicated due to the fact that there are typically multiple hydropower facilities present on a single river system, and thus the optimization must consider the operation of the system as a whole. Research into such optimization has taken many forms. Among the optimization methods applied to hydropower are mixed integer linear programming[1], mixed integer nonlinear programming[2], mixed integer quadratic programming[3], and genetic algorithms[4]. Dynamic programming (DP) has also occasionally been used, though typically not for daily operation, due to the large number of state and decision variables required to accurately model a hydropower system. Each optimization method has its own benefits, but in general, most neglect to utilize the highly structured nature of a hydropower system. In addition many of the methods used fail to fully account for the nonlinearities inherent in the relationship between head, flow rate, and power.

In order to facilitate fast optimization and accurate accounting for the variability of power production with head and net flow rate, it is useful to perform a preliminary analysis of each possible operating set of turbines for each facility. The goal of this preliminary analysis is to generate optimal efficiency and power surfaces for each unique operating set of turbines as functions of reservoir volume and net station flow. Sample results are shown in Figure 1.

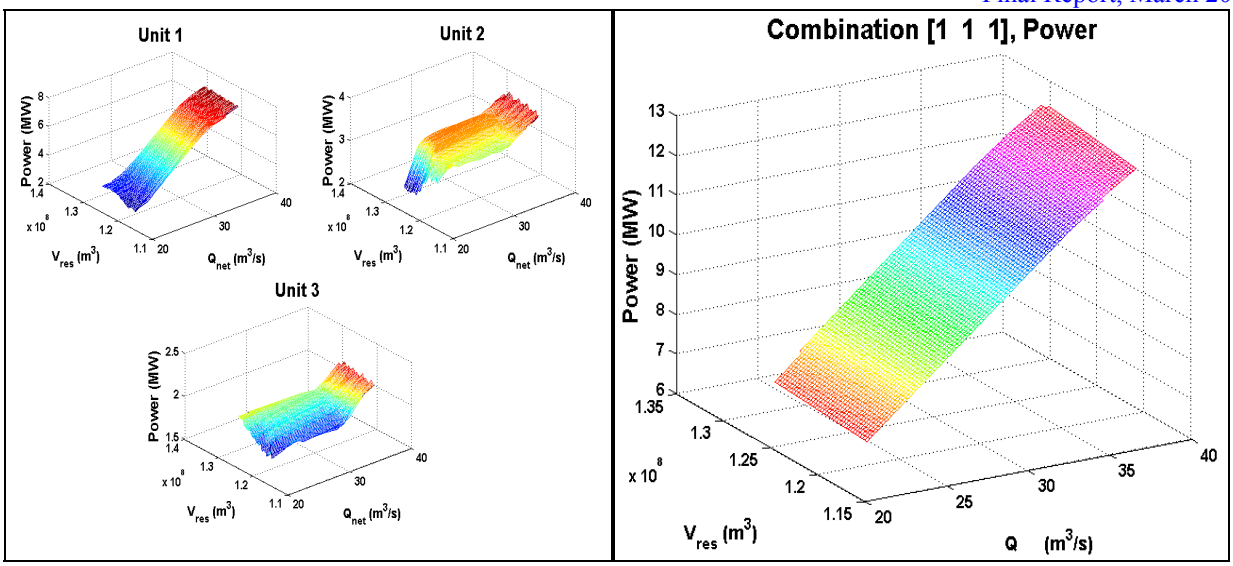

Figure 1. Preliminary optimization results for the optimal operation of an operating set of turbines consisting of three unique turbines. Above is the optimal power of each individual turbine (left) and the net optimal power (right).

When surfaces such as those shown in Figure 1 are used, future analyses need only determine the best operating set and net flow rate for each stage in the time horizon, rather than determining the on/off status and best flow rate for each individual turbine. This approach drastically reduces the number of required decision variables, thus speeding up future optimization of a hydropower system. For example, without the preliminary optimization, a discretized plant consisting of three unique turbines would have 6 decision variables (3 for the on/off status of the turbines, and 3 for the flow rates through the turbines), resulting in 343 unique possible decisions (if the flow rate of each turbine is discretized to 6 values) for each stage in the time horizon. The same facility, with the same level of discretization, would have only 2 decision variables (1 for the active operating set, and 1 for the net flow through the station), resulting in 67 unique possible decisions, which is less than 20% of the previous number of possible decisions. The savings increase drastically when the number of turbines increases and when the discretization is further refined. If the number of turbines is increased to 4, and the flow discretization is refined to include 10 points, then the application of the preliminary analysis changes the number of possible decisions from 14641 to 303, approximately 2% of the previously required number of decisions.

The preliminary analysis makes the application of DP to the optimization of a hydropower facility a very feasible option because of the greatly reduced number of decision variables. DP is a highly attractive optimization method because global optimality is guaranteed if it is applied correctly and the discretizations of the variables are sufficiently refined. Additionally, the inclusion of operational constraints due to environmental and recreational considerations are easily included in a DP analysis. Furthermore, the objective function used is easily modified to include various measures of optimality. Results are shown in Figure 2 for an analysis of an average spring day. The optimal

commitment in a deregulated market when power and regulation are both offered is compared to the optimal commitment when only power is offered.

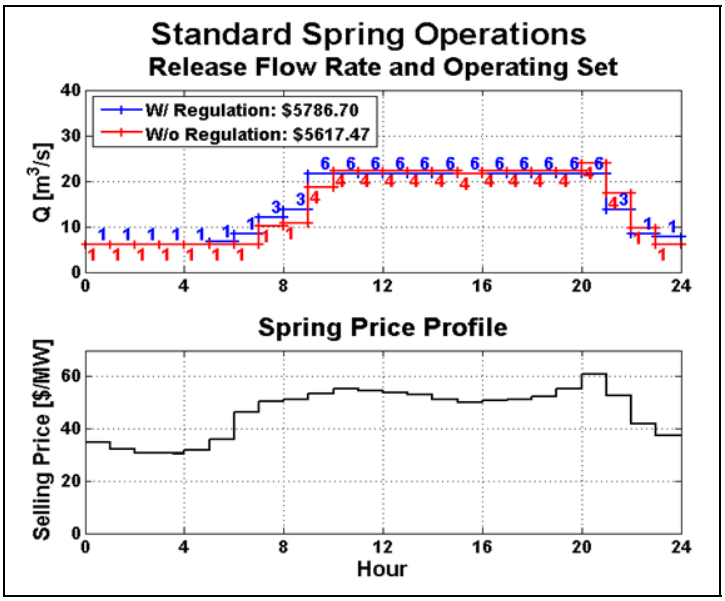

Figure 2. Preliminary optimization results for the optimal operation of an operating set of turbines consisting of three unique turbines. Above is the optimal power of each individual turbine (left) and the net optimal power (right).

Another consideration that must be accounted for when using DP, is that the results are only as good as the prediction of the power clearing price (and availability of water). Thus, it is desirable to compare the results of optimizing the operations for various predictions of future prices[5]. One method for doing so is to analyze the expected value of revenue and the conditional value-at-risk (CVaR) for the optimal strategies that result from each prediction. CVaR provides a measure of the risk taken in the worst case scenario. Several previous analyses performed using CVaR calculated the CVaR based on the probability density function (pdf) of expected revenue, and simply imposed a minimum acceptable value, or included the CVaR in the objective function in order to attempt to reach an acceptable balance between maximizing the expected value of profit and maximizing the profit in the worst case scenarios [6], [7]. However, basing the CVaR on the pdf of revenue fails to consider such an analysis simply guarantees that the CVaR will correspond to the revenue of the price profiles with the lowest values for price, and thus increasing CVaR simply results in the analysis being weighted more heavily toward the optimum for the low price scenarios. A much better assessment of risk is to consider loss to be the deviation of the profit produced by an operating strategy from the profit of the optimal operating strategy for each possible price scenario, and base the CVaR on this measure of loss. Furthermore, it can be useful to determine the Pareto frontier of a multi-objective optimization problem, rather than using a single-objective formulation. Utilizing these two considerations (modified CVaR and Pareto frontier) produces results very different from the optimum that would be obtained using previous methods. Over 200 price scenarios were considered, and the optimum operating strategy for each was calculated using the developed DP

optimization routine. Figures 3 and 4 show the results obtained from each method of measuring the CVaR.

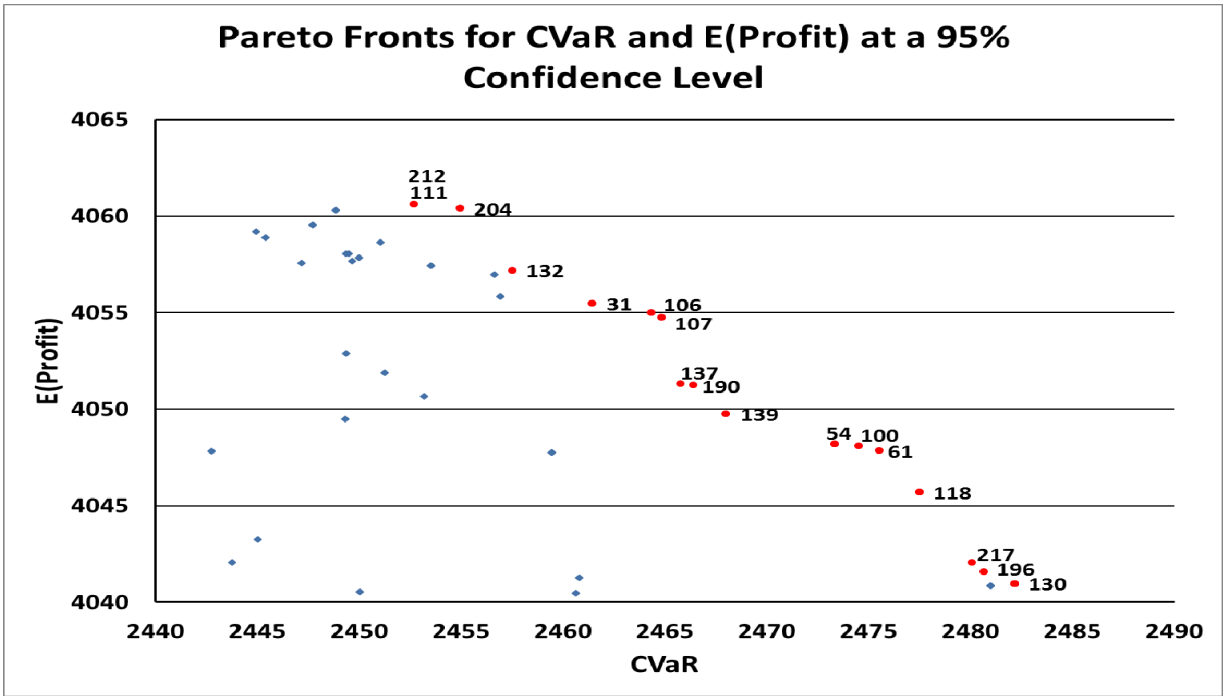

Figure 3. Resulting values of expected profit and CVaR when the CVaR is calculated based on the pdf of profit. Pareto frontier and is shown in red. Numbers correspond to the operating strategy utilized for neighboring points on the Pareto frontier.

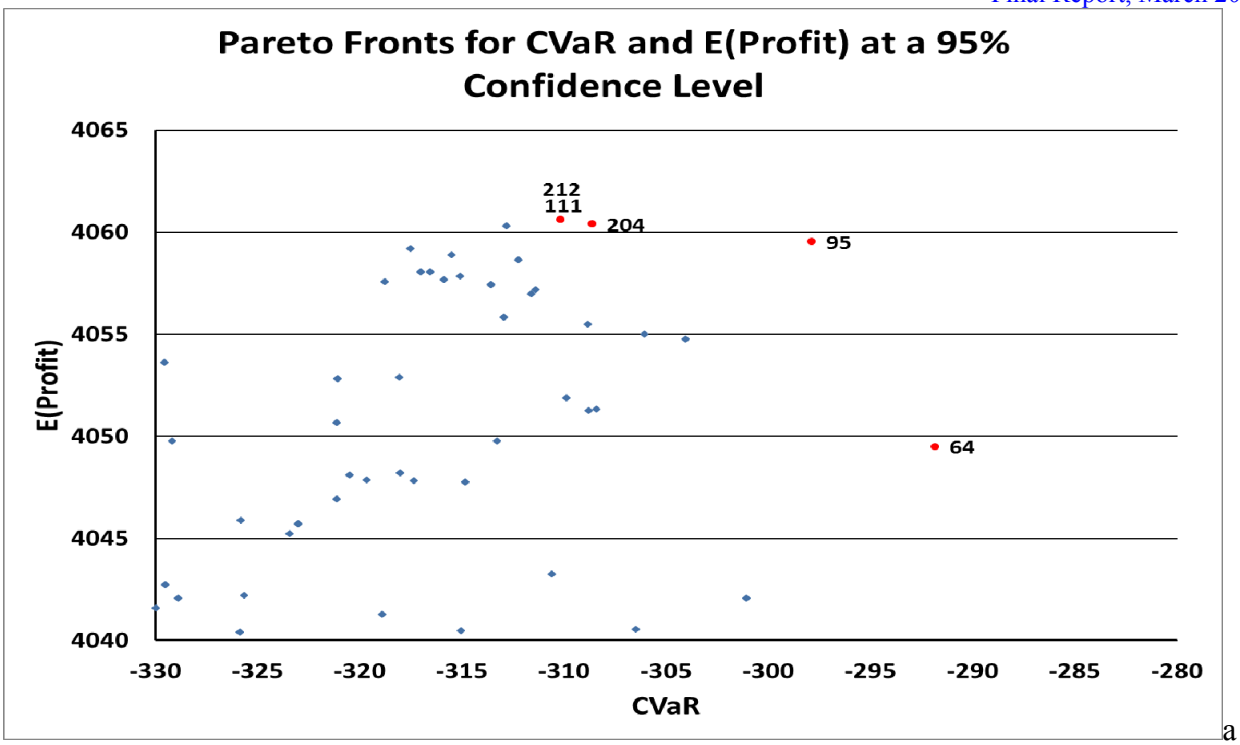

a

Figure 4. Results when CVaR is calculated based on the pdf of losses, as defined above.

It is worth noting that except for the operating strategies with the highest expected revenue, the points on the Pareto frontier are completely different for the different methods of calculating the CVaR.

The final objective is to extend this analysis to a system of hydropower facilities, rather than just a single facility. Unfortunately, the number of state and decision variables required to directly apply DP to a hydropower system consisting of more than two or three hydrologically connected facilities remains prohibitive. However, work is progressing to develop an optimization method that utilizes a combination of DP and gradient methods to take advantage of the speed and robustness of DP and the inherent structure of a hydropower system. The method as planned will optimize each facility in a hydropower system using DP, and then analyze the effect each facility has on its neighbors. Once the interactions between neighboring installations have been determined, gradient methods will be used to drive the operation of each facility toward the system optimum. The optimization will proceed by iterating between revenue gradient analysis and DP optimization of individual stations until convergence is achieved.

In summary, this work has developed a preliminary optimization step that greatly reduces the complexity of optimizing hydropower operations, and developed an improved method for analyzing and minimizing operational risks due to uncertainty. Further work is still progressing to improve previous results and extend application to consider systems of hydrologically connected hydropower facilities.

References:

1. G. W. Chang, M. Aganagic, J. G. Waight, J. Medina, T. Burton, S. Reeves, and M. Christoforidis, "Experiences with mixed integer linear programming based approaches on short-term hydro scheduling," Power, vol. 16, no. 4, pp. 743–749, 2001.
2. J. P. S. Catalao, S. J. P. S. Mariano, V. M. F. Mendes, and L. A. F. M. Ferreira, "Scheduling of Head-Sensitive Cascaded Hydro Systems, A Comparison Based On Numerical Simulation Results.pdf," International Journal of Power & Energy Systems, vol. 28, no. 2, pp. 128–134, 2008.
3. J. P. S. Catalão, H. M. I. Pousinho, and V. M. F. Mendes, "Scheduling of head-dependent cascaded hydro systems: Mixed-integer quadratic programming approach," Energy Conversion and Management, vol. 51, no. 3, pp. 524–530, Mar. 2010.
4. E. Santos and T. Ohishi, "A hydro unit commitment model using genetic algorithm," Evolutionary Computation, 2004. …, pp. 1368–1374, 2004.
5. L. Hongling, J. Chuanwen, and Z. Yan, "A review on risk-constrained hydropower scheduling in deregulated power market," Renewable and Sustainable Energy Reviews, vol. 12, no. 5, pp. 1465–1475, Jun. 2008.
6. J. P. S. Catalão, H. M. I. Pousinho, and J. Contreras, "Optimal hydro scheduling and offering strategies considering price uncertainty and risk management," Energy, vol. 37, no. 1, pp. 237–244, Jan. 2012.
7. J. Garciagonzalez, E. Parrilla, and A. Mateo, "Risk-averse profit-based optimal scheduling of a hydro-chain in the day-ahead electricity market," European Journal of Operational Research, vol. 181, no. 3, pp. 1354–1369, Sep. 2007.

Publications Resulting from this Project:

1. D. Beevers, L. Branchini, H. Perez-Blanco "Managing Renewable Variability with Pumped Hydro Storage," Undergoing revision prior to submission.
2. David Beevers, Poowanart Poramapojana, Fatih Tutuk, Kyle Reigh, "Optimizing and Managing Risk Due to Price Uncertainty in a Single Hydropower Station," Undergoing revision prior to submission.

DE-EE0002667
DOE/PSU Graduate Student Fellowship Program for Hydropower
The Pennsylvania State University
Final Report, March 2014

David Boger, PhD 2013. Advisor: Eric Paterson

A Continuous Adjoint Approach to Design Optimization in Multiphase Flow

Multiphase flow effects, including cavitation and air injection, are an important consideration for both expanding the operating range of hydroturbines and making them more environmentally friendly. For example, bulb turbines regularly encounter cavitation as a part of their normal operation, making it necessary to include cavitation effects during the design stage [Necker, 2010]. Kaplan runners typically allow some amount of cavitation during normal operation primarily as a tradeoff to a deeper setting of the machine. For Francis turbines, cavitation is generally considered intolerable, but in off-design conditions, swirling flow leaving the runner often forms a cavitating vortex rope. Air injection can be used to reduce pressure fluctuations from the vortex rope and other flow sources [Casanova 2009, Kirschner 2010]. Hydroturbines also tend to discharge water from the bottom of the reservoir, which can severely impact aquatic life downstream, so air injection is also used in that case to improve water quality [Bunea, 2010].

Multiphase CFD simulations for hydroturbines have become increasingly common in the last several years [Necker, 2010; Bunea, 2010; Liu, 2007; Liu 2009; Wu, 2010; Qian, 2007]. But even when CFD simulations are able to accurately predict problems with a design, it is usually still incumbent on the designer to correct these problems using traditional design tools and his own experience and intuition. CFD-based design optimization, on the other hand, can provide a direct link between the CFD solution and the required design improvements. Among optimization methods, gradient-based methods can be more efficient when the optimum is "nearby," so they are appropriate given the relative maturity of existing hydroturbines and the constrained design space that often accommodates retrofit operations. Among gradient-based methods, adjoint methods are of interest due to their ability to efficiently handle large numbers of design variables [Jameson, 1988].

With full-system multiphase calculations still in their infancy, researchers have not yet sought to systematically tie hydroturbine shape design to the results of multiphase analysis. In fact, generally speaking, adjoint methods do not appear to have been applied to multiphase flow at all. It is therefore of interest to investigate the extension of the continuous adjoint method to multiphase flow, which would allow design optimization methods to be applied to operating conditions in which cavitation or injected air exists either in the component being modified or in an adjacent stage of the machine. Continuous adjoint methods were developed in this project for design optimization in multiphase flow based on two homogeneous multiphase mixture models for cavitating flow --- a barotropic model and a transport-equation-based model [Boger, 2013].

The barotropic model consisted of variable-density mass and momentum equations and used an equation of state for the density that depends on only the local static pressure and the vapor pressure of the liquid [Delannoy, 1990]. In that case, the primary equations were homogeneous, and a conventional hybrid multistage explicit method based on central differencing and second- and fourth-order scalar artificial dissipation [Esfahanian, 2012] was applied to solve both the primary and adjoint systems. Results were obtained for both surface- and volume-based vapor minimization cost functions for a two-dimensional cavitating NACA66 hydrofoil in which the geometry was parameterized using B-splines [Boger, 2013]. Figure 1 (left) shows the primary solution for this case

in terms of the pressure distribution on the cavitating hydrofoil compared with measured data. The cost function gradients computed using the adjoint method were shown to compare well with gradients computed using complex-step finite-difference methods, particularly for the volume-based cost function, as shown in Figure 1 (right).

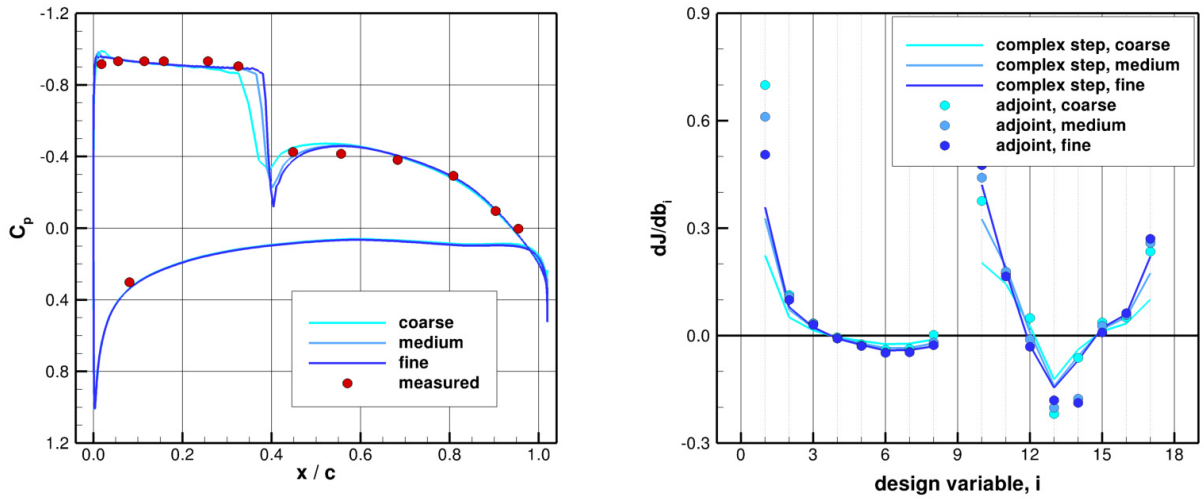

Figure 1. Multiphase pressure distribution from the barotropic model for a NACA66 hydrofoil at 4-degrees angle-of-attack (left) and cost function gradient for volume vapor minimization with using adjoint and finite difference methods (right).

The gradients were then used to inform a fixed-step method of steepest descent. Figure 2 shows an example of one such case in which a multi-objective cost function is constructed to minimize the amount of vapor throughout the computational domain while constraining the lift via a weighted penalty function for a NACA66 hydrofoil at 4 degrees angle-of-attack. Figure 2 (left) shows the evolution of the cost function for three cases where the lift is unconstrained, weighted, and more heavily constrained. Figure 2 (right) shows the resulting hydrofoil geometry in the vicinity of the leading edge compared with the original NACA66 geometry. The modified geometry eliminates the cavitation while maintaining the lift to within 0.02% of its original value. The case demonstrates that the adjoint-based gradients can be used to inform the optimization method but shows the well-known pitfall of single-point optimization in that the design is only optimal at a single operating condition.

For the transport-equation-based model, the governing flow equations included source terms that modeled the mass transfer between liquid and vapor [Kunz, 2000], and the fact that those source terms were not continuously differentiable with respect to the state variables gave rise to a discontinuity in the adjoint solution. A high-resolution fluctuation-splitting method with wave limiters was used to discretize the non-conservative, variable-coefficient linear system of equations [LeVeque, 2002], where the preconditioning matrix from the primary algorithm was included in the adjoint system to render it hyperbolic. Results were presented for several cost functions applied to quasi-one-dimensional flow through a converging-diverging nozzle [Boger, 2013]. The geometry was once again parameterized using B-splines, and once again, the cost function gradients computed using

the adjoint method were shown to compare well with gradients calculated using complex-step finite-difference methods.

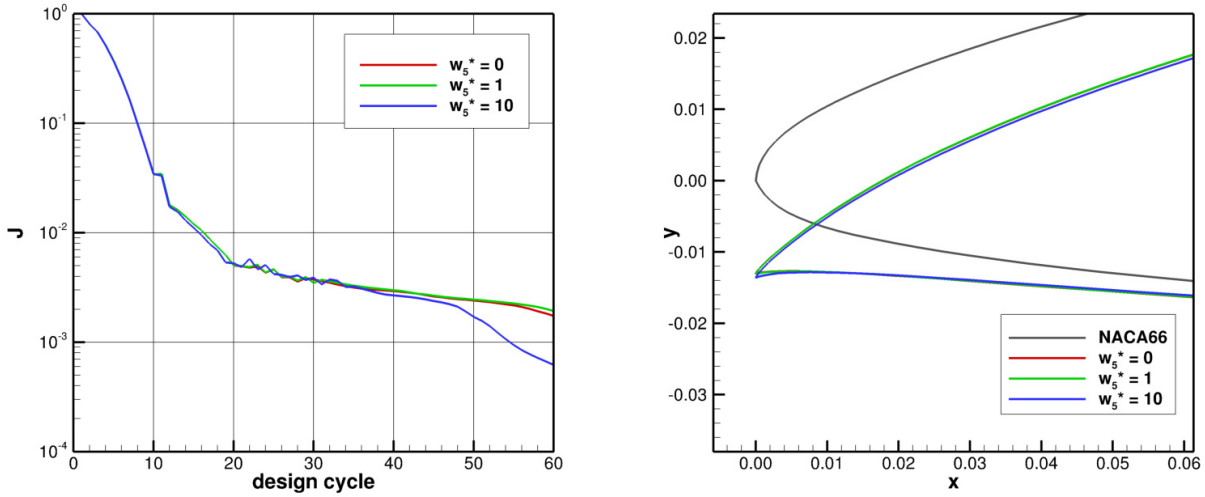

Figure 2. Evolution of the cost function (left) and final leading edge geometry (right) for shape optimization of a NACA66 hydrofoil at 4-degrees angle-of-attack to minimize cavitation while constraining lift via a penalty function with three different weights.

Exploration of several cost functions for the transport-equation-based model in multiphase flow revealed that the corresponding minimization surfaces were poorly conditioned and non-convex. Nevertheless, with careful cost function design and the use of a low-memory quasi-Newton descent method, the cost functions were minimized or significantly decreased in every case [Boger, 2013]. Figure 3 provides an example where the method is used to solve an inverse design problem for the quasi-one-dimensional nozzle with cavitating flow and a specified density distribution. Figure 3 (left) shows the evolution of the cost function, which should be driven to zero in the present case since the target density distribution is derived from the simulation of the target geometry. Figure 3 (right) shows the path of the minimization method for this two-variable inverse design problem and demonstrates that the quasi-Newton LBFGS-B method is able to navigate the non-convex minimization surface in this case.

In short, this work showed that continuous adjoint methods for shape optimization could be extended to multiphase flow and developed the analytical equations and numerical methods required to do so.

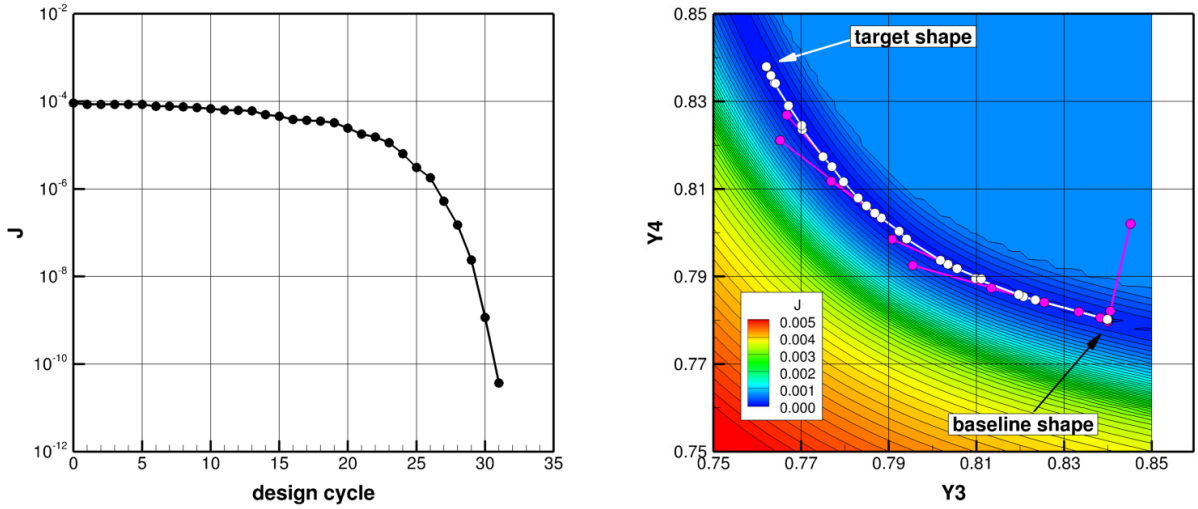

Figure 3. Evolution of the cost function (left) and minimization path (right) for inverse design of a quasi-one-dimensional cavitating nozzle using a specified density distribution and a transport-equation-based cavitation model

References:

1. J. Necker and T. Aschenbrenner (2010), Model test and CFD calculation of a cavitating bulb turbine, *IOP Conference Series: Earth and Environmental Sciences*, Vol. 12.
2. O. Kirschner, H. Schmidt, A. Ruprecht, R. Mader, and P. Meusburger (2010), Experimental investigation of vortex control with an axial jet in the draft tube of a model pump-turbine, *IOP Conference Series: Earth and Environmental Sciences*, Vol. 12(1):012092.
3. F. Bunea, S. Houde, G.D. Ciocan, G. Oprina, G. Baran, and I. Pincovschi (2010), Aspects concerning the quality of aeration for environmental friendly turbines, *IOP Conference Series: Earth and Environmental Sciences*, Vol. 12:012035.
4. Shuhong Liu, Qingguang Chen, and Yuliun Wu (2007), Unsteady Cavitating Turbulent Flow Simulation in a Kaplan Turbine, In 2nd IAHR International Meeting of the Workgroup on Cavitation and Dynamic Problems in Hydraulic Machinery and Systems, 24-26 October, 2007, Timisoara, Romania.
5. Shuhong Liu, Liang Zhang, Michihiro Nishi, and Yulin Wu (2009), Cavitating Turbulent Flow Simulation in a Francis Turbine Based on Mixture Model, *Journal of Fluids Engineering*, Vol. 131(5), pp. 1361-1364.
6. Yulin Wu, Shuhong Liu, Hua-Shu Dou, and Liang Zhang (2010), Simulations of unsteady cavitating turbulent flow in a Francis turbine using the RANS method and the improved mixture model of two-phase flows, *Engineering with Computers*.
7. Z. Qian, J. Yang, and W. Huai (2007), Numerical simulation and analysis of pressure pulsation in Francis hydraulic turbine with air admission, *Journal of Hydrodynamics, Ser. B.*, Vol. 19, pp. 467-472.
8. Antony Jameson (1988), Aerodynamic design via control theory, *Journal of Scientific Computing*, Vol. 3(3), pp. 233-260.

9. David A. Boger (2013), A Continuous Adjoint Approach to Design Optimization in Multiphase Flow, PhD Thesis, Penn State University.
10. Y. Delannoy and J. L. Kueny (1990), Two-Phase Flow Approach in Unsteady Cavitation Modeling, In Cavitation and Multiphase Flow Forum.
11. Vahid Esfahanian, Pooria Akbarzadeh, and Kazem Hejranfar (2012), An improved progressive preconditioning method for steady non-cavitating and sheet-cavitating flows, *International Journal for Numerical Methods in Fluids*, Vol. 68, pp. 210-232.
12. Robert F. Kunz, David A. Boger, David R. Stinebring, Thomas S. Chyczewski, Jules W. Lindau, Howard J. Gibeling, Sankaran Venkateswaran, and T. R. Govindan (2000), A preconditioned Navier-Stokes method for two-phase flows with application to cavitation prediction, *Computers & Fluids*, Vol. 29, pp. 849-875.
13. Randall J. LeVeque (2002), *Finite Volume Methods for Hyperbolic Problems*, Cambridge University Press.

Publications Resulting from this Project:

1. David A. Boger (2013), A Continuous Adjoint Approach to Design Optimization in Multiphase Flow, PhD Thesis, Penn State University.
2. David A. Boger and Eric G. Paterson, "A Continuous Adjoint Approach to Design Optimization in Cavitating Flow Using a Barotropic Model," Computers and Fluids, submitted April 2013 (under review).
3. David A. Boger and Eric G. Paterson, "A Continuous Adjoint Approach to Design Optimization for Cavitating Flow Using a Transport-Equation-Based Model," *Journal of Computational Physics*, submitted April 2013 (under review).

DE-EE0002667
DOE/PSU Graduate Student Fellowship Program for Hydropower
The Pennsylvania State University
Final Report, March 2014

Xibei Ding, MS 2011. Advisor: Alok Sinha
Sliding Mode/H_∞ Control of Hydropower Plants

Hydropower is a clean and renewable energy with high converting efficiency. In order to explore more hydro-energy for satisfying growing energy demand, we need to reduce the limitations of hydropower system. One of thresholds for the system is the control ability. A real case was brought at 2010 HydroVision International Conference [1]. Upgrading the old hydropower plant controller (a mechanical-hydraulic governor) made in 1960s to the modern digital controller, plant's controllability is improved. It is able to generate at least additional $327,743.00 per year during the regular drought water conditions when it could not operate using old control system with only total cost of $639,000.00. In addition, the mechanical and electrical hydraulic governor controllers were not designed to handling system uncertainties, such as parameters change due to wear and tear. The plant performance would decrease after prolonged use. Hence, by improving the control system, hydropower plant can provide more energy with economic profits.

The energy produced by power system flowing through the transmission line can be defined into two groups: active power and reactive power [2]. The active power control is related to frequency control and the reactive power control is related to voltage control. Since relatively constant frequency and voltage are very important for the quality of the power, active power control and reactive power control ability affect power system performance. The controller design for active power and reactive power can be separated. For active control, isolated systems and network systems have different design methods as shown in Figure 1. In this work, we focus on active power control or load frequency control on an isolated load system.

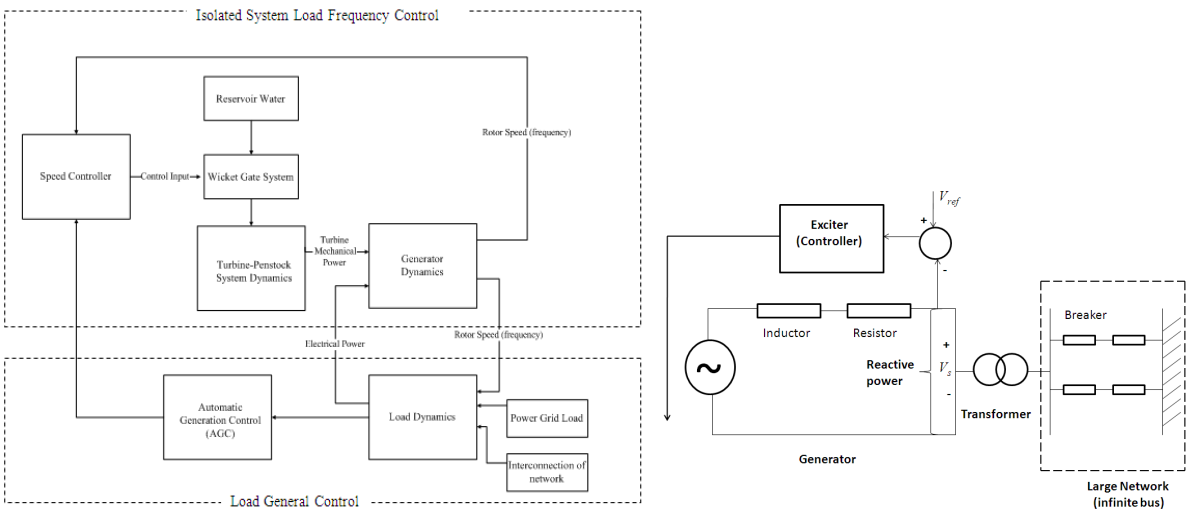

Figure 1. Block Diagram for Active Power Control of an Isolated System and Network Connected System [2] and Scheme of a Generator Connecting with Large Network, an Infinite Bus, through a Transformer. (Reactive Power Control) [3]

The control method for hydropower plant can be divided into two categories: PID linear controller for mechanical or electrical hydraulic governor and modern control algorithms for digital control system.

In the 1970's, electrical-hydraulic governors employing PID controller became popular. During the 1980's, several studies about variable structure control have been conducted [4], [5], [6]. Later, more modern control methods have been studied for hydropower plant, such as Robust Control [7], [8], Adaptive Control [9], Fuzzy Logic [10], [11] and Artificial Neural Networks [12], [13]. Unfortunately, most of the controller designs were based on linear model.

In order to investigate the control system for hydropower plant, we did a detail study on hydropower plant dynamic model. The basic hydro-power plant scheme is shown in Figure 2. Hydropower plant is usually consist of reservior, penstock, electric-hydraulic servo system, turbine and generator. Some plants with long penstock might have one or multiple surge tanks to reduce water hammer effect. The turbine and penstock dynamic model is the most important part of the system modelling. There are three types of turbine, Pelton, Francis and Kaplan. In this research, Francis turbine model is described in details. In general, there are two types of turbine penstock models. One is simplifed nonlinear anslytical model, which treats the hydro turbine model as a valve model. [2]. The other one is based on prototype characteristics [14]. Since model based on the valve model [2] is widely used in the power system simulation software such as PSS/E made by Siemens [15], it was used in our research for controller design. In general, each part can be modeled through its own dynamic equations. Linear or nonlinear model depends on how to model the turbine. The entire system model can be generated by combining each part's dynamic equation.
Our work about hydropower plant controller design can be divided into three parts. First, we designed a sliding mode controller with the H_∞ technique based on a linear hydropower plant model. Second, we applied feedback linearization to the nonlinear hydropower plant model for sliding model controller design. Third, we also investigated the application of second order sliding mode control for hydropower plant controller design due to certain disadvantage of traditional sliding model control method.

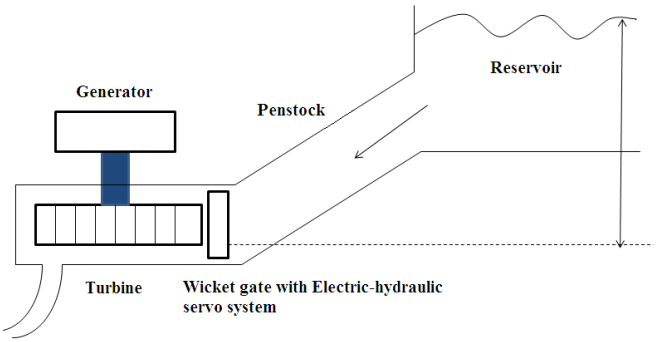

Figure 2. Simple Scheme of Hydropower Plant [2].

The sliding mode control (SMC) blended with robust optimal H_∞ theory, which is inspired by studies conducted in vibration area [16, 17], in which no assumptions on matching conditions are made. The H_∞ control provides the optimal choice of sliding surface and also minimizes the impact of external disturbances. The entire hydro-power plant system and a dynamic model was developed in MATLAB/Simulink software. The simulation results show the advantages of our method in comparison to other traditional control techniques. When the system is controlled by H_∞ / sliding mode method, the response of the system is quite insensitive to parametric uncertainties, Figure 3 (left) for -20% deviation in turbine model parameter only and -10% difference on all model

parameters. Note that the robustness of the traditional PI controller is significantly less as shown in Figure 3 (right).

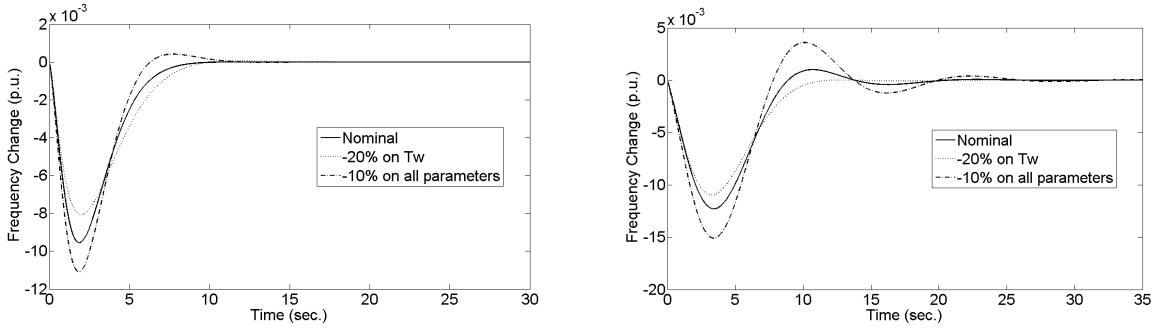

Figure 3. Frequency deviation $\Delta\omega$ with parametric uncertainties under H_∞ / sliding mode control and comparison with PI controller

After designed modern controller based on the linear model, a load frequency controller has been designed by using feedback linearization with sliding mode control on a nonlinear model. The central idea of feedback linearization is to algebraically transform the nonlinear system to a linear system without making any approximations. Then applying control algorithm to that linear system, the control input for the actual nonlinear system is generated. The input state feedback linearization is applied to cancel the nonlinearities of the system and then sliding mode control with integral feedback is implemented to reduce the frequency error to a small amount in the presence of load fluctuations. Due to the non-matching condition [8] of hydropower plant model, a sliding mode control blended with H_∞ method [19] is used for selecting sliding hyperplane so that the effects of disturbances are minimized. Initially, a solo nonlinear controller had very quick response, however, it could not fully reject disturbance as shown in Figure 4. Therefore, a second nonlinear controller was added to the control system. Simulation results (Figure 4) indicate that the two-stage nonlinear controller yields significantly better performance compared to the nonlinear controller with linear PI controller.

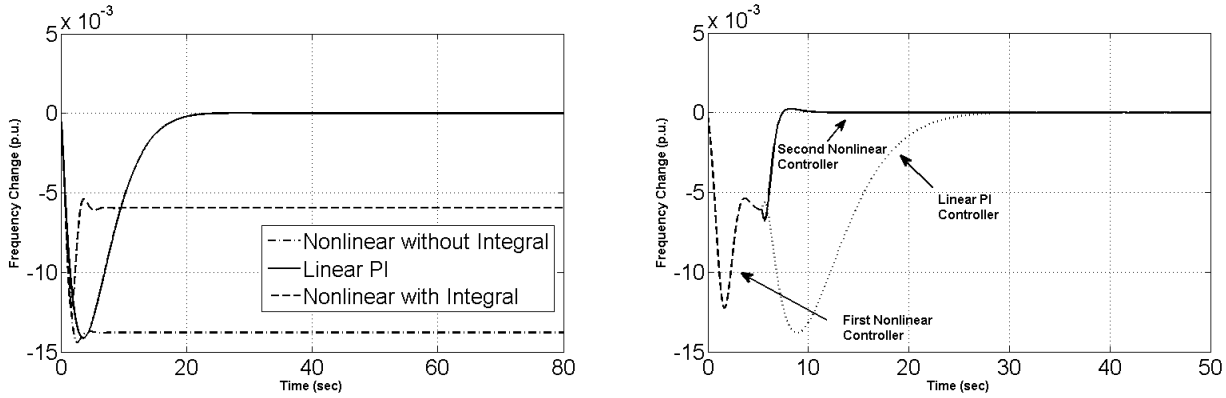

Figure 4. Frequency change responses from initial three control methods and nonlinear controller with second linear PI compared with PI controller

Although the sliding mode control has above advanced features, one issue is always associated with it: the unwanted high frequency oscillation of system trajectories along the sliding surface, which is called chattering effect. There are different ways to reduce the chattering effect, such as replacing the

"sgn" function with a saturation function [20]. Another method among them is the higher order sliding mode control [21-23]. It was introduced by Levant in the 1980s and has drawn great attentions of the control community, because it can not only reduce the chattering effect, but also retain the robustness feature from the first order sliding mode. The super-twisting algorithm, one of second order sliding mode control methods, is studied and applied to hydropower plant for frequency control. The sliding hyperplane vector is designed following the method introduced in [19, 20]. Then two modified controller design procedures have been proposed and tested. The simulations of both methods and regular first order sliding mode control with saturation function are conducted, and frequency change responses and control efforts are compared. It is found that one of the second order sliding mode methods dramatically reduces the chattering and maintains the robustness property of the regular sliding mode, especially under a large disturbance. Robustness of the second order sliding mode (Method 2) with system parametric uncertainties under a step disturbance is examined. The results are compared to the robustness of the regular sliding mode controller as shown in Figure 5. The robustness of the second order sliding mode (Method 2) is almost same or slightly better than that of the regular sliding mode controller. Therefore this second order sliding mode controller (Method 2) preserves all the robustness of the regular sliding mode and reduces the chattering effects.

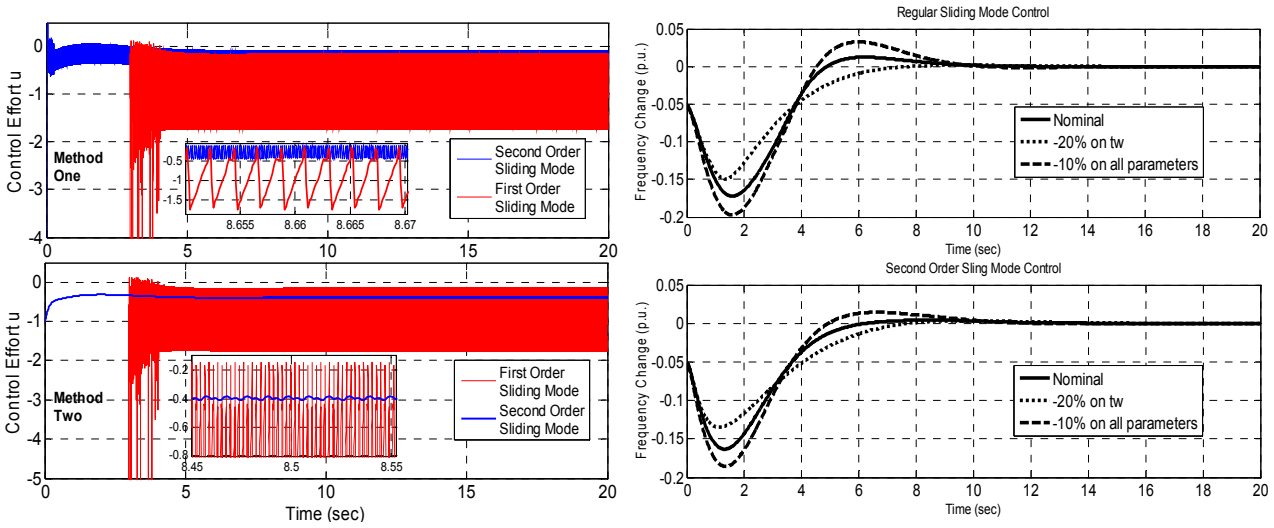

Figure 5. Control effort between two second order slide model controller and first/second order sliding model controller results comparison.

In short, this work showed the advantages of our modern control methods in comparison to other traditional control techniques.

References:

1. S. C. Onken, "Digital Governor Control of Large Pelton Turbines," HydroVision, Charlotte, N.C, July 27-30, 2010.
2. P. Kundur, *Power System Stability and Control*, New York, USA: McGraw-Hill, Inc., 1994.
3. Y. Wang, D. J. Hill, R. H. Middleton and L. Gao, "Transient Stability Enhancement and Voltage regulation of Power Systems", *IEEE Transactions on Power and Systems*, Vol. 8, No. 2, May, 1993.

4. N. Bengiamin and W. Chan, "Variable Structure Control of Electric Power Generation," *IEEE Transactions on Power Apparatus and Systems*, PAS-101. No.2, pp376-380, February, 1982.
5. C. Wah-Chun and H. Yuan-Yih, "Optimal Control of Electric Power Generation using Variable Structure Controllers," *Electric Power System Research*, Vol.6, No. 4, pp269-278, December, 1983.
6. A. Sivaramakrishnan, M. Hariharan and M. Srisailam, "Design of Variable-Structure Load-frequency Controller using Pole Assignment Technique," *International Journal of Control*, Vol. 40, No.3, pp 487-498, 1984.
7. J. Jiang, "Design of an Optimal Robust Governor for Hydraulic Turbine Generating Units," *IEEE Transactions on Energy Conversion*, Vol. 10, pp 188-194, 1995.
8. I. Eker, "Governors for Hydro-turbine Speed Control in Power Generation: a SIMO Robust Design Approach," *Energy Conversion* and *Management*, Vol. 45, pp 2207-2221, 2004.
9. L. Ye, S. Wei, Z. Li, O. Malik, G. Hope and G. Hancock, "An Intelligent Self-improving Control Strategy and its Microprocessor-based Implementation to a Hydro-turbine Governing System," Canada Journal of Electrical and Computer Engineering, Vol. 15, pp 130-138, 1990.
10. M.Mahmoud, K.Dutton, and M.Denman, "Design and Simulation of a Nonlinear Fuzzy Controller for a Hydropower Plant," *Electric Power Systems Research*, Vol.73, No. 2, pp87-99, February, 2005.
11. Z. Zhang, Z. Huo and Z. Xiao, "PID Control with Fuzzy Compensation for Hydroelectric Generating Unit," *International Conference on Power System Technology*, Vol. 4, pp 2348-2352, 2002.
12. G. Venayagamoorthy and R. Harley, "A Continually Online Trained Neurocontroller for Excitation and Turbine Control of a Turbogenerator," *IEEE Transactions on Energy Conversion*, Vol. 16, No. 3, September, 2001.
13. M. Djukanovi, M. Novicevic, D. Dobrijevic, B. Babic, D. Sobajic, Y. Pao, "Neural-net Based Coordinated Stabilizing Control for the Exciter and Governor Loops of Low Head Hydropower Plants," *IEEE Transactions on Energy Conversion*, Vol. 10, pp 760-767, 1995.
14. Working Group on Prime Mover and Energy Supply Models for System Dynamic Performance Studies, "Hydraulic Turbine and Turbine Control Models for System Dynamic Studies," *IEEE Transactions on Power Systems*, Vol. 7, pp. 167– 179, Feb. 1992.
15. H. Gao and C. Wang, "Effect of Detailed Hydro-turbine Models on Power System Analysis," Power Systems Conference and Exposition, pp. 1577-1581, October/November 2006.
16. A. Sinha*, Linear Systems: Optimal and Robust Control*. CRC Press Taylor & Francis Group, 2007.
17. M.C.Pai and A.Sinha, "Active Control of Vibration in a Flexible Structure with Uncertain Parameters Via Sliding Mode and H_∞/μ Techniques," *ASME Vibration and Noise Control*, vol. DE-Vol. 97/DSC-Vol. 65, pp. 1–7, 1998.

18. B. Drazenovic, 1969. "The Invariance Condition in Variable Structure Systems", *Automatica*, vol.5, pp. 287-295
19. X. Ding and A. Sinha, 2011. "Sliding Mode/ H_∞ Control of a Hydropower Plant", *Presented at American Control Conference*, San Francisco, California, USA, June 29 - July 1.
20. A. Sinha, 2007. Linear Systems: Optimal and Robust Control, 1st ed. CRC Press Taylor & Francis Group, New York, Chap. 6.
21. A. Levant, 2003. Introduction to Higher-order Sliding Modes. <http://www.tau.aci.il/levant/hosm2002.pdf >
22. A. Levant, 1993. "Sliding Order and Sliding Accuracy in Sliding Mode Control". *International Journal of Control*, 59(6), pp 1247-1263.
23. G. Bartolini and E. Punta, 2000. "Chattering Elimination with Second-order Sliding Modes Robust to Coulomb Friction". *Journal of Dynamic Systems, Measurement and Control*, 122, pp 679-686.

Publications Resulting from this Project:

1. Xibei Ding (2011), Sliding Mode/ H_∞ Control of Hydropower Plants, MS Thesis, Penn State University.
2. X. Ding and A. Sinha, 2011. "Sliding Mode/ H_∞ Control of a Hydropower Plant", Presented at American Control Conference, San Francisco, California, USA, June 29 - July 1

DE-EE0002667
DOE/PSU Graduate Student Fellowship Program for Hydropower
The Pennsylvania State University
Final Report, March 2014

Hosein Foroutan, PhD Candidate. Advisor: Savas Yavuzkurt

Simulation, Analysis and Prevention of Vortex Rope Formation in Draft Tubes

Hydropower is a renewable and sustainable energy source with many technical, economical, and environmental benefits. Storage capability and fast response make hydropower an ideal form of power generation. However, the variable energy demand requires hydraulic turbines to be operated over an extended range of conditions quite far from their design point (the best efficiency point). Hydraulic turbines operating at partial load have a high level of swirl at the draft tube inlet as the difference between the swirl generated by the wicket gates and the angular momentum extracted by the runner. The decelerated swirling flow in the draft tube may lead to flow instabilities resulting in the formation of a helical precessing vortex called the "vortex rope" [Zhang et al., 2009]. The flow instability with formation of the vortex rope is the main cause of efficiency reduction and pressure fluctuations experienced by a Francis turbine operating at part-load conditions. These pressure fluctuations become more serious if their corresponding frequency approaches the natural frequency of the power plant structures. This can result in vibration of the whole installation [Dörfler et al., 2013]. Given the strong effects that vortex rope can have, the analysis and investigation of its formation as well as the control or elimination of its effects are necessary for improving hydropower plant efficiency over a wide range of operating conditions, and preventing structural vibrations. These were addressed in this research study using computational fluid dynamics (CFD). Therefore, the present study is directly related to the improvement of conventional and/or pumped storage hydropower technologies and operations.

Turbulent swirling flow was investigated numerically using a systematic, step-by-step approach starting from the simplest and advancing towards the most complicated flow structure. First, a detailed evaluation and investigation of different turbulence closure approaches for simulation of flow in a simplified conical draft tube was performed [Foroutan and Yavuzkurt, 2012]. Simulations were carried out for axisymmetric as well as three-dimensional grid (for a symmetric geometry) for both steady and unsteady cases using ANSYS-FLUENT and OpenFOAM CFD codes. It was shown that steady simulations of the axisymmetric and three-dimensional flow geometry using RANS turbulence models give the same results; namely, they underpredict the levels of turbulent kinetic energy and axial velocity near the centerline of the draft tube as shown in Fig. 1. The deviation between numerical simulations and experimental data increases as one goes farther from the best efficiency point. This is due mainly to the precessing vortex rope which increases the level of mixing and turbulence production that cannot be predicted using steady simulations.

By performing unsteady simulations it was found that Unsteady Reynolds-Averaged Navier-Stokes (URANS) models cannot capture the self-induced nature of the vortex rope and result in steady solutions. Small scale unsteadiness of the vortex rope is averaged off by the URANS approach. Therefore, hybrid URANS/LES models were considered as an alternative turbulence closure approach. These models aim at combining the best of Reynolds-Averaged Navier-Stokes (RANS) and Large Eddy Simulation (LES) turbulence models. In this approach, the URANS models are employed in the near-wall region, while LES treatment is applied to regions far away from the wall. By applying hybrid URANS/LES models detailed unsteady features of the flow and a precessing vortex rope were captured sufficiently as shown in Fig. 2 [Foroutan and Yavuzkurt, 2012]. Therefore, it was concluded that choosing the correct turbulence model is essential in modeling draft tube vortex rope.

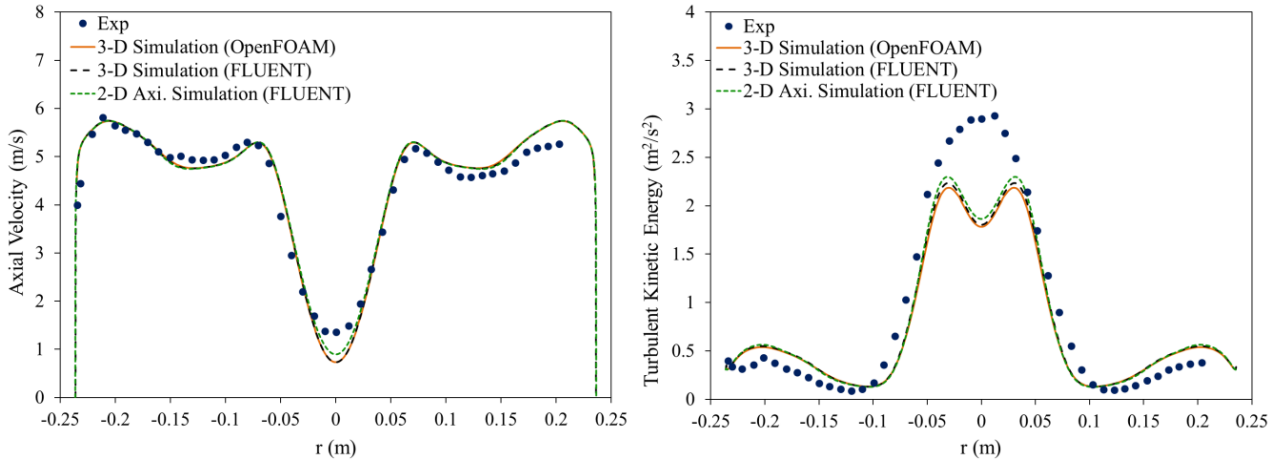

Figure 1. Axial velocity (left) and turbulent kinetic energy (right) profiles in the draft tube; Comparison of 2-D axisymmetric and 3D RANS simulations using FLUENT and OpenFOAM.

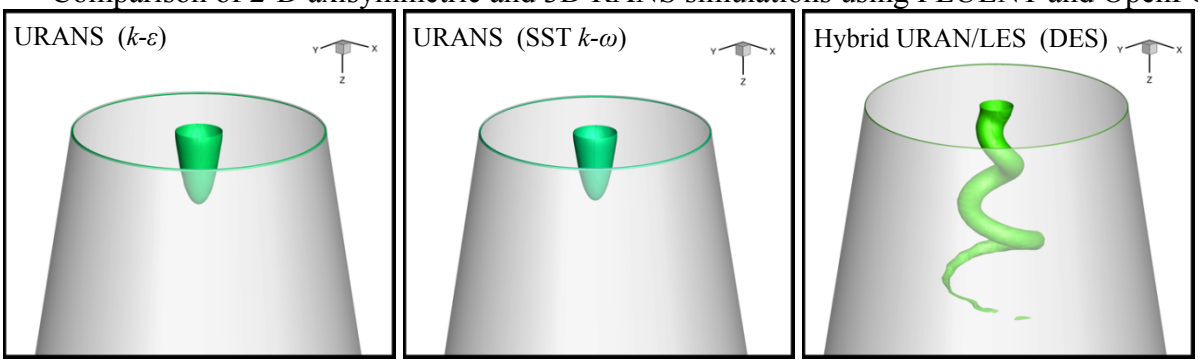

Figure 2. Iso-pressure surfaces (representing the vortex rope) in the draft tube for an instance in time, comparing different turbulence closure approaches [Foroutan and Yavuzkurt, 2012]

One of the challenges this research study faced was the lack of a test case for which the geometry and boundary conditions, as well as detailed experimental data are available. These experimental data were needed for assessment and validation of numerical simulations within this project. The measurements should include not only pressure fluctuations, but also profiles of velocity components as well as turbulent quantities. Among the several experimental studies reviewed, those related to the FLINDT project [Avellan, 2000] contain these details. The FLINDT project experimental investigations were carried out on a Francis turbine scale model of specific speed 0.56 in the Laboratory of Hydraulic Machines at EPFL. The turbine model has a spiral case, stay ring of 10 stay vanes, a distributor made of 20 guide vanes, a 17-blade runner of 0.4 m outlet diameter, and a symmetric elbow draft tube with one pier. However, it was found out that the exact geometry of the draft tube is not available in open literature and is restricted to the project partners only. Therefore, a comprehensive investigation of the previously published articles within the FLINDT project is performed in this study, in order to build a complete database on details of the draft tube geometry (as much as possible) and available experimental data. Using this database the three-dimensional FLINDT draft tube geometry was rebuilt. Therefore, this study can provide a publicly available test case with all details required for a CFD simulation.

Aiming to better predict the vortex rope behavior, a new hybrid URANS/LES model within the Partially-Averaged Navier-Stokes (PANS) framework was developed [Foroutan and Yavuzkurt,

2013] in this project. In the PANS approach [Girimaji, 2006], the extent of partial averaging is controlled by the unresolved-to-total ratios of turbulent kinetic energy, k, and turbulent dissipation rate, ε, which depend upon the computational grid spacing. Therefore, PANS closure model can be used at any grid resolution ranging from Reynolds-Averaged Navier-Stokes (RANS) to Direct Numerical Simulation (DNS). The present PANS model was used in unsteady simulations of flow in the FLINDT draft tube. An operating condition with the head coefficient of $\psi = 1.18$ and flow rate coefficient (discharge coefficient) of $\varphi = 0.26$ (corresponding to 70% of the BEP flow rate) was considered. Simulations could predict a strong precessing vortex rope in the draft tube, which is visualized by the iso-pressure surfaces in Fig. 3. Unsteady pressure fluctuations due to the precession of the vortex rope were monitored for several points on the draft tube wall. The frequency of the precession was found to be 0.32 of the frequency of the runner, which is in very good agreement (only 7% deviation) with experimental data [Ciocan et al., 2007].

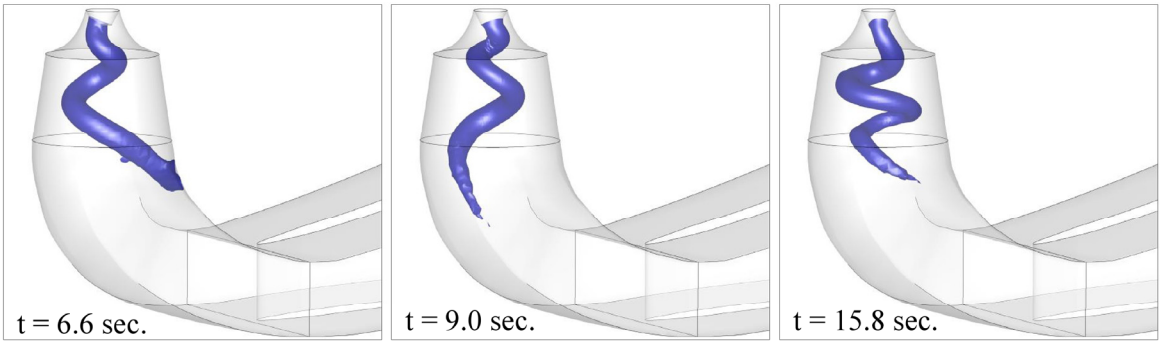

Figure 3. Vortex rope formation inside a draft tube (three instances of time). Simulations are performed using a newly developed Partially-Averaged Navier-Stokes (PANS) model.

Furthermore, studies at PSU confirmed that the vortex rope forms due to the shear layer at the interface of an inner low velocity region (stagnant region or wake of the crown cone) and a highly swirling outer flow. Therefore, a control technique including water jet injection from the runner crown cone downstream into the draft tube to mitigate the vortex rope was considered and investigated [Foroutan and Yavuzkurt, 2014]. The main idea is to increase the momentum of the stagnant flow in the centerline of the draft tube, to reduce the wake or stagnant region, and to eliminate the high velocity gradients, which result in formation of the shear layer and helical vortex rope. Figure 4 includes a sequence of figures showing the iso-pressure surfaces in the draft tube as well as the axial velocity contours (the darker the color, the higher the axial velocity) on the meridian plane. The sequence starts at the onset of jet injection (top left) and continues to the final frame (bottom right) where the water jet is completely developed. The time between each frame is 0.083 s. It is seen that without jet injection a relatively large vortex rope exists in the draft tube wrapped around a low axial velocity (light color) region. When the water jet is applied, the axial velocity (flow momentum) within the center of the draft tube increases (see the darker color at the center), therefore, the velocity gradients within the free shear layer between the stagnant region and outer flow decreases. This reduces the potential that the shear layer would roll-up and form the vortex rope; hence the vortex strength is weakened and the rope is practically eliminated. However, some low pressure pockets are still seen in the flow.

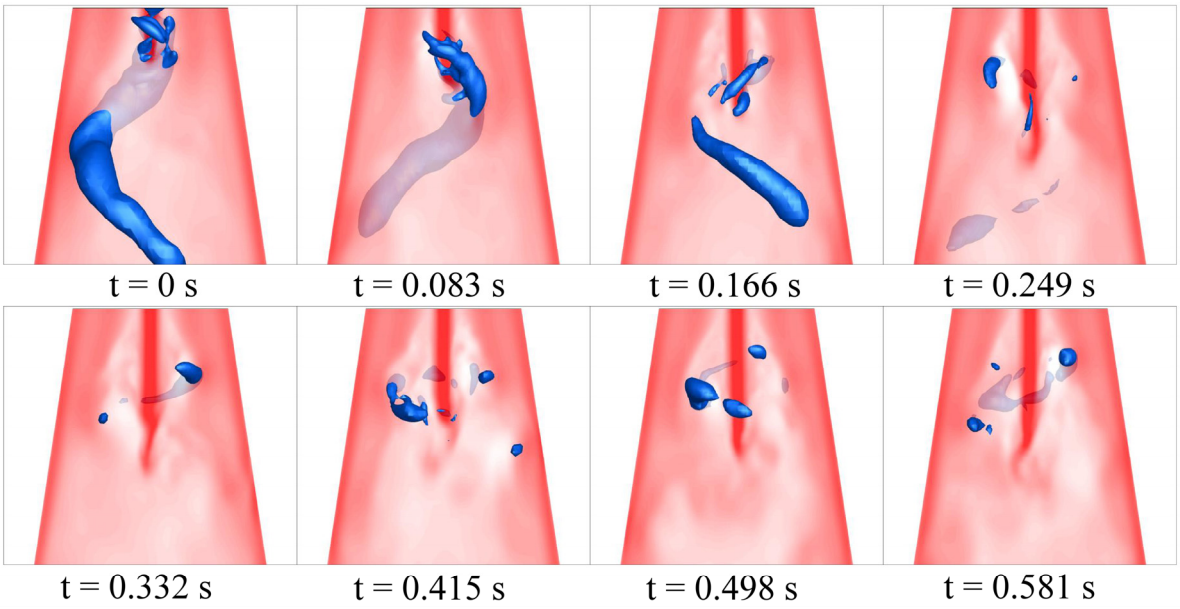

Figure 4. Time evolution of the controlled draft tube flow by water jet injection showing the reduction and elimination of the vortex rope (top left to bottom right) [Foroutan and Yavuzkurt, 2014].

References:

1. Zhang R. K., Mao F., Wu J. Z., Chen S. Y., Wu Y. L., and Liu S. H. (2009), Characteristics and control of the draft-tube flow in part-load Francis turbine, *ASME J. Fluids Engr.*, **131**, pp. 021101-1–13.
2. Dörfler P., Sick M., and Coutu A. (2013), *Flow-induced pulsation and vibration in hydroelectric machinery*, Springer, London, UK, chap. 2.
3. Foroutan, H. and Yavuzkurt, S. (2012), Simulation of flow in a simplified draft tube: turbulence closure considerations, IOP Conf. Ser.: Earth and Environmental Science, Vol. 15, p. 022020.
4. Avellan F. (2000) Flow investigation in a Francis draft tube: the FLINDT project, *Proc. 20th IAHR Symp. on Hydraulic Machinery and Systems*, Charlotte, North-Carolina, USA.
5. Foroutan, H. and Yavuzkurt, S. (2013), Partially-averaged Navier-Stokes modeling of turbulent swirling flow, Bulletin of the American Physical Society, Vol. 58, No. 18, 66th Annual Meeting of the APS Division of Fluid Dynamics, Pittsburgh, PA.
6. Girimaji, S. S. (2006), Partially-averaged Navier-Stokes model for turbulence: A Reynolds-averaged Navier-Stokes to direct numerical simulation bridging method, *Journal of Applied Mechanics*, **73(3)**, pp. 413–421.
7. Ciocan G. D., Iliescu M. S., Vu T. C., Nennemann B., and Avellan F. (2007), Experimental study and numerical simulation of the FLINDT draft tube rotating vortex, *ASME J. Fluids Engr.*, **129**, pp. 146–158.
8. Foroutan, H. and Yavuzkurt, S. (2014), Flow in the simplified draft tube of a Francis turbine operating at partial load - Part 2: Control of the vortex rope, Journal of Applied Mechanics, In Press

Publications/Presentations Resulting from this Project:

1. Foroutan, H. and Yavuzkurt, S. (2014), Flow in the simplified draft tube of a Francis turbine operating at partial load - Part 1: Simulation of the vortex rope, *Journal of Applied Mechanics*, In Press.
2. Foroutan, H. and Yavuzkurt, S. (2014), Flow in the simplified draft tube of a Francis turbine operating at partial load - Part 2: Control of the vortex rope, *Journal of Applied Mechanics*, In Press.
3. Foroutan, H. and Yavuzkurt, S. (2013), Partially-averaged Navier-Stokes modeling of turbulent swirling flow, *Bulletin of the American Physical Society, Vol. 58, No. 18,* 66th Annual Meeting of the APS Division of Fluid Dynamics, Pittsburgh, PA.
4. Foroutan, H. (2013), Simulation, analysis and control of the draft tube vortex rope, Seminar presentation in *Penn State Fluid Dynamics Research Consortium*, The Pennsylvania State University.
5. Foroutan, H. and Yavuzkurt, S. (2012), Simulation of flow in a simplified draft tube: turbulence closure considerations, *IOP Conf. Ser.: Earth and Environmental Science*, Vol. 15, p. 022020.
6. Foroutan, H. and Yavuzkurt, S. (2012), Analysis and prevention of vortex rope formation in the draft tube cone of a hydraulic turbine, *ASME 2012 International Mechanical Engineering Congress & Exposition*, Houston, TX.
7. Foroutan, H. and Yavuzkurt, S. (2012), Unsteady simulation of flow in the draft tube cone of a hydraulic turbine using different turbulence closure models, Poster presentation in *9th College of Engineering Research Symposium*, The Pennsylvania State University (Awarded the best poster).
8. Foroutan, H. and Yavuzkurt, S. (2012), Analysis and prevention of vortex rope formation in the draft tube cone of a hydraulic turbine, Poster presentation in *27th Annual Graduate Exhibition*, The Pennsylvania State University (Awarded the second place).
9. Dhiman, S., Foroutan, H., and Yavuzkurt, S. (2011), Simulation of flow through conical diffusers with and without inlet swirl using CFD, *Proceedings of ASME-JSME-KSME Joint Fluids Engineering Conference 2011*, Hamamatsu, Japan.
10. Foroutan, H. and Yavuzkurt, S. (2011), Two applications of OpenFOAM: evaluation of k-ε models in boundary layer predictions under high free stream turbulence and simulation of the flow in simplified draft tube of a Francis turbine, *6th OpenFOAM Workshop*, The Pennsylvania State University.

DE-EE0002667
DOE/PSU Graduate Student Fellowship Program for Hydropower
The Pennsylvania State University
Final Report, March 2014

Zack Francis, MS ., Abridged by H. Perez-Blanco

Firming up renewables via PHS w/ Pelton Wheel and bypass: Response and Revenue.

Although wind and solar have free fuel sources, they do not always act in a predictable fashion, or follow the demands of customers. These variations can be thought of as natural cycles whose length can vary from short to long term [1]. Figure 1 shows the timescales of these natural cycles for different renewable resources.

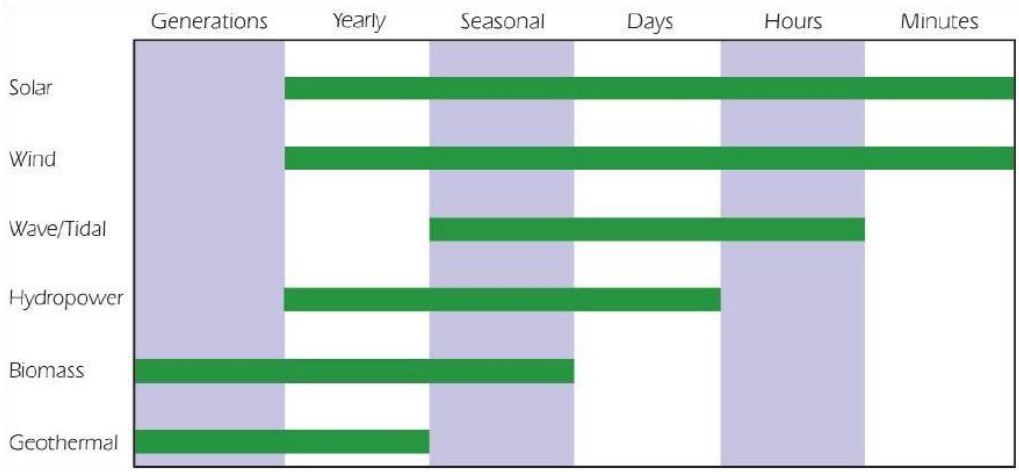

Figure 1 Renewable energy sources and their cycle timescales [1]

The variability of wind is seen by the grid operator as unscheduled changes in power, and consequently a change in frequency that must be balanced [2].

When the penetration of wind and solar power increases, there is a greater need for fast ramping generators. If the mitigating generators are gas driven, they can offset some of the environmental benefits of renewable power [3]. With cumulative wind power capacity in the United States growing rapidly (16% in 2011), variations from renewable sources will likely cause problems in the near future [4]. We study the possibilities of a special type of plant to balance the grid. Pumped hydroelectric storage (PHS) can have good round trip efficiencies for the energy stored (70%-80%), and much higher storage and generating capacities when compared to other technologies [1].

The goal of this research is to study the performance of a fast-response PHS plant [5]. The unit was modeled with the Pelton wheel in a hydraulic short circuit similar to figure 2.

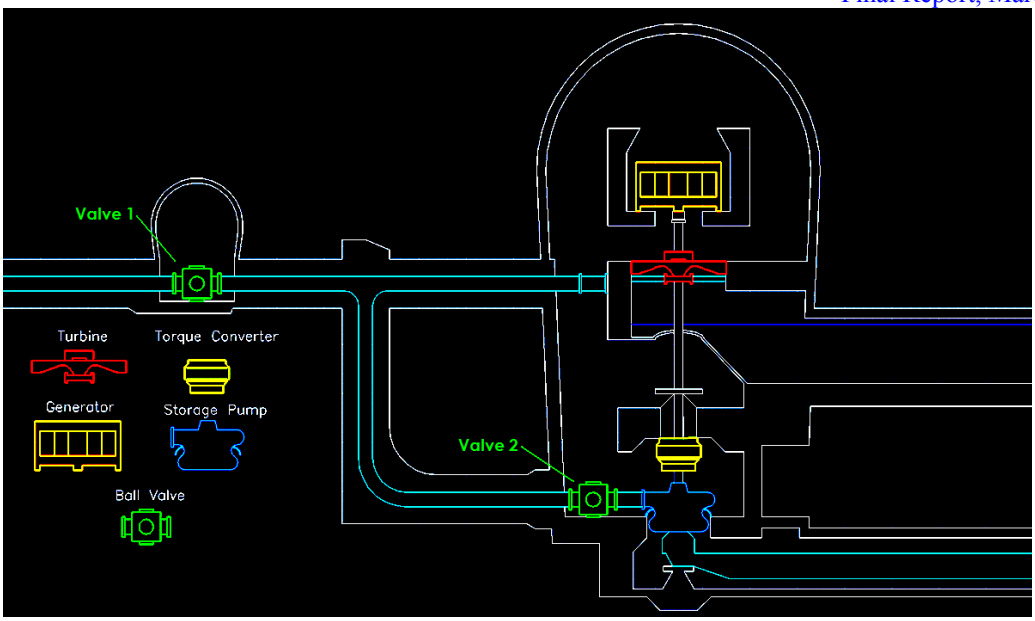

Figure 2 Pumped storage utilizing a bypass component diagram

The separate turbine and pump can work together to allow for variable pumping. A Pelton wheel PHS unit has 4 main components on the generator shaft that need to be modeled; namely the turbine, the generator, the hydraulic clutch, and the pump [6]. The penstock and valves response times must also be considered.

The simulated unit, must be able to profit from energy arbitrage [7] and from offering frequency regulation. According to Perekhodtsev [8], frequency regulation can provide some of the highest revenues for pumped storage plants when compared to the other ancillary services.

Each component is modeled separately via analog programming, and then the model is assembled in VisSim. Turbine calculations reflect that the change in the angular momentum of the flow per unit time also gives the value of the torque imparted on the turbine . The Euler equation gives for torque, [ZACK]

$$T = \dot{m}_3 V_{u3} R_{out} - \dot{m}_2 V_2 R_{in} + (\dot{m}_2 - \dot{m}_3) R^2 \omega \qquad 2.1$$

Eq 2.1 shows that the unsteady torque imparted on the Pelton wheel depends on the entering and exiting mass flow rates, their velocities, and radii. The angular velocity of the Pelton wheel/motor/pump is given by:

$$\dot{\omega} = \frac{T - T_m - T_p}{I} \qquad 2.2$$

Where T is the torque imparted on the turbine by the water, T_m is the torque required by the motor/generator, and T_p is the torque of the pump on the shaft of the motor/generator and turbine. I is the moment of inertia for the system (wheel and generator, or wheel, generator, and pump depending on clutch status). T_m for the motor/generator is positive when the synchronous machine is acting as a generator and producing energy and negative when it is acting as a motor and consuming electricity. Integrating the $\dot{\omega}$ value yields the shaft rotational speed.

The turbine efficiency, varies with the turbine input flow . The adopted efficiency curve was fitted from data given in [9] for a generic turbine. The penstock response time to flow changes is limited [10]. To calculate the fastest opening and closing times, the inertia time constant, and a z term need to be calculated first.

$$T_W = \frac{LV_p}{gH_t} \qquad z = \frac{H_t}{H_{nominal}} \qquad 2.3$$

These two values can be used with the assumption of a long, elastic penstock to find the minimum achievable opening and closing times for the penstock.

$$T_{closing} = \frac{2T_W}{1-z} \qquad 2.4$$

$$T_{opening} = \frac{2T_W\sqrt{z}}{1-z} \qquad 2.5$$

These limits determine the maximum speed at which the needle valve, which controls the flow to the turbine, can open or close.. These opening and closing times allowed for a measured maximum positive ramp rate of about 242 MW/min, and maximum negative ramp rate of about 236 MW/min.

Pump calculations were done under the assumption that each stage of the three stage pump had equal power input and pump head. The total head for the pump was defined as the height difference between reservoirs plus head loss. Both the total head and total power were divided equally among the three stages. The mass flow rate could be found using Eq 2.6

$$\dot{m}_{pump} = \frac{P_{stage}\eta_p}{gH_{stage}} \qquad 2.6$$

Controls to determine the pump, turbine, and stored power focus on the motor input. When the input power for the simulation is negative, the synchronous machine is acting as a motor and consuming power. Since the pumps must run at 100% (150 MW) when being used, the turbine must supply power that is equal to the difference between the required pump power and power supplied by the motor.

$$150\,MW = P_{motor} + P_{turbine} \qquad 2.7$$

The proportional, integral, derivative (PID) controller for the turbine adjusts the needle valve. The power stored is then found using the mass flow rate sent to the upper reservoir and the head between reservoirs:

$$\dot{m}_{pumped} - \dot{m}_{turbine} = \dot{m}_{stored} \qquad 2.8$$

$$P_{stored} = g \cdot H_p \cdot \dot{m}_{stored} \qquad 2.9$$

The pump in this particular configuration is linked to the same shaft as the turbine and generator/motor via a hydraulic torque converter. When the facility is running in turbine mode, the torque converter remains empty so that the turbine and generator can run freely. When the plant needs to switch into pumping mode, the torque converter is flooded with water and the pump is brought up to speed with the motor and turbine [11]. The torque converter was modeled as a rotational damper, where the damping constant, D, was adjusted so that the startup time was about 25 seconds to match measured data [12]. The angular acceleration of the pump shaft was found using Eq 2.10.

$$\dot{\omega}_p = \frac{D(\omega - \omega_p)}{I_p} \qquad 2.10$$

The pump's angular acceleration is integrated and set as the new angular velocity. Pump torque was related to the angular velocity with the use of a generic speed-torque curve for a centrifugal pump with open discharge [13], Eq 2.11,

$$T_p = \frac{T_{design}}{100}\left[192\left(\frac{\omega_p}{\omega_{synch}}\right)^4 - 434\left(\frac{\omega_p}{\omega_{synch}}\right)^3 + 428\left(\frac{\omega_p}{\omega_{synch}}\right)^2 - 93.7\left(\frac{\omega_p}{\omega_{synch}}\right) + 7.3\right] \qquad 2.11$$

The valves have a closing and opening time of 20 seconds; this process was assumed to vary linearly with time [14].. Penninger and Benigni gave flow coefficients as a function of angle for a variety of ball valves [14]. These curves were used to generate a generic flow coefficient curve on the zero to one scale, which could then be related to the head loss.

To complete the physical characteristics of the system, the motor/generator was modeled as a salient pole synchronous machine which is most common in hydropower units [15]. The electrical torque output of such a machine is determined by considering the angle known as delta [16], which measures a phase angle between the generator voltage and the load voltage, the rated machine voltage [17], generator voltage and values for line and load reactances [19], combined in a final equation for electrical torque,

$$T_e = 557460 \sin\delta + 280000 \sin 2\delta - 500000(\omega - \omega_{rated}) \qquad 2.12$$

The synchroounes machine was simulated with 12 poles.

Controls

The unit's main goal is to meet power requests of the grid, so the unit was

modeled to operate even in low efficiency situations. However, this does not mean that the unit is able to constantly follow the grid operator's requests because it takes time to switch between pumping and generating modes.

When in generating mode, a PID controller uses the current power and the

requested power to control the needle valve area passing more or less flow to the turbine. If the grid operator signal drops below zero, the system goes into generating shutdown. Ball valve one and the needle valve both close as quickly as possible. During this time, the synchronous machine power output deviates from following the requested signal, Fig 3.

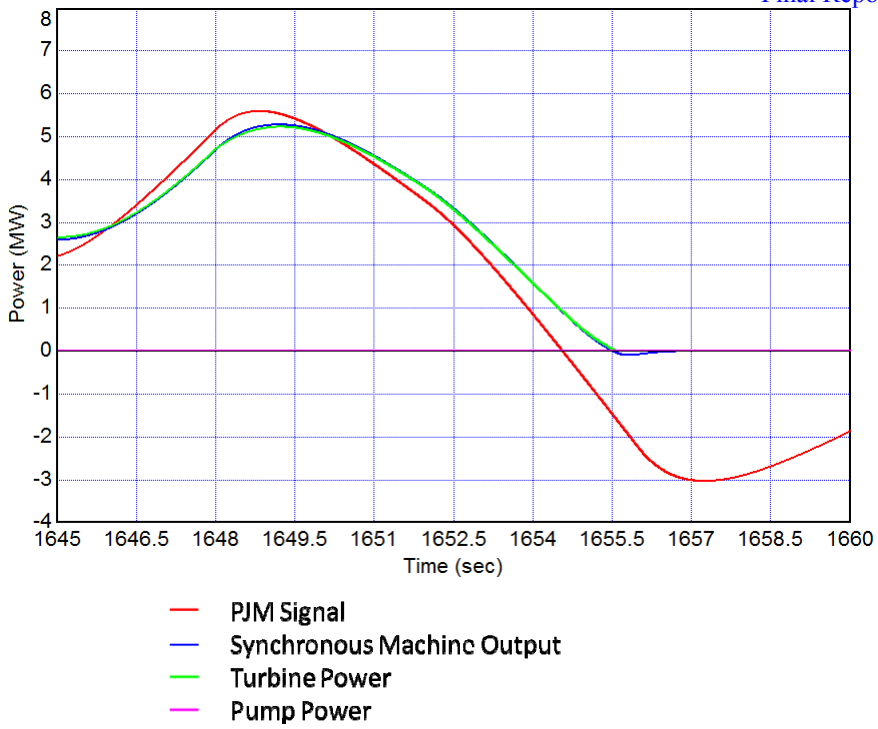

Figure 3 Generation shutdown process

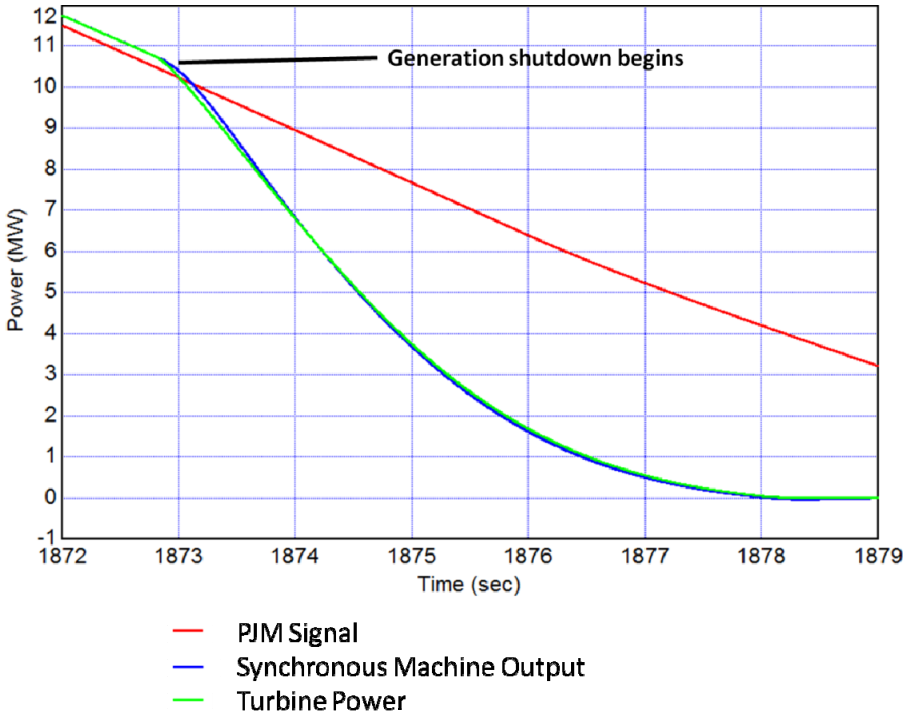

Figure 3b Generation shutdown process

If the signal remains below zero, the unit will go into pump startup immediately after shutting down generation. The pump startup sequence can be seen below, in Figure 7.

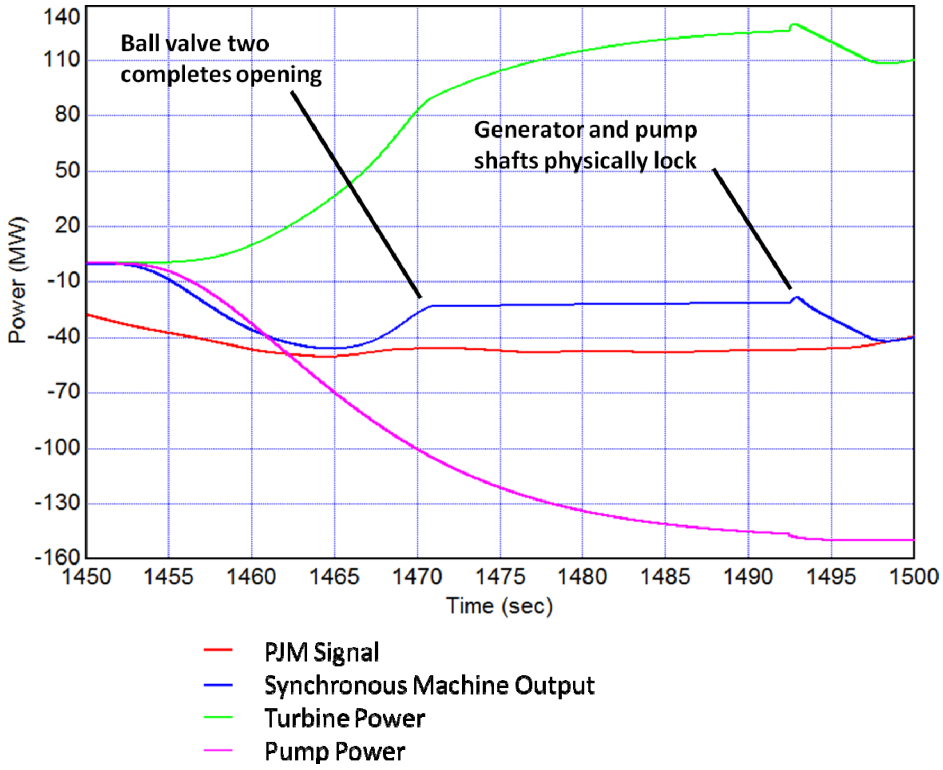

Figure 7 Pumping start up process

The hydraulic clutch fills with fluid, and the pump starts the sequence to come up

to speed. While this is happening, ball valve one remains closed while ball valve two and the needle valve begin to open. This results in the entire pumped flow rate beingbypassed to the turbine to assist in pump startup. Once the pump shaft speed reaches 99.5% of the motor/generator shaft speed, the two physically interlock. After this happens, ball valve one opens and water starts to be stored. This process allows the generator output to once again match the PJM signal.

Similar considerations apply when the requested power moves again above zero, and the pump is shutdown while generation recommences.

When the input signal moves out of the dead band and into the generating region above 10.5 MW, generation startup begins. The needle valve and ball valve one begin to open, the power removed from the system by the generator also increases to the input signal. The generation startup procedure is shown in Fig 2.8.

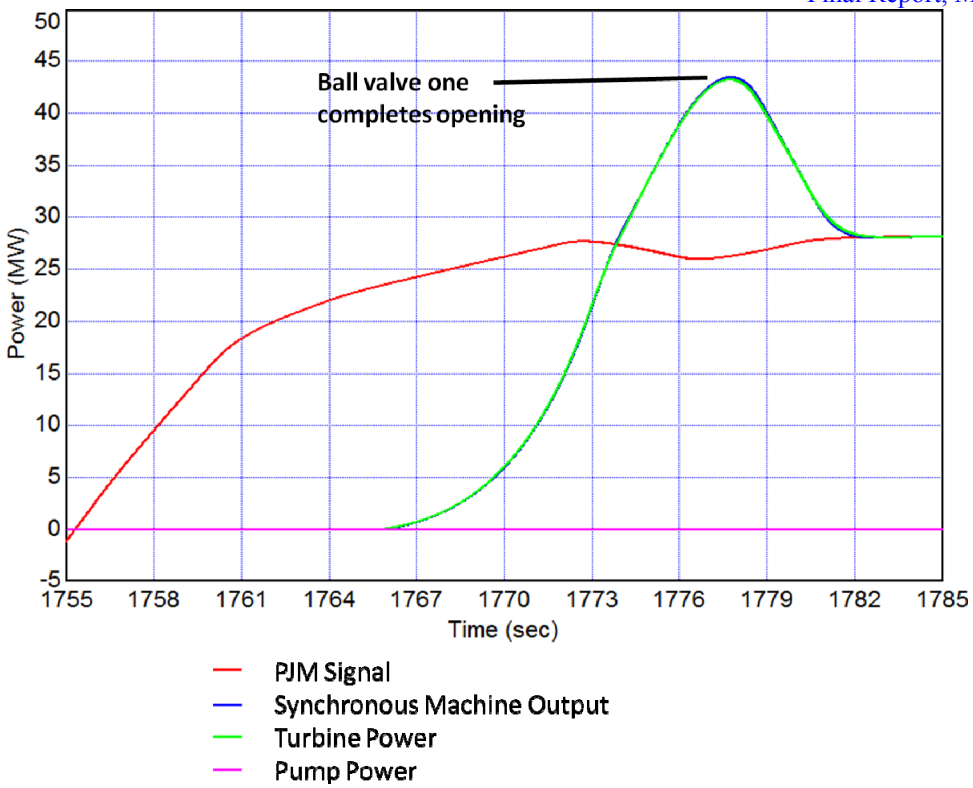

Figure 7b. Generation start up process

To simulate a unit that operates independently in the market, a regulation signal was required. A PJM regulation signal from the day of March st 2012 was obtained, and split into 24 separate hours. The data needed to be split into individual hours because the VisSim model was incapable of running a full day's worth of data at once. The regulation data from PJM had a resolution of 4 seconds. To make the system more realistic, this was filtered through a simple first order Bessel filter with a frequency cutoff of 1 rad/s.

The regulation data were used in conjunction with PJM market prices for seasonal simulations. An 'average month' was constructed for January 2012, April 2012, July 2012, and October 2011 to allow for simplified simulations that gave insight into the trends of each respective season. The hourly DALMP (Daily Locational Marginal Price), RTLMP (Real Time Locational Marginal Price), and RMCP (Regulation Market Clearing Price) were averaged for each hour and compiled to form an average 24 hour day that represents its month. This setup allowed for fewer simulation runs, results that could reflect each individual season, and when all averaged together, an entire year.

Data to simulate the output of a set of real world wind farm was taken from Richard's thesis [7]. A Fast Fourier Transform was performed on the one minute resolution data across 4096 points to find the fundamental frequencies. Fifteen of the most prominent frequencies and magnitudes were measured to create a function to be used in the simulation. These frequencies ranged from 0.007 to 0.080 radians/second and the scaled magnitudes varied from 18 to 2.6 MW. This variation was

added to a constant value to give the final simulated wind power output and is compared to an "offer" or target output value.

The investigation of how profitable, or not, the modeled unit could be when used in the real world begins by calculating the ORC (operating reserve charge) and UDS (uninstructed deviation settlement) of a simulated wind farm with and without the pumped storage plant over the course of one hour. The ORC was calculated using Eq 2.20,

$$ORC = ORR \times \int |P_{prod} - P_{offer}| dt \qquad 2.20$$

The UDS was given by,

$$UDS = RT\ LMP \times \int (P_{prod} - P_{offer}) dt \qquad 2.21$$

The amount of variability reduced by implementing pumped storage is also calculated in the simulation. This calculation involves the integral of the difference of power production and the offer, but compares the two separate values with or without PHS operation. The equation used can be seen below.

$$Variation\ reduction = 1 - \frac{\int |P_{prod\_p} - P_{offer\_p}| dt}{\int |P_{prod} - P_{offer}| dt} \qquad 2.22$$

Frequency regulation is an ancillary service in PJM that can easily be provided by hydro plants during generation. A unique feature of the modeled Pelton wheel in a hydraulic short circuit is that it can also provide regulation during pumping, as well as regulation about a set point of zero. Regulation during simulations was calculated using Eq 2.23.

$$Reg_{credit} = RMCP \int P_{reg\_offer} dt \qquad 2.23$$

When the unit must come away from its scheduled load, it gets compensated for it in the form of lost opportunity cost (LOC). The lost opportunity cost credits compensate the generator for the energy they could be producing had it not been called upon to provide regulation. The LOC can reach significant values if the RTLMP is high compared to what the DALMP is during unscheduled hours. LOC credits and LOC are calculated with the following equations.

$$LOC_{credit} = LOC \int (P_{offer} - P_{setpoint}) dt \qquad 2.24$$

$$LOC = max[RTLMP - ED, 0] \qquad 2.25.$$

ED is defined according to PJM as the average DALMP at the hydro unit bus for the appropriate on-peak or off-peak period excluding those hours during which all available units at the hydro plant were operating [18].

Present worth analysis was completed to identify the investment value of the modeled plant in each of the three simulated scenarios. The present worth calculation took into consideration three major cost/revenue sources which included labor expenses, operations and maintenance expenses, and revenue.

Labor expenses in hydropower plants are fairly low since the plants are automated and require few employees [21]. Because of this, labor costs were estimated at $1,200,000 in the first year. Employment costs in the United States have grown at about 2.9% since 2004 according to the Bureau of Labor Statistics, so that number was also used for the labor expense inflation for the present worth [22]. Operation and maintenance costs were fixed at $3/MWh and $50 million every 15 years [23]. Also included in this section was the initial investment cost of $482 million, and

recovery income at $200/kW. The costs and revenue in this section did not take inflation into account.

Revenue of the plant was obtained from seasonal simulations. Adjustments for purchases from other type of plants, [23] and for inflation of energy prices at a rate of 1.1% [24] were incorporated. The three main factors discussed above were then summed together and adjusted for a corporate tax rate of 35% [25]. Since hydropower is a renewable resource, the plant is able to receive a renewable energy production tax credit of 1.1 ¢/kWh for the first ten years of operation [26]. A discount rate of 5% was used to discount future income to the present value .

The seasonal simulations were completed under the assumption that the operators correctly forecasted when to pump and when to generate throughout the day to maximize profit. Simulations were done on an hourly basis with constant prices for the DALMP, RT LMP and RMCP throughout the hour. In figure 3.1 below, an hour of generating at a set point of 100MW while regulating 50MW is shown, and an hour with a set point of 0MW and regulating 150MW is shown in figure 3.2, this has been termed zero-band regulation.

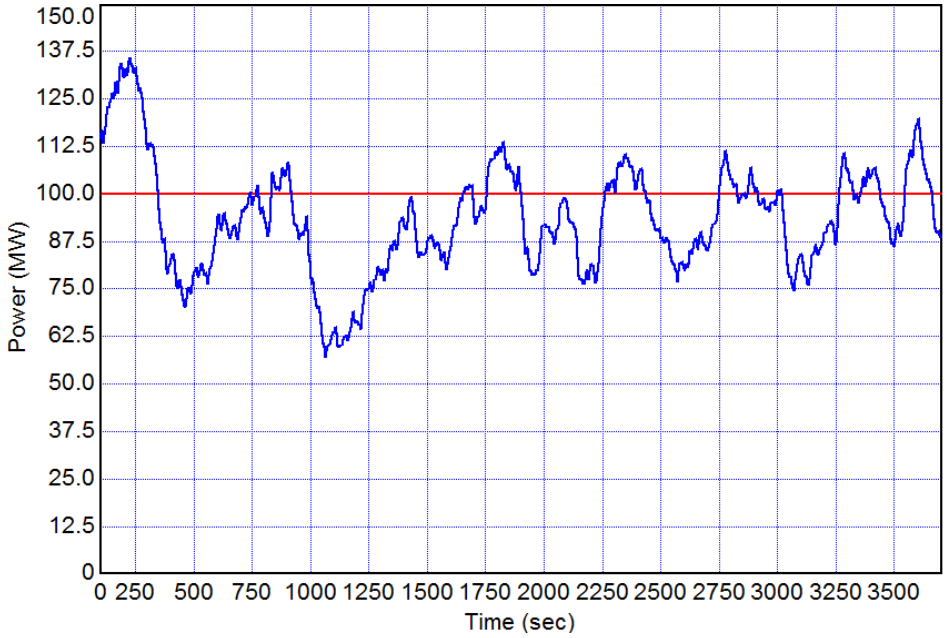

Figure 3.4 Generating at 100 MW with 50 MW regulation

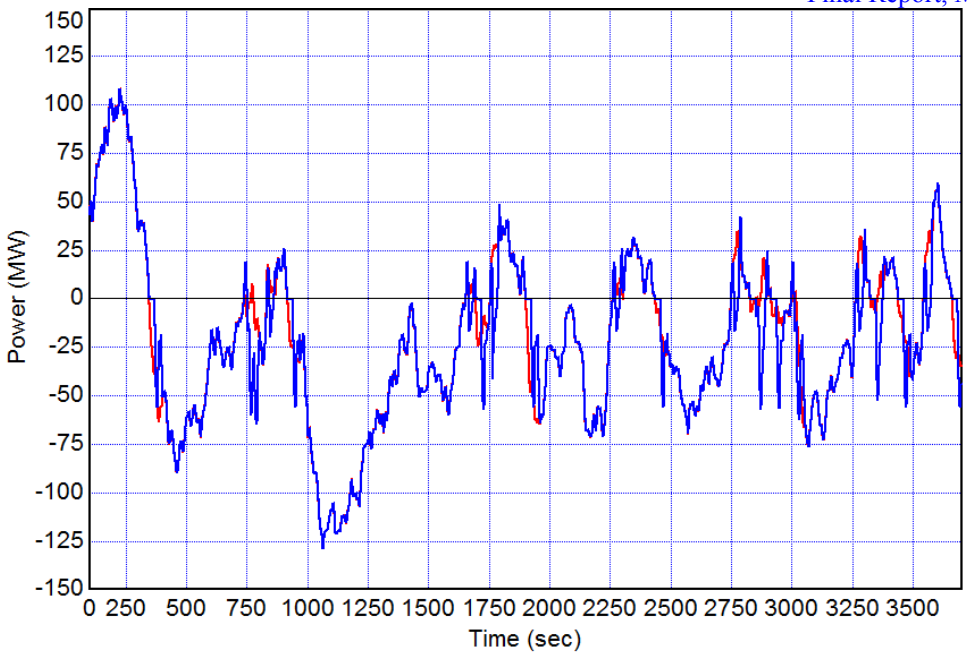

Figure 3.5 150 MW zero-band regulation

Simulation results show that participation in the regulation market can greatly increase daily revenue. Figure 3.3 compares pumping and generating at a maximum power of 150MW with pumping, generating at 100MW while contributing 50 MW to the regulation market without zero-band regulation, and generating at 100MW while contributing 50 MW to the regulation market with zero-band regulation. Participating in regulation and arbitrage as well as zero band regulation allowed the unit to gross about $20,000 more regardless of the season. Throughout the year, arbitrage with zero band regulation earns the unit a gross average of $44,150 per day while arbitrage alone makes a gross average of $24,009 per day.

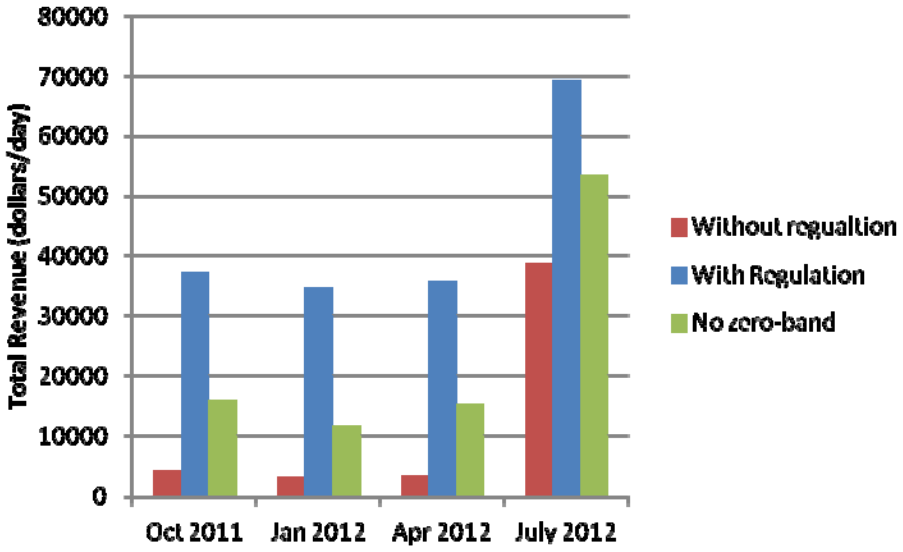

Figure 3.6 Gross daily revenue

July's high price peaks allow the unit to benefit from higher arbitrage revenues for all three scenarios. A finer look at the three scenarios during July can be seen in Figure 3.4.

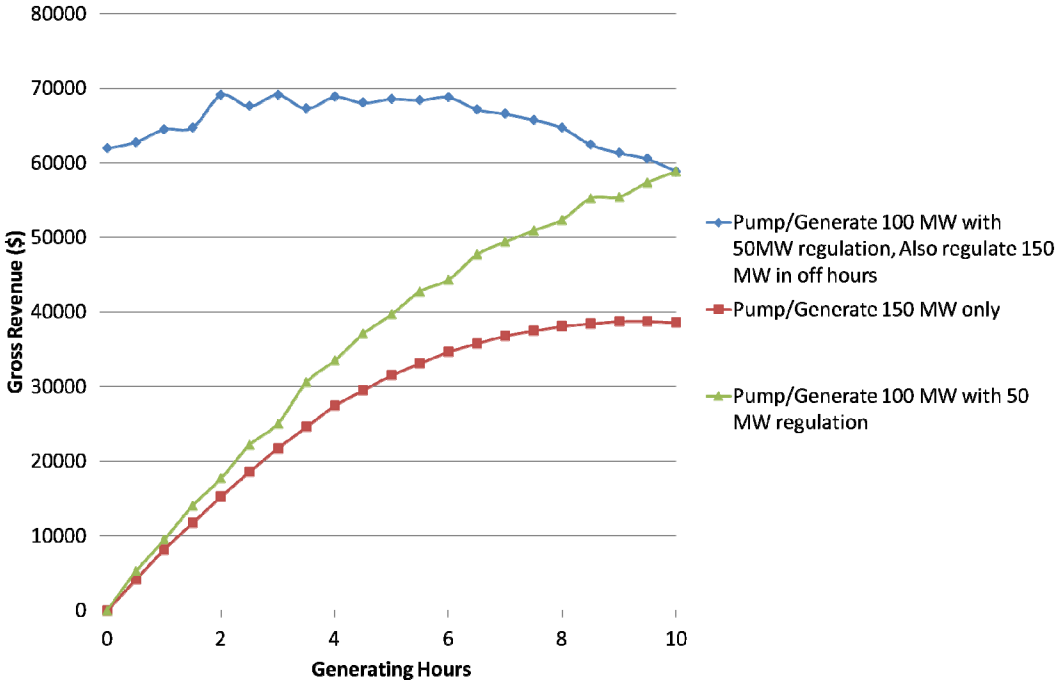

Figure 3.7 July gross daily revenue by generating hours

Both scenarios without zero band regulation have increasing revenue with increased generating hours until the price difference between the most expensive pumping hour and the cheapest generating hour is too small. Arbitrage only (red trace) reaches a maximum at nine hours of

generation with gross revenue of $38,753. Arbitrage with 50 MW of regulation, but without zero band regulation, is less affected by the decreasing price differences and reaches a maximum gross revenue of $58,828 at ten hours of generation. Ten hours of generation is the maximum amount of generation possible in the simulation because fourteen hours of pumping are required to balance out the reservoirs to have zero net flow. Arbitrage with 50 MW of regulation, and zero band regulation, behaves differently than the other two scenarios. Implementing zero band causes the unit to maximize revenue at three hours of generation with a gross of $69130. The gross revenue stays close to this value until it drops off around six hours of generation. At six hours it is noticeable that more money is generated from zero band regulation rather than from increased generating hours.

A Sensitivity analysis with respect to the assumed parameters was performed on the July simulations discussed above. Results can be found in [Zack Thesis].

The present worth of the investment was calculated for the same three scenarios used in section 3.1, namely 24 hr operation w/ arbitrage, arbitrage plus regulation, and arbitrage only. Results are shown in Fig 3.6.

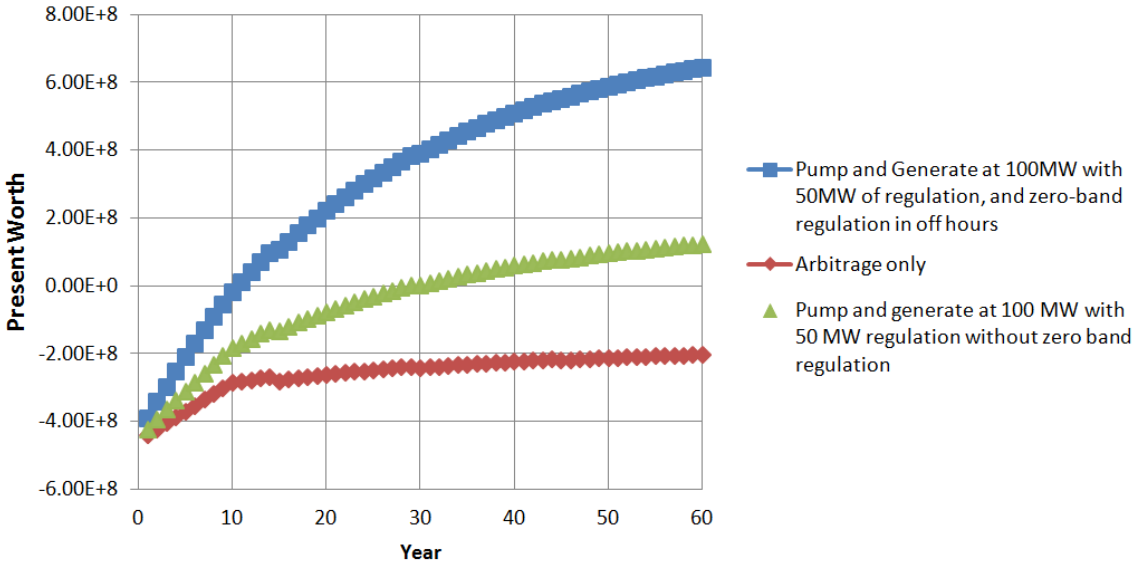

Figure 3.8 Present worth vs. years since initial investment

The most profitable case, with zero band, present worth becomes positive in the eleventh year, and ends the sixty year period with a present worth of $645 million. In the second most profitable case, with regulation but without zero band, present worth becomes positive in the 29th year, and ends the sixty year period with a present worth of $126 million. The least profitable case, involving no regulation, did not reach a positive present worth in the time period, and ended with a present worth of -$203 million.

The model was successful in showing that a Pelton wheel used in a hydraulic short circuit can achieve very high ramp rates. The limiting factor for ramps rates proved to be the penstock dynamics, and not the machinery. The current ramp rates allow the unit to follow the regulation curve given by PJM, even when that curve is spread across the entire capacity of the modeled unit. The largest deviations from the regulation curve occurred at the startup and shutdown of the

pumping process. To better follow the regulation curve improvements should be made to pumping mode transitions rather than ramp rates.

Seasonal simulations show that participating in regulation with the typical energy arbitrage increases average daily revenue. Revenue can be increased further when the unit participates in zero band regulation during hours in which the unit is not operating in arbitrage. This was true for every month's simulation as well as all of the sensitivity analysis results.

The revenue for the most profitable case begins to drop if the unit participates in over six hours of arbitrage generation. This represented the point where it would be more profitable to operate in zero band regulation as opposed to further arbitrage. This occurred because the more arbitrage the plant participates in, the lower the difference between the buying and selling price of energy.

Sensitivity analysis with varying regulation offers reinforced that engaging in more regulation increases revenues. When the operating set point was dropped by 10 MW and the regulation offer increased by 10 MW, the unit was able to increase its average gross daily revenue in July by over $2,000.

Sensitivity analysis showed interesting results when it came to how much the roundtrip efficiency affected the revenue of the plant. A 10% change in roundtrip efficiency yielded less than a 5% change in gross revenue. It is also important to note that the difference in revenue between 77% and 80% roundtrip efficiency is $1,910 and the difference between 70% and 77% is only $1,394. This jump in revenue is unexplained, and would likely need further analysis to determine the efficiency factors that affect revenue.

The present worth analysis shows that operating this type of setup without participating in regulation is not a good investment. For future work, further analysis of individual days, as opposed to the average days that were used, would serve to verify if the average days constructed were good representations of the month. Alternate pump start up and shutdown procedures should also be analyzed to determine if there is a procedure that allows the unit to follow the grid operator curve more closely.

BIBLIOGRAPHY

[1] Gül, Timur, and Till Stenzel. "Variability Of Wind Power And Other Renewables." *www.uwig.org*. International Energy Agency, Web. <http://www.uwig.org/IEA_Report_on_variability.pdf>.

[2] Parsons, B., and Et. Al. "Grid Impacts of Wind Power Variability: Recent Assessments from a Variety of Utilities in the United States." *Nrel.gov*. National Renewable Energy Laboratory, Web. 11 Feb. 2013. <http://www.nrel.gov/docs/fy06osti/39955.pdf>.

[3] Su, Han-I, and Abbas El Gamal. "Modeling and Analysis of the Role of Fast-Response Energy Storage in the Smart Grid." *Ieee.org*. Institute of Electrical and Electronics Engineers, 28-30 Sept. 2011. Web. 11 Feb. 2013. <http://ieeexplore.ieee.org/stamp/stamp.jsp?tp=>.

[4] U.S. Department of Energy. "2011 Wind Technologies Market Report."*Www.eere.energy.gov*, Aug. 2012. Web. <http://www1.eere.energy.gov/wind/pdfs/2011_wind_technologies_market_report.pdf>.

[5] Vorarlberger Illwerke AG. "Under Pressure." *Omicron Magazine* 1.1 (2010): 18-21.*Omicron.at*. Omicron. Web. <http://www.omicron.at/fileadmin/user_upload/files/pdf/en/OMICRON-magazine-issue1-ENU.pdf>.

[6] Vorarlberger Illwerke AG. *Hydropower Plant Kops II*. Vorarlberger Illwerke AG, *Kopswerk.at*. Vorarlberger Illwerke AG. Web. Aug. 2012. <http://www.kopswerk2.at/downloads/Folder_061006_englisch.pdf>.

[7] Richards, Scott. *Technoeconomic Analysis of Pumped Hydroelectric Storage as a Means to Mitigate the Variability of Renewable Generation*. Thesis. Penn State, 2012.

[8] Perekhodtsev, Dmitri. "Essay: Economics of Hydro Generating Plants Operating in Markets for Energy and Ancillary Services." Thesis. Carnegie Mellon University, 2004.*Tepper.cmu.edu*. Web. <http://wpweb2.tepper.cmu.edu/ceic/theses/Dmitri_Perekhodtsev_PhD_Thesis_2004.pdf>

[9] Dixon, S.L.; Eng, B. (1998). Fluid Mechanics and Thermodynamics of Turbomachinery (5th Edition). (pp: 308-317). Elsevier.

[10] Kjølle, Arne. "Chapter 4: Governing Principles." *Hydropower in Norway*. Trondheim: Norwegian University of Science and Technology, 2001. Web. <http://www.ehu.es/inwmooqb/Centrales%20electricas%20I/06_chapter4.pdf>

[11] Voith. "Pumps." *Products and Services*. Web. <http://www.voith.com/en/products-services/hydro-power/pumps-566.html>.

[12] "Under Pressure." *Omicron Magazine*. Omicron Electronics, 2010. Web. <http://www.omicron.at/fileadmin/user_upload/files/pdf/en/OMICRON-magazine-issue1-ENU.pdf>.

[13] "Starting Torque - Speed Curve Analysis." *CR4.globalspec.com*. Web. <http://cr4.globalspec.com/thread/73003>

[14] Penninger, Gerhart, and Helmut Benigni. *NUMERICAL SIMULATION AND DESIGN OF SPHERICAL VALVES FOR MODERN PUMP STORAGE POWER PLANTS. 14th Intern. Seminar on Hydropower Plants*. Institute for Waterpower and Pumps, 2006. Web. <http://www.hfm.tugraz.at/fileadmin/user_upload/pdf/Benigni_ISHPP2006.pdf>.

[15] Mayer, Jeffrey. "AC Machine Fundamentals." EE 387. Penn State. Lecture.

[16] Mayer, Jeffrey. "Synchronous Machine" EE 387. Penn State. Lecture.

[17] Hindelang, Bernd. "KOPS II, AN EXTRAORDINARY TURBINE/GENERATOR ARRANGEMENT." *VA Tech Hydro News* 8 (June 2005): 6-7. *Vatech-hydro.com*. Virginia Tech. Web. <http://atl.g.andritz.com/c/www/00/04/04/266832675/40450/1/1/0/hydro-media-media-center-hn8_masterfile_e_final_1_.pdf>.

[18] PJM. "Regulation Hydro Lost Opportunity Cost Calculation Examples." *Pjm.com*. N.p., n.d. Web. <http://www.pjm.com/markets-and-operations/ancillary-services/~/media/markets-ops/ancillary/20090915-regulation-hydro-lost-opportunity-cost-calc-examples.ashx>.

[19] Masoum, Mohammad. "SYNCHRONOUS MACHINE DYNAMICS." Lecture. Electrical Machines 302. Curtin University of Technology. 2006. Web.

<http://bauhaus.ece.curtin.edu.au/~em302/Lecture%20Notes/Lec%208-10%20SM%20Dunamics.PDF>.

[20] PJM State and Member Training Department. "Demand Side Response in the Ancillary Service Markets." *Www.pjm.com*. N.p., Aug. 2012. Web. <http://www.pjm.com/~/media/training/core-curriculum/ip-dsr/dsr-in-the-ancillary-service-markets.ashx>.

[21] "Hydropower Generation." SETIS, 7 June 2010. Web. <http://setis.ec.europa.eu/newsroom-items-folder/hydropower-generation>.

[22] "Cost of Employment." *Bls.gov*. Bureau of Labor Statistics, Web. <http://data.bls.gov/cgi-bin/surveymost>.

[23] "The Dynamics of Pumped Hydro Storage with a Pelton Wheel and Bypass." Voith Hydro, Personal interview. 28 Feb. 2013.

[24] "Rising Electricity Costs: A Challenge For Consumers, Regulators, And Utilities." *Eei.org*. Edison Electric Institute, May 2006. Web. <http://www.eei.org/whatwedo/PublicPolicyAdvocacy/StateRegulation/Documents/rising_electricity_costs.pdf>.

[25] "Cost of New Entry Combustion Turbine Power Plant Revenue Requirements." *Pjm.com*. Pasteris Energy, Inc., 16 Nov. 2009. Web. <http://www.pjm.com/~/media/committees-groups/committees/cmec/postings/20091130-cone-ct-revenue-requirements-report.ashx>.

[26] "Renewable Electricity Production Tax Credit (PTC)." *Energy.gov*. U.S. Internal Revenue Service, Web. <http://energy.gov/savings/renewable-electricity-production-tax-credit-ptc>.

Daniel Leonard, expect PhD Dec. 2014. Advisor: Jules Lindau

Computation of Cavitating Flow in Hydroturbines

Cavitation refers to the physical process of the inception, transport, and desinence of vapor cavities within an originally homogeneous liquid medium. Cavitation inception occurs in localized regions of the liquid which have fallen below a material property of the liquid called the vapor pressure. At a fixed temperature, if the liquid drops below this very low pressure in some region, a phase change will occur in that region (*i.e.* vapor cavities will form). This is a similar mechanism to boiling but at roughly constant temperature. The cavities may then be transported through the liquid, interacting with it, and possibly changing flow structure if they develop to a relatively large enough scale. In this manner, cavitation within hydraulic machinery can affect performance. When the cavities are transported into a region of higher pressure, they will collapse, changing phase to liquid once again. The collapse of cavities is usually a violent process which produces high intensity noise, causes severe vibration to nearby solid structures, and can easily pit and erode hard metals such as steel.

In hydroturbines, cavitation can cause a sharp decrease in efficiency, as well as erosion from collapsing vapor clouds, resulting in premature wear, large component repair costs, and significant loss in revenue during machine repair downtime [1,2,3]. Furthermore, it is the present trend in the hydro industry to attempt to extract more power from current and future installations over a wider operating range [4,5,6]. Consequently, there is more current and expected operation at off-design conditions, where cavitation is likely to occur. Thus, understanding cavitation is of utmost importance to allow for operation at the off-design conditions the energy market demands, while mitigating cavitation's undesirable effects.

Although there is a great deal of CFD research for hydroturbines, and a wealth of CFD analysis of cavitating flow in turbomachinery, investigations of hydroturbines utilizing multiphase CFD are rather scarce. This is even more surprising when we recall how large of an impact cavitation has on the hydroturbine industry. Of the few cavitating CFD studies published, some have only simulated the draft tube region, and neglected the upstream components such as the runner and guide vanes [7]. Susan-Resiga et al. [8] and Panov et al. [9] simulated steady, periodic cavitating flow in the stationary and rotating components of Francis turbines. Panov et al. clearly displayed the performance breakdown of the machine with decreasing cavitation number (increasing extent of cavitation), and the results compared favorably with experiments. Lui et al. [10] and Wu et al. [11] simulated steady and Unsteady Reynolds Averaged Navier Stokes cases of a full 360 degree Francis turbine. The steady results displayed performance breakdown which compared well with experimental values, and the unsteady pressure fluctuation amplitudes and frequencies were predicted much more reliably than the corresponding single-phase cases. These results are all very promising, but this research area is still in its early stages, and much progress can still be made with further investigations into cavitating CFD in hydroturbines.

This project computed cavitating flow in a Francis hydroturbine, for which the geometry and experimental data was provided by industry partner Weir American Hydro. The computational domain included the stay vanes, guide vanes, runner, and elbow draft tube as pictured in Figure 1a. The stay vane, guide vane, and runner, were all calculated with single-blade passages that required periodic boundaries, while the draft tube was the full 360 degree non-axisymmetric diffuser. The steady flow, single-blade computations, with the assumption of periodicity, allow for accurate performance predictions. The draft tube plays a large role in the losses of the machine, and thus, using the full draft tube provides more realistic results. The runner was computed in a rotating reference frame, which included centrifugal and Coriolis acceleration terms in the equations of motion, to account for rotational effects in the steady, fixed mesh computation. To deal with the variable periodicity between stages of

the turbine, mixing planes were used to circumferentially average the pressure, velocity and volume fraction at interfaces highlighted in Figure 1b. The mixing planes conserve mass, angular & radial momentum, and surface averaged pressure. Simulations were completed on Department of Defense (DoD) computer Harold, and a density-based solver with a homogenous mixture approach [12] along with the Kunz mass transfer model [13] were used to compute the cavitating flow field. Gravitational effects were also considered.

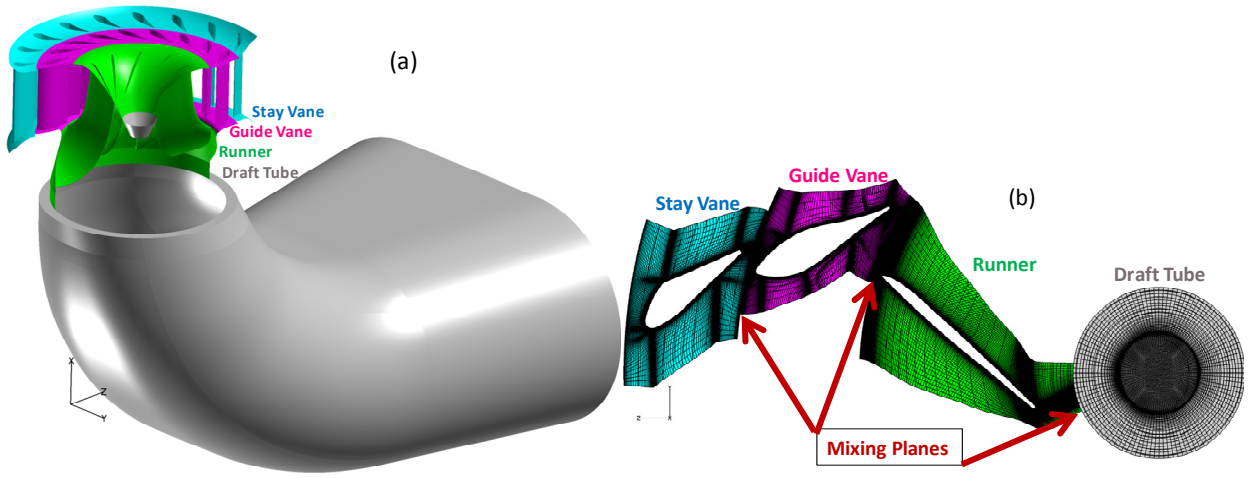

Figure 1. Write stuff here.

Figure 2a displays the results of power coefficient over a range of Thoma numbers for the model-scale coarse and fine meshes compared with the model test experiments. All cases are within 2 percent error, and because the results do not vary much between coarse and fine meshes (5 and 10 million cells, respectively), it implies that the mesh has little effect on the torque results (displays mesh convergence). As cavitation develops on the runner with lower Thoma number, the power coefficient can be seen to begin to breakdown. Figure 2b shows the efficiency is predicted within 5 percent of the experiments for both meshes. However, the losses are being over predicted, and while the fine mesh is approaching the experimental values, the mesh still needs to be refined more, particularly in the draft tube, to correctly capture the efficiency. Another level of mesh refinement is in progress.

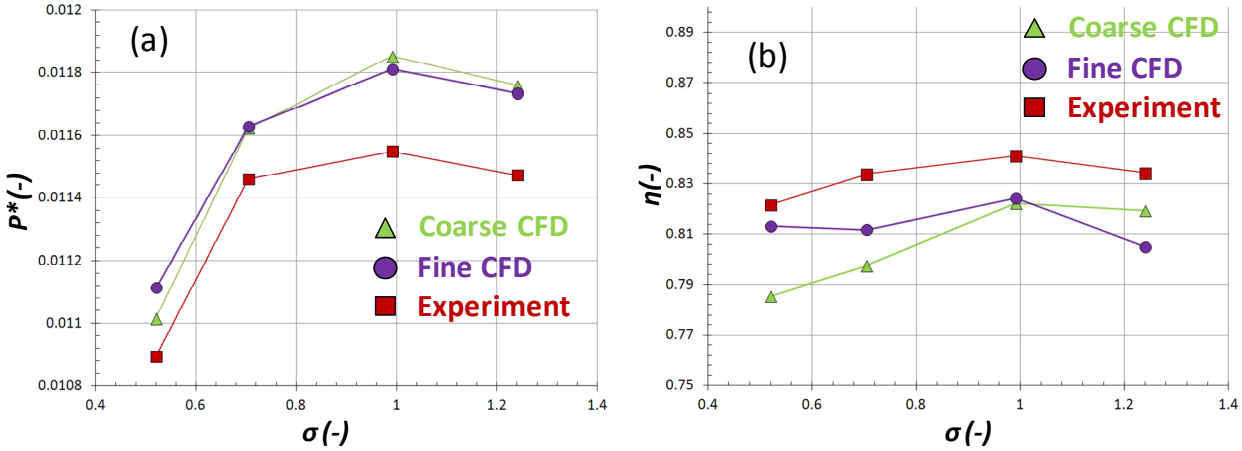

Figure 2. Write stuff here.

Figure 3a and 3b qualitatively compare the cavitation for the highest and lowest Thoma number cases, least and most cavitating cases, respectively, to their corresponding experimental photos and drawings. The streamlines in Figure 3a clearly display the vortex rope structure in the draft tube. The mesh is too

coarse in the axial direction to capture the cavitating core of the rope fully but cavitation does appear underneath the hub. Also, in this case, no cavitation is observed on the leading edge suction side although it was reported to occur to a minimal degree in the experiments. Both cases display cavitation beneath the overhang of the guide vane which also occurred in the experiments. This may be the first time that cavitation has been predicted with CFD in the guide vane region. Figure 3b shows the torch like hub cavitation is predictied well, and the vortex rope is much weaker than for the case with less cavitation (or this cases corresponding single-phase simulation, not shown). This is direct evidence that cavitation plays a large role on the structure of the vortex rope. Furthermore, the large amount of cavitation along the suction side of the blade, at the band, is consistent with the experiments. These results were presented in at a conference [14].

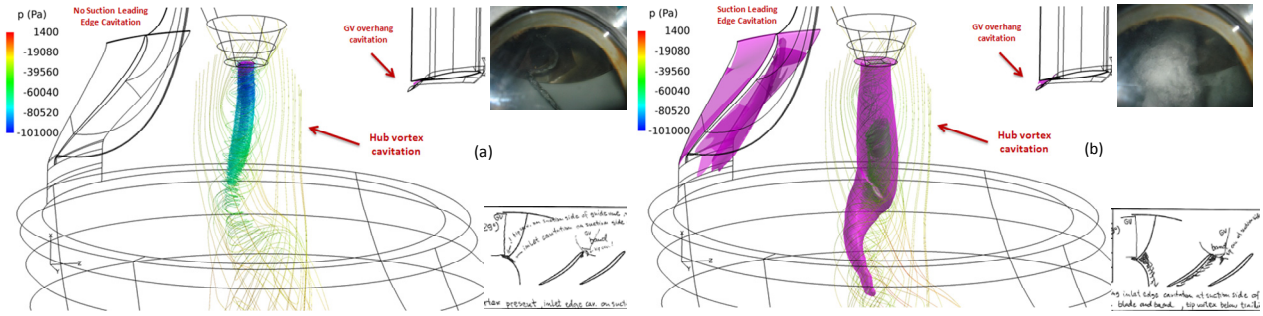

Figure 3. Write stuff here.

While the performance predictions, such as efficiency and power, can be reliably calculated with steady simulations, unsteady calculations are necessary to indicate how cavitation affects vibration, noise, erosion, and damage. Unsteady simulations have begun, using periodic domains and the full draft tube. The unsteady flow in the draft tube displays a precessing vortex for the cases with the least cavitation and this is consistent with the experiments. The unsteady power coefficient for each case is plotted in Figure 4. It can be seen that these oscillations do not occur for the cavitation cases which do not have a precessing vortex structure. These simulations are in preliminary stages and they still must be advanced for a greater period to overcome the transient and produce more reliable results. These preliminary unsteady results were presented in a recent seminar [15].

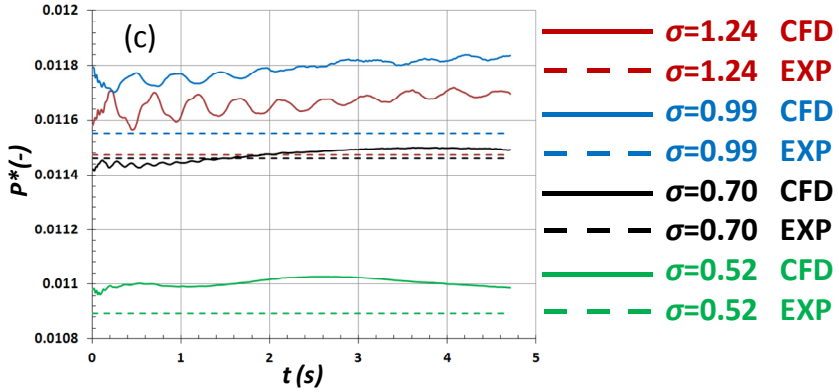

Figure 4. Write stuff here.

This project received a fellowship award from the Hydro Research Foundation in April 2013. Funding from the Foundation will continue until December 2014. The steady results will continue with mesh refinement and also calculations of the prototype-scale machine. There does not seem to be any literature presently available of cavitating hydroturbine CFD which displays the differences due to lack of Froude scaling, due to the hydrostatic pressure gradient, between model and prototype scales. This is

an important topic because cavitation can end up being fundamentally different between the model scale and the full scale machine. Displaying these differences is something that CFD can easily accomplish by computing at both scales. Preliminary results are already being obtained for the prototype scale. Further present and future work is to calculate full wheel unsteady cavitating results for the fully coupled stationary and rotating components using Unsteady Reynolds Average Navier-Stokes (URANS) and Detached Eddy Simulation (DES) approaches. This work is expected to be completed by December 2014.

References:

1. Bourdon, P., Farhat, M., Mossoba, Y., and Lavigne, P. (2004). Hydro turbine profitability and cavitation erosion.
2. Gordon, J. L. (1992), Hydroturbine cavitation erosion, *Journal of energy engineering* 118.3: 194-208.
3. Avellan, F. (2004). Introduction to cavitation in hydraulic machinery*, The International Conference on Hydraulic Machinery and Hydrodynamics*, Timisoara, Romania.
4. Susan-Resiga, R., Muntean, S., Hasmatuchi, V., Anton, I., & Avellan, F. (2010). Analysis and prevention of vortex breakdown in the simplified discharge cone of a francis turbine. *Journal of Fluids Engineering*, *132*(5), 051102.
5. Susan-Resiga, R. F., Muntean, S., Avellan, F., & Anton, I. (2011). Mathematical modelling of swirling flow in hydraulic turbines for the full operating range. *Applied Mathematical Modelling*, *35*(10), 4759-4773.
6. Alligné, S., Nicolet, C., Allenbach, P., Kawkabani, B., Simond, J. J., & Avellan, F. (2008, October). Influence of the vortex rope location of a Francis turbine on the hydraulic system stability. In *Proceedings of the 24th IAHR Symposium on Hydraulic Machinery and Systems, Foz do Iguassu, Brazil*.
7. Dorfler, P., Keller, M., Braun, O. (2010). Francis full-load surge mechanism identified by unsteady 2-phase CFD, *25th IAHR Symposium on Hydraulic Machinery and Systems*, 2010
8. Susan-Resiga, R., Muntean, S., Bernad, S., & Anton, I. (2003, September). Numerical investigation of 3D cavitating flow in Francis turbines. In *Proc. of the Int. Conf. on Modell. Fl. Flow (CMFF03)* (pp. 950-57).
9. Panov, L. V., Chirkov, D. V., Cherny, S. G., Pylev, I. M., & Sotnikov, A. A. (2012). Numerical simulation of steady cavitating flow of viscous fluid in a Francis hydroturbine. *Thermophysics and Aeromechanics*, *19*(3), 415-427.
10. Shuhong Liu, Liang Zhang, Michihiro Nishi, and Yulin Wu (2009), Cavitating Turbulent Flow Simulation in a Francis Turbine Based on Mixture Model, *Journal of Fluids Engineering*, Vol. 131(5), pp. 1361-1364.
11. Yulin Wu, Shuhong Liu, Hua-Shu Dou, and Liang Zhang (2010), Simulations of unsteady cavitating turbulent flow in a Francis turbine using the RANS method and the improved mixture model of two-phase flows, *Engineering with Computers*.
12. Venkateswaran, S., Lindau, J. W., Kunz, R. F., & Merkle, C. L. (2002). Computation of multiphase mixture flows with compressibility effects. *Journal of Computational Physics*, *180*(1), 54-77.
13. Robert F. Kunz, David A. Boger, David R. Stinebring, Thomas S. Chyczewski, Jules W. Lindau, Howard J. Gibeling, Sankaran Venkateswaran, and T. R. Govindan (2000), A preconditioned Navier-Stokes method for two-phase flows with application to cavitation prediction, *Computers & Fluids*, Vol. 29, pp. 849-875.

14. Leonard D.J. (January 30 2014). Computation of Cavitating Flow in a Francis Hydroturbine, *Penn State Fluid Dynamics Research Consortium Seminar Series*, University Park, PA
15. Leonard D.J., Lindau J.W. (November 24-26 2013). Computation of Cavitating Flow in a Francis Hydroturbine, *American Physical Society 66th annual meeting of the Division of Fluid Dynamics*, Pittsburgh, PA

Publications Resulting from this Project:

1. Leonard D.J. (January 30 2014). Computation of Cavitating Flow in a Francis Hydroturbine, , *Penn State Fluid Dynamics Research Consortium Seminar Series*, University Park, PA
2. Leonard D.J., Lindau J.W. (November 24-26 2013). Computation of Cavitating Flow in a Francis Hydroturbine, *American Physical Society 66th annual meeting of the Division of Fluid Dynamics*, Pittsburgh, PA

Bryan Lewis, PhD 2014. Advisor: John Cimbala
Improving Unsteady Hydroturbine Performance During Off-Design Operation Through Controlled Wicket Gate Trailing-Edge Blowing

Hydroturbines operate at very high efficiency (up to approximately 95%) at their best efficiency point (BEP). However, with the ever-increasing penetration of alternative electricity generation, it has become common to operate hydroturbines at off-design conditions in order to maintain stability in the electric power grid. This work demonstrated a method for improving hydroturbine performance during off-design operation by injecting water through slots at the trailing edges of the wicket gates. The injected water causes a change in bulk flow direction at the inlet of the runner, and reduces in the unsteady rotor stator interactions. The change in flow angle from the wicket gate trailing edge jets provided the capability of independently varying the flow rate and swirl angle through the runner, which in current designs are both determined by the wicket gate opening angle.

Many methods have been studied for reducing the intensity of the vortex shedding. Donaldson studied the effect of trailing edge shape on the flow induced vibrations of hydrofoils, and found that by adding a bevel to the hydrofoil trailing-edge, the amplitude of wake shedding was deduced to 1% of that observed with a blunt trailing edge [Donaldson 1956]. Naudascher studying the behavior of turbulent momentumless-wakes, where the drag on the body was balanced by a fluid jet at the trailing edge, and found that the decay rate for the centerline velocity deficit was much faster for the momentumless wake than for the pure wake [Naudascher 1965]. By combining these two methods, a uniquely designed wicket gate trailing-edge was developed, that included a symmetric beveled trailing edge, and dual slot jets that were inclined inward from the beveled surface (see Figure 1). The optimal location and inclination angle of the jets were determined through a Taguchi method.

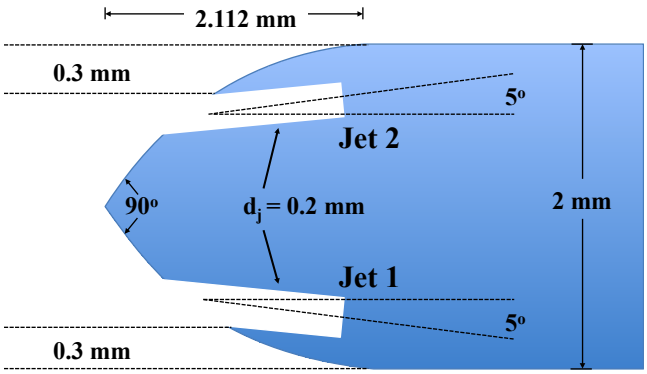

Figure 1. Final design of the trailing edge geometry for the jet channels added to the wicket gates of the GAMM Francis Turbine. The blunt trailing edge was replaced with a beveled shape, and the jets were inclined toward the center of the vane to improve the maximum turning of the water.

The unsteady flow through the hydroturbine was simulated in OpenFOAM®, an open source CFD solver. The governing equations and boundary conditions are consistent with the industry standards. The effects of blowing from the wicket gate trailing-edge jets were evaluated using unsteady quasi-2-D simulations of the distributor channel with various jet designs (Figure 2(a)), 3-D steady-state simulations of a single distributor vane and runner blade passages (Figures 2(b) and (c)), and unsteady simulation of the

complete GAMM Francis Turbine [Parkinson 1995, Sottas and Ryhming 1989], including the dynamic rotation of the runner wheel (Figure 2(d)).

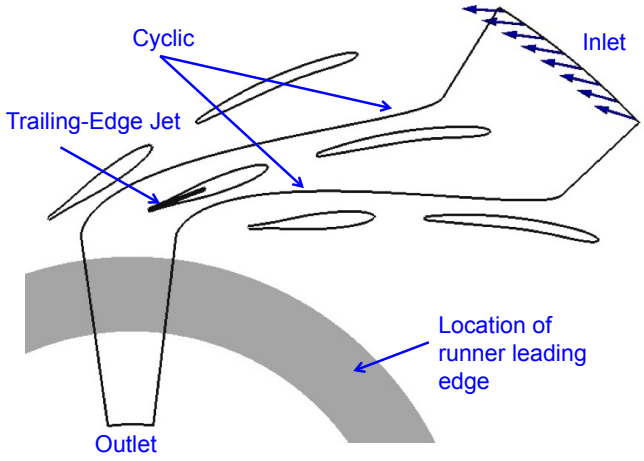

(a) Quasi-2-D distributor passage

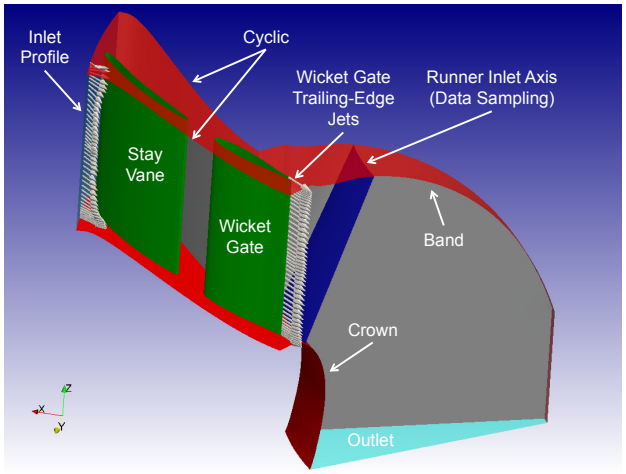

(b) 3-D distributor vane passage

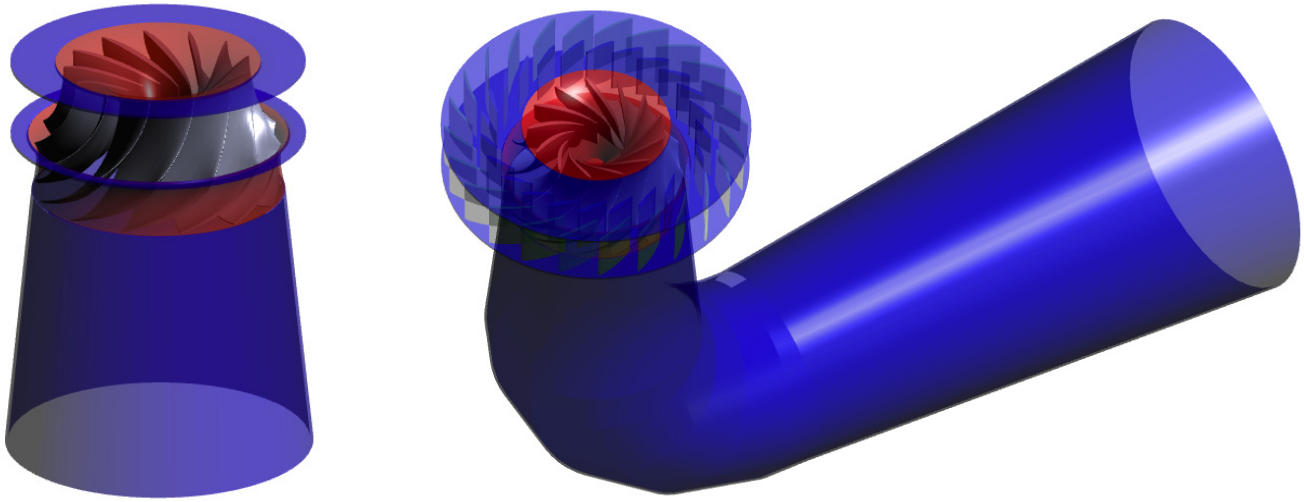

(c) 3-D runner passage (only one blade included in the simulation)

(d) 3-D full-wheel simulation of the complete GAMM turbine

Figure 2. Geometry used for the various CFD simulations needed to evaluate the design of the wicket gate trailing-edge jets, and the impact on the turbine performance.

From the quasi-2-D simulations of a single distributor vane passage, the effects of blowing from trailing-edge jets were explored, with both blunt and beveled trailing edges. By introducing blowing from the blunt trailing-edge wicket gate, or adding a beveled shape to the trailing edge of the wicket gate, the unsteadiness in the wake due to large von Kármán vortex shedding was significantly reduced. As shown in Figure 3, both the blunt trailing edge with blowing and the beveled trailing edge effectively eliminate the von Kármán vortices downstream. With the addition of blowing from the beveled trailing edge shape, a ±5° change in swirl angle at the location of the runner leading edge was observed. This amount of turning was achieved by blowing from each jet independently with a jet speed of 14.9 m/s, or 3% of the inlet flow rate at BEP.

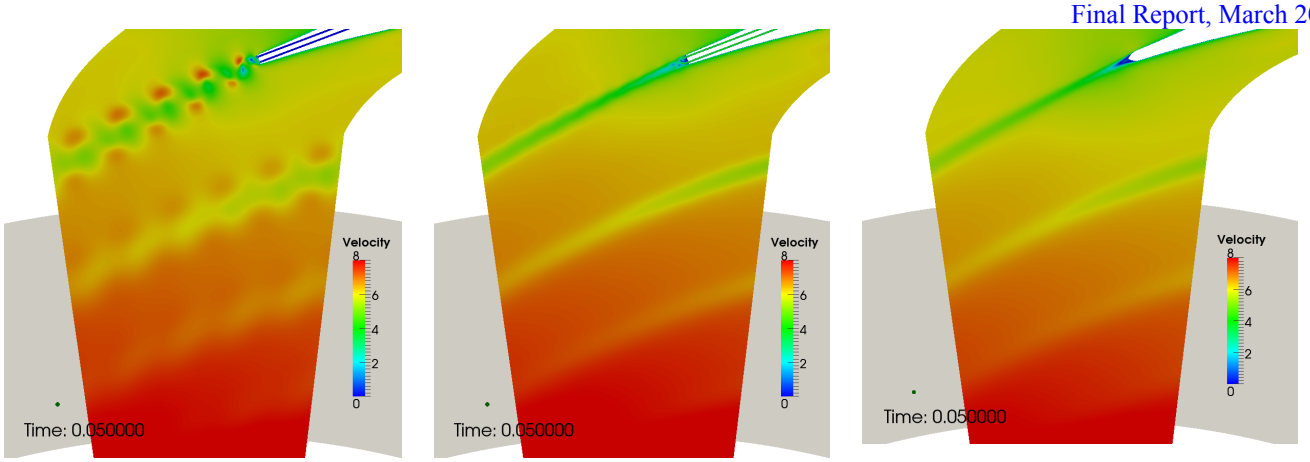

(a) Blunt trailing edge, no blowing **(b)** Blunt trailing edge, with blowing **(a)** Beveled trailing edge, no blowing

Figure 3. Instantaneous velocity contour plots (in m/s) for the flow in a 2-D periodic distributor-vane channel with a blunt trailing edge and a beveled trailing edge, without blowing.

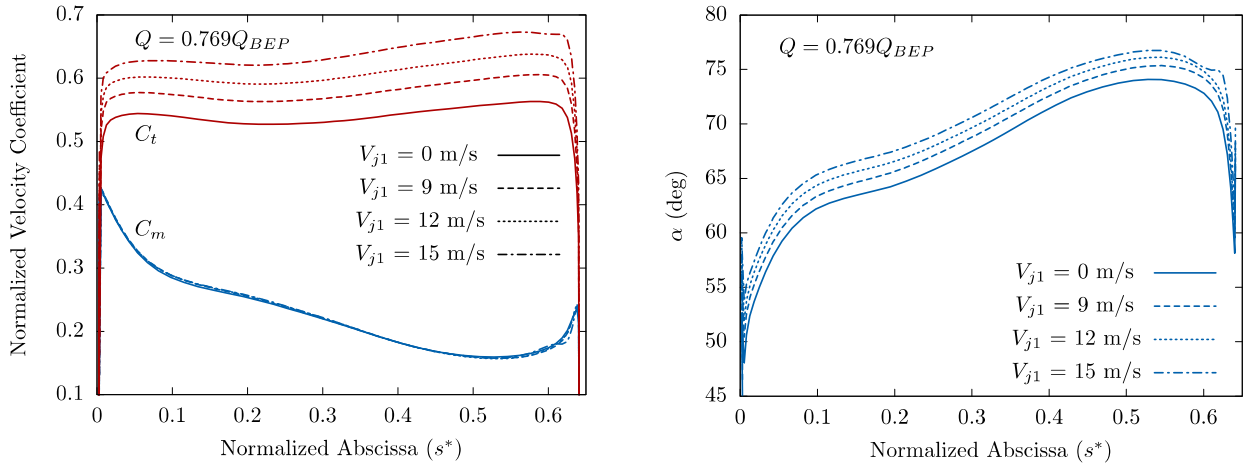

(a) Low Flow, $Q = 0.769\ Q_{BEP}$

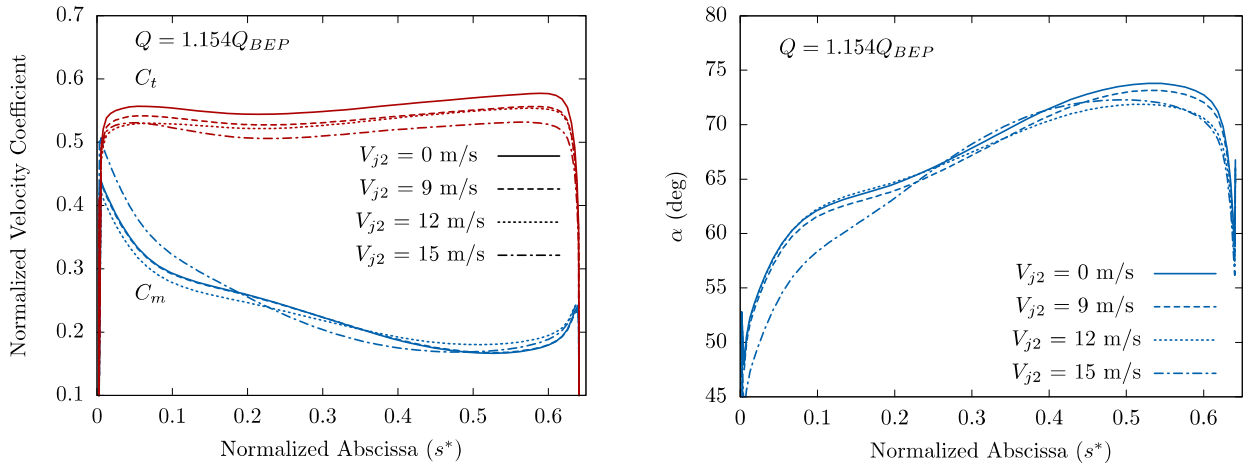

(b) High Flow, $Q = 1.154\ Q_{BEP}$

Figure 4. Circumferentially averaged velocity and flow angle profiles at the runner inlet. Profiles are

plotted with respect to a normalized abscissa s^*, where $s^* = 0$ is located at the band.

The results of the 3-D single distributor vane passage simulations are shown in Figure 4. The inlet volume flow rate to the domain was adjusted, corresponding to the jet flow rate, in order to achieve a consistent total flow rate through the turbine. The direction of swirl angle change was chosen based on the runner velocity triangles for the corresponding high and low head operating points.

For the low flow case, fluid was injected from the pressure side jet (Jet 1 in Figure 1). The addition of blowing resulted in an approximately uniform increase in tangential velocity, while the meridional velocity was unaffected. This resulted in a uniform increase in swirl angle over the span of the runner inlet. For the high flow case, fluid was injected from the suction side jet (Jet 2 in Figure 1). The addition of blowing resulted in a uniform decrease in tangential velocity; however, blowing altered the meridional velocity distribution, particularly for the higher jet speeds. It was concluded that this jet design is well suited for operating conditions that require an increase in swirl to improve the performance, as decreasing the swirl may cause additional changes in the flow distribution entering the runner, and significantly alter the operation of the turbine. Further analysis is required to fully understand the dynamic effect of blowing from the suction side jet, and the interaction with the runner flow distribution and performance.

As a coupled solution of the wicket gate and runner was not possible with blade passage simulations, the effect of blowing on the runner performance was analyzed for an isolated runner blade passage. The inlet velocity profile was obtained from experimental measurements, and modified to simulate a ±6° change in swirl angle caused by the wicket gate trailing-edge jets. For the unmodified inlet conditions, the simulations matched the measured head and torque to within approximately 1% for the BEP case, 5% for low flow case, and 4% for the high flow case. This was a significant improvement over previous computational studies [Nilsson and Davidson 2001, 2002, and 2003]. With the change in inlet swirl, the turbine efficiency improved by approximately 4% for the low flow condition, as a result of a 3° increase in swirl angle, and by approximately 2% for the high flow condition, as a result of a 3° decrease in swirl angle (see Figure 5). The 3-D single distributor vane passage simulations predicted that these amounts of swirl angle change could be achieved with a jet speed of $V_{j1} = 12$ m/s for the low flow case and $V_{j2} = 15$ m/s for the high flow case.

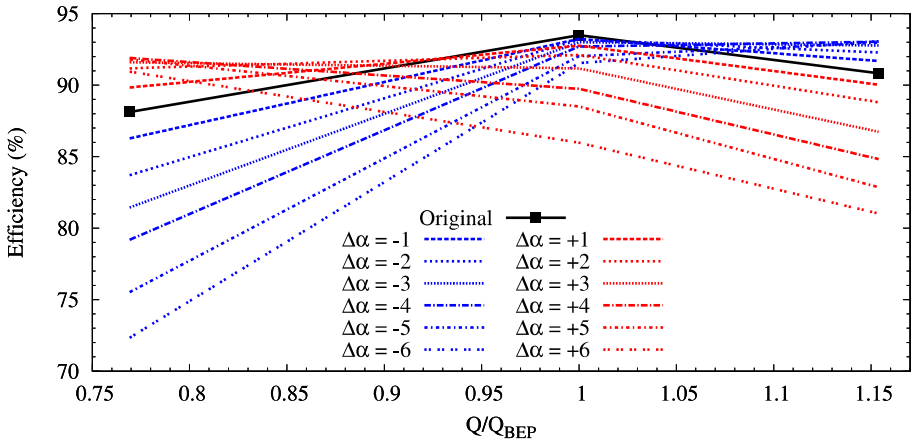

Figure 5. Change in runner efficiency as a result of modifying the inlet swirl angle of the extrapolated experimental velocity profile.

Unsteady simulations of the complete turbine, including the dynamic rotation of the runner, were necessary to understand the detailed effects of blowing on the rotor-stator interactions, the unsteady load changes on the runner blades and wicket gates, and the draft tube performance. The results of the full-wheel simulations were within approximately 3% of the measured torque and head values for both the low flow and BEP operating conditions. As the high flow condition required a decrease in swirl angle to improve the turbine efficiency, full-wheel simulations was not performed at this flow rate.

Blowing was introduced at the low flow condition, and a 22% increase in head and a 26% increase in torque, and 2.7% increase in runner efficiency were observed. The change in head was evaluated only across the runner wheel, as the addition of mass through the wicket gate jets would skew the results if calculated from the normal measurement locations. Although a significant improvement in efficiency, the single blade passage simulations predicted an increase in efficiency of approximately 4%. Furthermore, a 15 m/s jet, or 2.98% of the inlet volume flow rate, was required to achieve the desired amount of swirl angle change, while the 3-D distributor passage simulations predicted that only a 12 m/s jet, or 2.39% of the inlet volume flow rate, would be needed. The downstream presence of the runner, which was not modeled in the single distributor vane simulations, was clearly affecting the overall turning behavior of the wicket gate trailing-edge blowing.

Contours of the velocity distribution were analyzed at several axial locations through the turbine. Due to the high curvature of the runner blades, changes in local flow velocity, blade speed, and blade angle produced a significant variation in the velocity triangle at the runner leading edge along the span of the blade. Near the lower distributor wall, the runner blades and wicket gates are in close proximity, and the wakes from the wicket gates were distorted due to the interaction with the passing runner blades. Near the crown, only minor wake distortion was observed, as the leading edge of the runner blades is located at a larger distance from the wicket gates.

With the addition of blowing, the inlet swirl was increased, which significantly improved the flow distribution in the runner passage at the low flow condition (see Figure 6). For the upper span of the runner, near the crown, the present change in swirl was sufficient to properly align the inlet velocity triangle; however, for the lower portion of the runner, near the band, an additional increase in swirl would further improve the flow in this region.

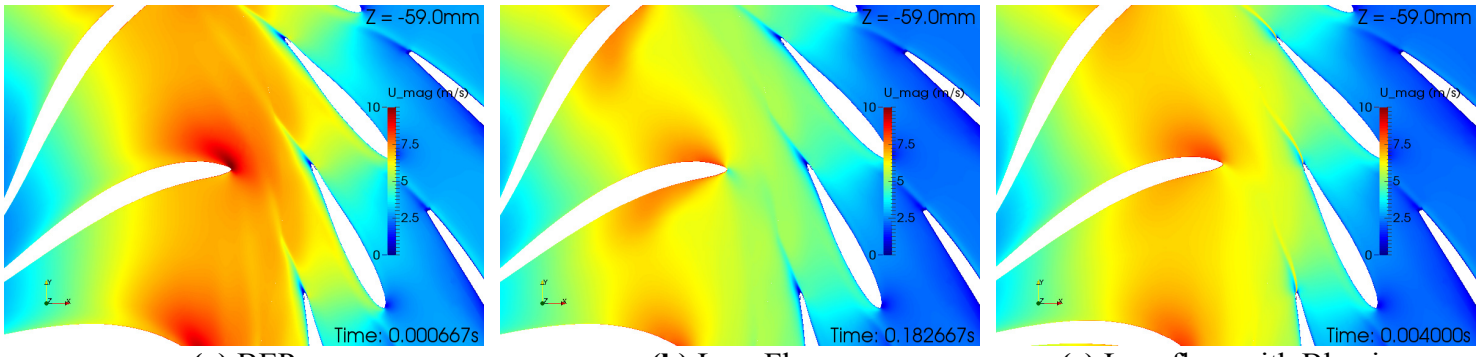

(a) BEP **(b)** Low Flow **(c)** Low flow with Blowing

Figure 6. Instantaneous contours of velocity magnitude in the distributor and runner region for the BEP, low flow, and low flow with blowing cases, showing the changes in flow behavior near the runner for the three operation conditions. Contours were taken at constant values of *Z*.

The dynamic behavior of the forces on individual runner blades and wicket gates were also studied to evaluate the effect of blowing on the unsteady blade force oscillations. Dominant oscillations were clearly observed at the runner passing frequency and the wicket gate passing frequency, respectively. Blowing at the low flow rate resulted in a minor increase in amplitude of force oscillations; however, the amplitudes remained below the values observed at the BEP flow rate.

Many other aspects of the unsteady turbine performance were studied from the full-wheel simulations, including the global pressure oscillations resulting from flow variations in the draft tube, the behavior of surface-streamlines as a result of the changes in flow rate and swirl angle, and the performance and pressure recovery achieved in the draft tube, as observed by the unsteady pressure distribution along the draft tube. Each of these analyses provided interesting insight into the complex unsteady nature of the flow through Francis hydroturbines, as well as the affect of blowing from the wicket gate trailing-edge jets.

In conclusion, the addition of blowing from the trailing-edge of the wicket gates successfully increases the swirl angle at the inlet of the runner at the low flow case, and resulted in 2.7% improvement in runner efficiency. However, the relative velocity at the runner leading edge was still positioned at a negative angle of attack for the lower portion of the runner blade. Therefore, increased amounts of blowing should be used in future work. The feasibility of implementing this technology should also be considered, in particular, the design of the internal jet channels, and the coupling of the jets to the penstock, without disabling the pivoting function of the wicket gate.

References:

1. R. M. Donaldson (1956), Hydraulic turbine runner vibration, *J. Engineering for Power*, Vol. 78, pg. 1141-1147
2. E. Naudascher (1965), Flow in the wake of a self-propelled body and related sources of turbulence, *J. Fluid Mechanics*, Vol. 22, pg. 625-656
3. H. Nilsson and L. Davidson (2001), A Validation of parallel multiblock CFD against the GAMM Francis water turbine at best efficiency and off-design operating conditions, Department of Thermo and Fluid Dynamics, Chalmers University of Technology, Göteborg, Sweden, Aug. 2001
4. H. Nilsson and L. Davidson (2002), Validation and Investigation of the Computed Flow in the GAMM Francis Runner and the Hölleforsen Kaplan Runner, Proc. 21st IAHR Symposium on Hydraulic Machinery and Systems (Lausanne, Switzerland, Sep. 2002)
5. H. Nilsson and L. Davidson (2003), Validations of CFD against detailed velocity and pressure measurements in water turbine runner flow, *Int. J. Numerical Methods in Fluids*, Vol. 41
6. E. Parkinson (1995), Turbomachinery Workshop ERCOFTAC II, Test Case 8: Francis turbine
7. G. Sottas and I. L. Ryhming (1989), *3D-Computation of Incompressible Internal Flows. Proceedings of the GAMM Workshop held at EPFL, 13-15 September 1989, Lausanne, Switzerland*, Series: Notes on Numerical Fluid Mechanics, Vol. 39, Vieweg, Braunschweig/Wiesbaden

Publications Resulting from this Project:

1. Bryan John Lewis, “Improving Unsteady Hydroturbine Performance During Off-Design Operation Through Controlled Wicket Gate Trailing-Edge Blowing”, PhD Dissertation, Penn State University, 2014.

2. Lewis, B., Cimbala, J., Wouden, A., “Wicket Gate Trailing-Edge Blowing: A Method for Improving Off-Design Hydroturbine Performance by Adjusting the Runner Inlet Swirl Angle”, Penn State College of Engineering Research Symposium, April 2014
3. Lewis, B., Cimbala, J., Wouden, A., “Wicket Gate Trailing-Edge Blowing: A Method for Improving Off-Design Hydroturbine Performance by Adjusting the Runner Inlet Swirl Angle”, 27th IAHR Symposium on Hydraulic Machinery and Systems, Montreal, Canada, Sep. 2014 (under review)
4. Lewis, B., Cimbala. J., “Major Historical Developments in the Design of Hydroturbines”, IAHR Symposium on Hydraulic Machinery and Systems, Montreal, Canada, Sep. 2014 (under review)
5. Lewis, B., Cimbala, J., Wouden, A., "Modified Design of Hydroturbine Wicket Gates to Include Liquid Control Jets," APS 66th Annual DFD Meeting, Pittsburg, Pennsylvania, Nov. 2013
6. Lewis, B., Cimbala, J., Wouden, A., "Investigation of Distributor Vane Jets to Decrease the Unsteady Load on Hydroturbine Runner Blades", *Journal of Physics, IOP Conference Series*, Vol. 15, No. 022006, 2012 (presented at 26th IAHR Symposium on Hydraulic Machinery and Systems, Beijing, China, Aug. 2012)
7. Lewis, B., Cimbala, J., Wouden, A., "Analysis and Optimization of Guide Vane Jets to Decrease the Unsteady Load on Mixed Flow Hydroturbine Runner Blades", 7th International Conference on Computational Fluid Dynamics (ICCFD7), Big Island of Hawaii, July, 2012
8. Lewis, B., Cimbala, J., Wouden, A., "Caution: Precision Error in Blade Alignment Results in Faulty Unsteady CFD Result”, APS 65th Annual DFD Meeting, San Diego, California, Nov. 2012
9. Lewis, B., Cimbala, J., Wouden, A., “Applying Turbulence Models to Hydroturbine Flows: A Sensitivity Analysis Using the GAMM Francis Turbine”, APS 64th Annual DFD Meeting, Baltimore, Maryland, Nov. 2011
10. Lewis, B., Wouden, A., Cimbala, J., Paterson, E., “OpenFOAM Validation of the GAMM Francis Runner using SimpleSRFFoam and MRFSimpleFoam : Additions to the Turbomachinery SIG ”, 6th OpenFOAM Workshop, State College, Pennsylvania, June 2011

Keith Martin, MS 2014. Advisor: John Cimbala

Effects of Pre-whirl on Efficiency and Operating Range of a Reversible Francis Pump-turbine in Pumping Mode

Since the introduction of reversible pump-turbines in 1928, Francis pump-turbines have become the most common machine used for hydro pumped storage in the United States. Pumped storage provides generation and ancillary services to electrical grids because of its high power density and flexible generation characteristics. Operating pump-turbines over a wide range of flows is desirable because it allows for greater grid stabilization and has recently become more important because of increased penetration of intermittent generation sources such as wind and solar.

Traditional Francis pump-turbines are single-speed machines that operate on a performance curve determined by a one-to-one correlation between head and capacity. Advances in power electronics have made it possible to decouple the speed of large pumps from the grid frequency with variable speed motor/generators. Variable speed pumps operate over a range of flow rates and power described by a hill chart similar to the one used in turbine mode and can improve the capacity of a plant to store power [Anagnostopoulos, 2007]. Modifying flow characteristics is another approach to regulating power and achieving a larger operating envelope in pumping mode. Researchers have shown that it is possible to improve the performance of some compressors and centrifugal pumps by controlling pre-whirl at off design conditions [Tan, 2010; Tan, 2012; Xiao, 2007; Zhou, 2012]. For example, positive pre-whirl induced by three dimensional guide vanes at part load operation in a centrifugal pump was shown to reduce reverse flow and improve efficiency by up to two percent [Tan, 2010].

Despite the application of flow straighteners and inlet guide vanes in compressors and some industrial centrifugal pumps, pre-whirl control has not been applied to pump-turbines. The current research investigates the effects of pre-whirl on the operating range and performance of a single speed pump-turbine with fixed impeller and flow passage dimensions in pumping mode. Typical power losses through a centrifugal pump impeller are outlined in Figure 1 (left). Pre-whirl is used to address part load recirculation and other hydraulic losses. Part load recirculation can occur at the inlet and outlet of the pump impeller at low flow conditions, often appearing around 60% of the BEP flow, due to local flow separation and pressure differential normal to the mean through-flow. Severely recirculating flow at 40% of BEP flow is shown in Figure 1 (right). Flow enters the draft tube diffuser cone along the band and generates a positive pre-whirl that decreases from the wall to the axis of rotation. This naturally induces positive pre-whirl improves the incidence angle at low flow but causes instability and non-uniform flow. Hydraulic losses include viscous losses due to shearing of non-uniform flows and poor incidence angles on the leading edge of the impeller blade. The goal of the research is to investigate whether pre-whirl can be used to improve off-design operation of a synchronous pump by a) increasing efficiency by reducing internal losses, b) providing variable power storage by controlling torque, and c) expanding the operating range by delaying cavitation and suppressing the onset of recirculation at low flow operation.

CFD analysis of an existing pump was used to predict performance and stage losses. The pump has nine impeller blades and fixed distributor vanes in the spiral case. After an initial analysis of steady-state flow through a single periodic blade passage, the computational domain was expanded to include the draft tube, complete pump impeller, and spiral case. Unsteady full-wheel simulations were carried out in ANSYS-FLUENT using a k-ω SST turbulence model on a fully structured grid of approximately 11

million cells shown in Figure 2. Figure 3 shows normalized head and efficiency from steady state analysis using multiple reference frames, transient full-wheel CFD simulations, and experimental results provided by the manufacturer. As expected, steady state simulations did a poor job modeling the rotor-stator interaction and flow in the spiral case and over predicted losses. Transient simulations predicted efficiencies within 2% of the experimental values.

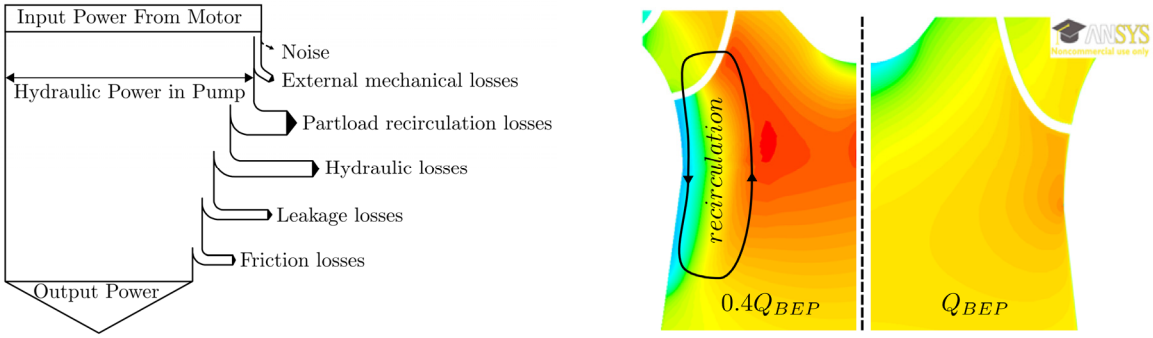

Figure 1. Typical sources of mechanical and hydraulic losses through a centrifugal pump impeller [Gülich, 2008] (left) and velocity magnitudes in the draft tube diffuser cone at BEP and 40% of BEP flow. Reverse flow is present in the blue areas along the outer wall (right).

Pre-whirl was introduced by adding blowing through slits in the draft tube diffuser wall at the pump inlet. Positive swirl angles indicate swirling flows aligned with impeller rotation, and negative swirl angles indicate swirling flows in the opposite direction as impeller rotation. Peripheral jets were chosen to allow for active control and a means of influencing angular momentum and axial flow near the diffuser wall where reverse flow occurs. Blowing is parameterized by a circumferential and meridional blowing angle and flow rate through one of the the jets as shown in Figure 2. An orthogonal test matrix was constructed reduce the number of required simulations to test three levels of peripheral swirl, axial flow, and flow intensity.

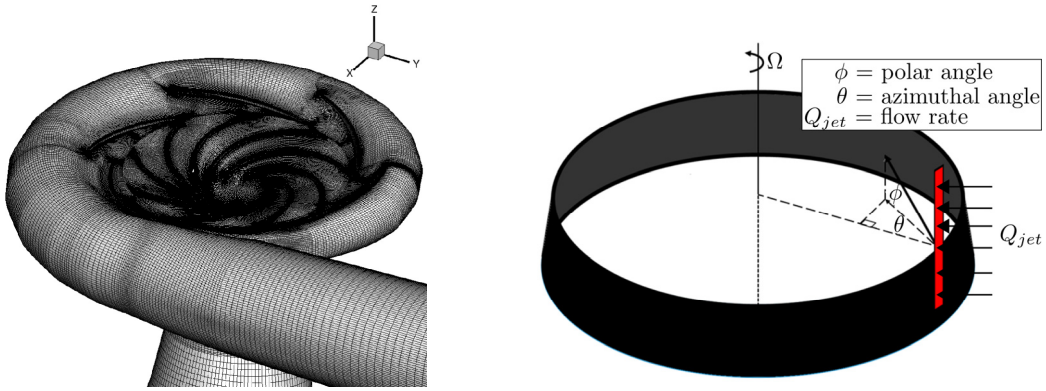

Figure 2. Computational domain of complete draft tube, impeller, and spiral case and is meshed with approximately 11 million fully structured cells (left) and blowing parameters shown at one of eight slits in the draft tube wall (right).

Taguchi level averaging showed that the magnitude of flow through the jets had the greatest effect on pump efficiency. This result was expected because of the power needed to inject water. Swirl angle was

also a significant indicator of pump efficiency. The Euler turbomachinery equations are consistent with the normalized head and efficiency for one combination of parameters that generate positive pre-whirl are shown in red in Figure 3. Parasitic losses from the jets at off-design conditions can be offset by enforcing uniform velocity distribution along the leading edge of blades to correct incidence angles. Minimal changes of less than one percent in efficiency were observed with pre-swirl conditions. Transient flow in the impeller passage at low flow and the rotor-stator interaction are being examined more closely. Future work could include testing pre-swirl generated by guide vanes in a small draft tube test stand. Ideally, researchers with proper facilities could validate CFD results with a complete test loop

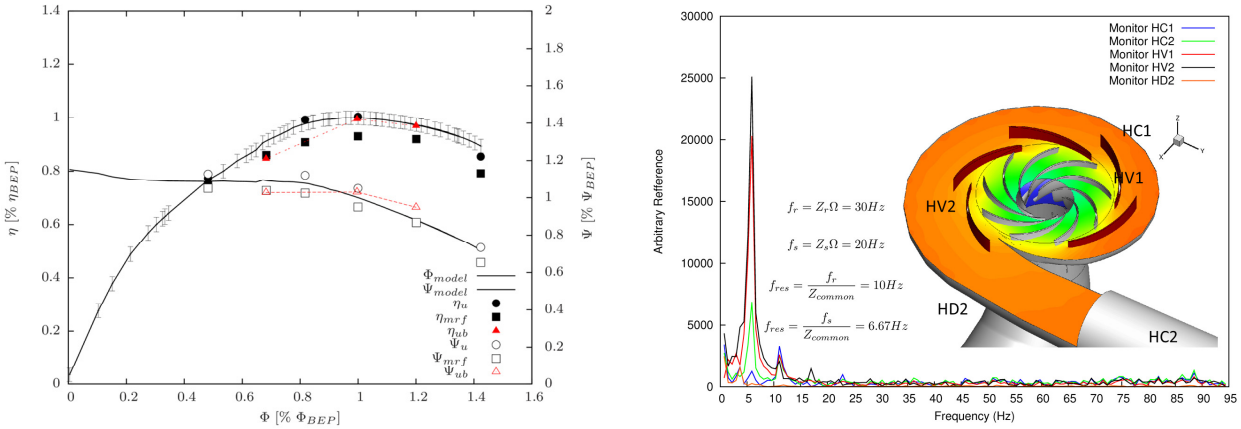

Figure 3. Normalized head and efficiency curves predicted by full-wheel steady state (mrf), and unsteady (u) CFD simulations compared to experimental data (left) and pressure pulsations on spiral case and guide vane walls (right).

.

References:

1. Gülich, J. F. (2008). *Centrifugal pumps*. Berlin: Springer.
2. Anagnostopoulos, J. S., & Papantonis, D. E. (2007). Pumping station design for a pumped-storage wind-hydro power plant. *Energy Conversion and Management*, *48*(11), 3009-3017.
3. Tan, L., Cao, S., & Gui, S. (2010). Hydraulic design and pre-whirl regulation law of inlet guide vane for centrifugal pump. Science China Technological Sciences, 53(8), 2142-2151.
4. Tan, L., Cao, S., Wang, Y., & Zhu, B. (2012). Influence of axial distance on pre-whirl regulation by the inlet guide vanes for a centrifugal pump. Science China Technological Sciences, 55(4), 1037-1043.
5. Xiao, J., Gu, C., Shu, X., & Gao, C. (2007). Performance analysis of a centrifugal compressor with variable inlet guide vanes. Frontiers of Energy and Power Engineering in China, 1(4), 473-476.
6. Zhou, C. M., Wang, H. M., Huang, X., & Lin, H. (2012, November). Influence of the positive prewhirl on the performance of centrifugal pumps with different airfoils. In IOP Conference Series: Earth and Environmental Science (Vol. 15, No. 3, p. 032020). IOP Publishing.

Tyler Quinzán-Singer, B.S. 2012. Advisor: H. Perez-Blanco

DYNAMIC MODEL OF A PUMPED STORAGE HYDRO PLANT FOR SIMULATING RAMP RATES AND FINANCIAL VIABILITY

Abridged by: H. Perez-Blanco

The purpose of this report is to show how to model a Pumped Hydro Storage (PHS) plant that can be used to mitigate the variability of wind caused by increased penetration into the energy market. This is a continuation of Scott Richard's work in this field. The purpose of this continuation is to enhance research on how the specific characteristics of a pumped storage plant affect its ability to handle fast changes in power demand. This report seeks to yield insight into how to best manage a power plant to both enhance profitability and increase grid stability.

The plant model is created within a dynamic modeling platform called VisSim. The physics of the penstock, the pump-turbine, and the motor-generator responding to changes in power demand are simulated. The power plant has a maximum head of 600m with a Francis type pump-turbine with variable speed in pump mode. A schematic of the proposed plant is shown below. Table 1 shows the key variables adopted for simulation, largely based on the specifications of the Serbian power plant in Bajina Bašta, Serbia.

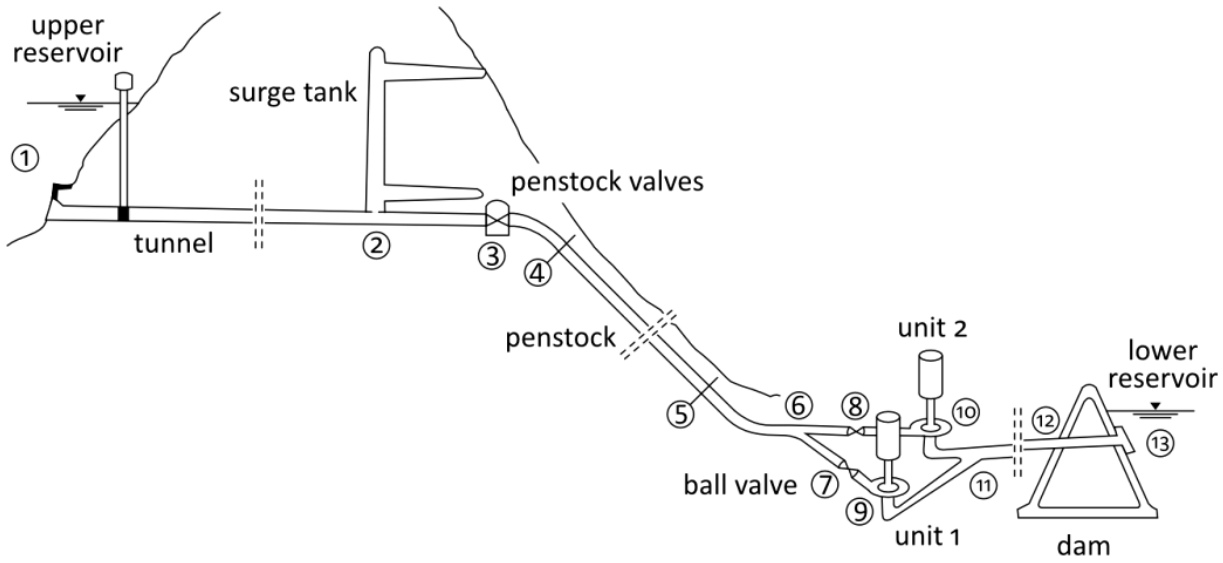

Figure 1: Pumped Storage Hydropower Plant Schematic

Table 1. Main Parameters used for Simulation [1]	
Turbine Ratings	
Net Head, m	Maximum: 600.3
	Design: 554.3
	Minimum: 497.5
Power, MW	At Maximum Head: 315
	At Design Head: 294
	At Minimum Head: 243

Rotational Speed, rpm	428.6
Maximum Flow Rate, m^3/s	63
Efficiency	89%
Runner Diameter, m	4.82
Moment of Inertia, $kg \cdot m^2$	$1.5x10^6$
Runner Material	Stainless Steel , 13% Cr, 3.5% Ni
Pump Ratings	
Pumping Head, m	Maximum: 621.3
	Minimum: 531.7
Pumping Discharge, m^3/s	At Maximum Head: 36.7
	At Minimum Head: 50.8
Maximum Pump Input (MW), at speed (rpm) MW	310, 428.6
Length of Penstock (estimated) , m	845

The dynamic performance f the plant depends on the combined response of the penstock and runner to variations in power demand. Once a turbine is synchronized with the grid, and within certain limits, the rotor of the generator/motor is locked to the grid frequency, and hence frequency and voltage variations are minute and absorbed by a linear control strategy labelled 'droop control'. The ideas behind this type of control seem simple enough: if the grid frequency drops due to increased load, the generator responds with increased power, and so do other generators connected in parallel to the load. If the voltage drops due to increased load, then the reactive power is increased via changing the generator excitation phase. Clearly, we are interested here in adjusting the active power response. The worst possible case would be a nearly isolated plant balancing wind/solar load variations, and this is the scenario assumed by default. The same assumption is employed for generation and pumping.
The penstock diameter and area follow the guidelines in [2,3]. Details can be found in [4].

$$D_{pen} = \frac{D_{pen} \times h_o}{h_o} = \frac{2400m^2}{840m} \approx 4\,m \qquad (1.1)$$

The area of the penstock is then calculated as

$$A_{pen} = \pi \cdot \left(\frac{D}{2}\right)^2 \qquad (1.2)$$

Whenever the head in the turbine is changed through the adjustment of the wicket gates the flow rate changes according to the following equation Eq 1.3, [5]. The flow continues to change until the total available head is equal to the sum of the head losses in the penstock and the net head through the turbine:

$$\frac{dQ}{dt} = (h_o - h_l - h_t) \cdot \frac{gA_{pen}}{L_{pen}} \qquad (1.3)$$

The total head losses in the penstock are calculated using the following equation

$$h_l = f_{pen} \cdot \frac{L_{pen} \cdot V_{pen}^2}{2gD_{pen}} \qquad (1.4)$$

The velocity in the penstock is a function of area of the penstock and the volume flow rate

$$V_{pen} = \frac{Q}{A_{pen}} \qquad (1.5)$$

The Reynolds number in the penstock is given by

$$Re_{pen} = \frac{\rho_{water} V_{pen} D_{pen}}{\mu_{water}} \quad (1.6)$$

And the Darcy friction factor of the flow in the penstock is calculated by

$$f_{pen} = \frac{1}{3.24 \cdot \left[\log\left[\frac{6.9}{Re_{pen}} + \left(\frac{\epsilon_{steel}}{3.7 \cdot D_{pen}}\right)^{1.11}\right]\right]^2} \quad (1.7)$$

The turbine head at a given wicket gate angle and flow is calculated using a Hill chart [6]. The chart below (Fig 2) is an example of a generic chart for a Francis turbine and the flow coefficient is decreased by a factor of 0.225 to better match the operating parameters of the chosen plant.

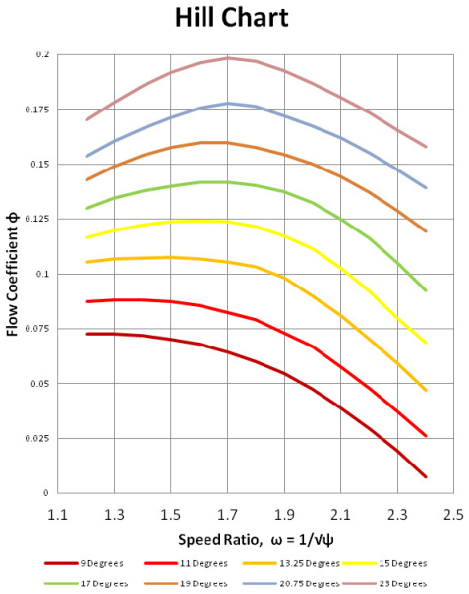

Figure 2: Flow Coefficient vs. Speed Ratio at Various Wicket Gate Angles

The head in the turbine is calculated using the speed ratio and the flow coefficient.

$$\omega_{11} = \frac{1}{\sqrt{\psi}} = \sqrt{\frac{\omega^2 D_t^2}{2gh_t}} \quad (2.1)$$

$$\varphi = \frac{Q}{D_t^2 \sqrt{2gh_t}} \quad (2.2)$$

Using the hill chart above each wicket gate angle has a given relationship between φ and ω found in Excel using a second order best fit polynomial equation. Table 2 contains all the coefficients.

$$\varphi = f(\omega_{11}) = a\omega_{11}^2 + b\omega_{11} + c \quad (2.3)$$

$$k_I \int de + k_P e + k_D \frac{de}{dt} \quad (3.7)$$

Table 2: Third Order Polynomial Coefficients for Francis Hill Chart

angle	a	b	c
9	-0.012528409	0.033095061	-0.00551427
11	-0.013778721	0.03827304	-0.006612662
13.25	-0.016535027	0.048915865	-0.0115943
15	-0.018201174	0.05682711	-0.01610537
17	-0.018288274	0.059331949	-0.015992757
19	-0.016807568	0.055883616	-0.010641028
20.75	-0.01841471	0.063227023	-0.014788074

The turbine head is evaluated at each given wicket gate angle. Interpolation is then used to find the turbine head at any wicket gate angle between 9 and 20.75 degrees.

The Euler equation yields the torque ensuing form the flow angular momentum change,

$$T_{flow} = mfr \cdot (V_\theta - V_{\theta_2}) \cdot r_t \quad (3.1)$$

The incoming swirl velocity is determined using the radial velocity as well as the vane angle

$$V_\theta = \frac{V_r}{\tan(\alpha)} = \frac{Q}{\pi \cdot z \cdot D_t \cdot \tan(\alpha)} \quad (3.2)$$

The energy lost in swirl $(V_\theta - V_{\theta_2})$ is a percentage of V_θ found from turbine efficiency which is calculated from a general Francis efficiency chart [7]

$$T_{flow} = Q \cdot \rho \cdot \eta_H \cdot (V_\theta \quad V_{\theta_2}) \cdot \frac{D_t}{2} \quad (3.3)$$

Which simplifies to

$$T_{flow} = \frac{Q^2 \cdot \rho \cdot \eta_H}{2\pi \cdot z \cdot \tan(\alpha)} \quad (3.4)$$

The torque from the generator is power demanded from the system divided by the rotational speed. The power demanded is a given function obtained from past regulation data from PJM's website.

$$T_{gen} = \frac{P_D}{\omega} \quad (3.5)$$

The angular acceleration is the difference between the two opposing torques divided by moment of inertia of the Francis pump-turbine and the motor/generator.

$$\frac{d\omega}{dt} = \frac{T_{flow} - T_{gen}}{I} \quad (3.6)$$

A PID controller is used to adjust the wicket gate angle. The Zeigler-Nichols method of tuning was used to determine the constants of each controller component,

The ideal head is calculated using Euler's equation, multiplying the ideal tangential exit velocity by the tip speed of the impeller.

$$H_t = \frac{-E_t}{g} = \frac{V_{\theta_{2i}} U_2}{g} \quad (4.1)$$

The tip speed is calculated by the product of the rotational speed and the radius of the pump-turbine

$$U_2 = \omega r_2 \quad (4.2)$$

And the ideal tangential exit velocity is found geometrically according to Figure 3, namely

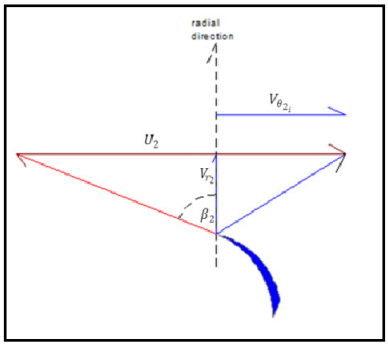

Figure 3: Schematic of Pump Exit Velocities

$$V_{\theta_{2i}} = U_2 - V_{r_2}\tan(\beta_2) \quad (4.3)$$

V_{r_2} is the radial direction of the exit velocity, which can be calculated using the exit area and mass flow rate.

$$V_{r_2} = \frac{Q}{2\pi r_2 z} \quad (4.4)$$

Combining equations 4.1, 4.2, 4.3, and 4.4 the ideal head of the pump is found as follows

$$H_t = \frac{\omega r_2\left[\omega r_2 - \frac{Q}{2\pi r_2 z}\tan(\beta_2)\right]}{g} \quad (4.5)$$

To correct the pump output, the slip coefficient is calculated using the following correlations with U_2, $V_{\theta_{2i}}$, β_2, and nB.

$$\eta_{slip} = 1 - \frac{\pi\omega r_2\cos(\beta_2)}{\left[\omega r_2 - \frac{Q}{2\pi r_2 z}\tan(\beta_2)\right]nB} \quad (4.6)$$

The Impeller head is the product of the ideal pump head and the slip coefficient

$$H_{imp} = H_t\eta_{slip} \quad (4.7)$$

The volumetric efficiency is used to take into account the loss of flow from leakage between the impeller and the casing. Equation (6.1) is used to calculate a volumetric efficiency for the pump,

$$\eta_v = 1 - 2\frac{C}{Q^n} \quad (5.1)$$

The coefficients C and n correlate with the design flow, and can be found in [4]. The head efficiency is used to take into account the losses in the rotor and the diffuser and is calculated using equation (5.2), with the flow rate in gpm,

$$\eta_H = 1 - 2.2\frac{0.8}{Q^{\frac{1}{4}}} \quad (5.2)$$

The overall hydraulic efficiency is the product of the volumetric efficiency and of the head efficiency. The mechanical and electrical efficiencies are incorporated by formulating an additional efficiency, so that the range from 93% to about 85% corresponds from minimum to maximum head respectively. Equation (5.3) hence is an additional efficiency, and it is a linear relationship to meet the efficiency range specified in the previous sentence,

$$\eta_{dif} = \eta_{dif_{max}} - \frac{(531.7 - H_{pump})}{(531.7 - 621.3)}\left(\eta_{dif_{max}} - \eta_{dif_{min}}\right) \tag{5.3}$$

The overall efficiency is the product of the volumetric, hydraulic, and additional efficiencies.

$$\eta_o = \eta_v \eta_h \eta_{dif} \tag{5.4}$$

The head produced by the impeller multiplied by the overall efficiency gives the actual head.

$$H_{pump} = H_{imp}\eta_o \tag{5.5}$$

The head in Eq 5.5 depends on the flow, since the efficiencies depend largely on the flow. The flow is evaluated solving for the flow that equates the required head and the available head.

Because this is a variable speed pump the rotor is allowed to accelerate according to the following equation.

$$\dot{\omega} = \frac{T_{motor} - T_{impeller}}{I} \tag{6.1}$$

Where the motor torque is given by,

$$T_{motor} = \frac{P_{input}}{\omega} \tag{6.2}$$

And the impeller torque is govenrned by the required azimuthal flow velocity, namely

$$T_{impeller} = Q \cdot \rho \cdot V_{\theta_{R_i}} \cdot \eta_{slip} \cdot r_i \tag{6.3}$$

In order to determine the financial benefits of regulation in combination with arbitrage, a financial analysis was completed. This was accomplished by using data from one example day of regulation according to the PJM website along with hourly prices from one day of each season. The models for both the pump and turbine were run at each hour for one day. These computations resulted in a predicted amount of water discharged as well as MWhr produced or used for each hour. The turbine was run at a set point of 240 MW with 60 MW of regulation while the pump was set at 241 MW with 44 MW of regulation. Once all the data was compiled pumping and generating hours were assigned for each day, balancing the water volume discharge to calculate the maximum revenue under no volume change at day's end. These calculations were completed according to the following equations.

The total revenue is the sum of three classes of revenue when regulating. The first type is labeled as "Actual Energy Revenue" , or AER. This represents the total profit from buying and selling energy at low and high prices respectively. The next is the Lost Opportunity Cost (LOC). This represents the amount of money that PJM compensates a participant in the regulation market because it is not running at full capacity. Finally the regulation revenue (RR) is the amount of money that the plant is paid for being available to quickly change its energy output for the purpose of regulating the frequency.

$$Total\ Revenue = AER + LOC + RR \tag{7.1}$$

The AER depends on hourly energy price, denominated the Locational Marginal Price, or LMP. In this model there are example prices for one day in each of the four seasons

$$AER = \frac{\int Power\ (MW)}{3600} * LMP\left(\frac{\$}{MWhour}\right) \tag{7.2}$$

The integral $\frac{\int Power(MW)}{3600}$ represents the value for MWhours produced or used, determined in the model using regulation data from one example day in March.
The LOC is determined via Eq 7.3, namely, [8]

$$LOC = Foregone\ Energy\ (MW) * (LMP - ED)\left(\frac{\$}{MWhour}\right) * 1\ hour \quad (7.$$

$Foregone\ Energy\ (MW)$ is the number of MW used for regulation, and ED is the average on-peak/off peak LMP excluding the hours in which the pump-turbine is running.
The Regulation Revenue is calculated via Eq 7.4, namely,

$$RR = Foregone\ Energy\ (MW) * RMCP\left(\frac{\$}{MWhour}\right) * 1\ hour \quad (7.4)$$

Where $RMCP$ is the regulation market clearing price. This is the amount of money a plant gets paid per MW it makes available to provide regulation.
The PJM power demand curve scaled for this plant, in red in Fig 4, is closely followed by the blue trace, which is the output calculated by the model. The power adjustments are obtained by continually adjusting the position of the wicket gates.

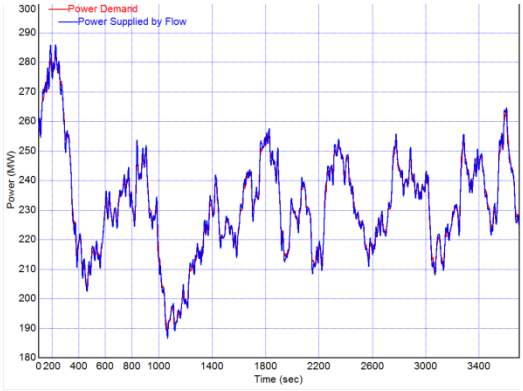

Figure 4: Power vs. Time for Hour 1

Whereas the turbine speed is projected to stay constant while in synchronicity with the grid, an isolated system may have to respond to power demand changes with small changes in rotational frequency. The model projections show that the speed stays well within 2% of design.

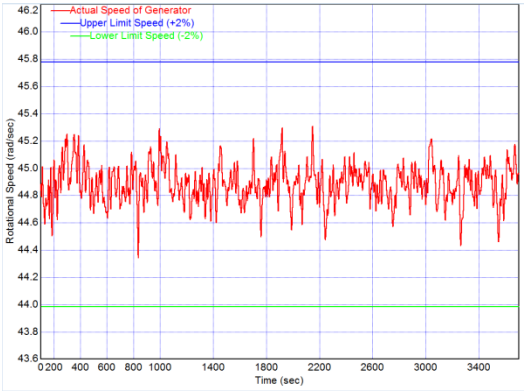

Figure 5: Runner Speed vs. Time for Hour 1

The required flow rate and wicket angles to produce the output of Fig 1 are shown in Figs 6 and 7 respectively.

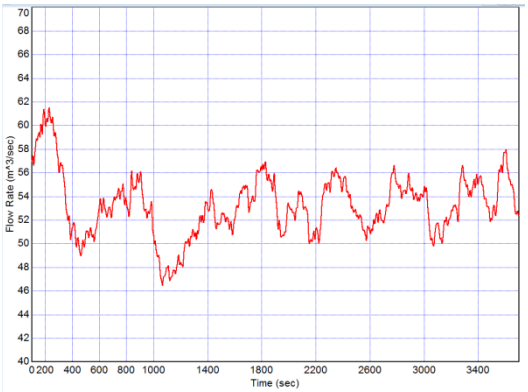

Figure 6: Volumetric Flow Rate vs. Time for Hour 1

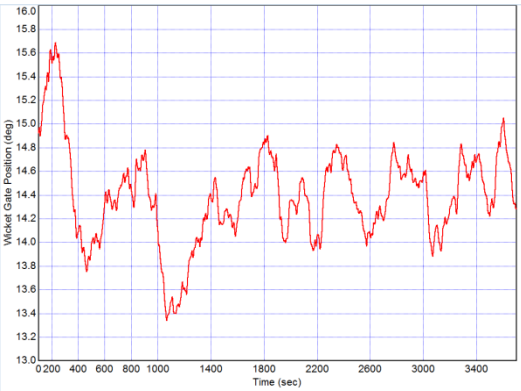

Figure 7: Wicket Gate Angle vs. Time for Hour 1

Sudden variations in the supply of wind and solar call for meeting steep ramp rates. The capabilities of the simulated plant to meet such ramps are illustrated in Fig 8. This power demand curve shows the maximum power demand ramp rate that this plant can regulate while maintaining within 2% of design speed

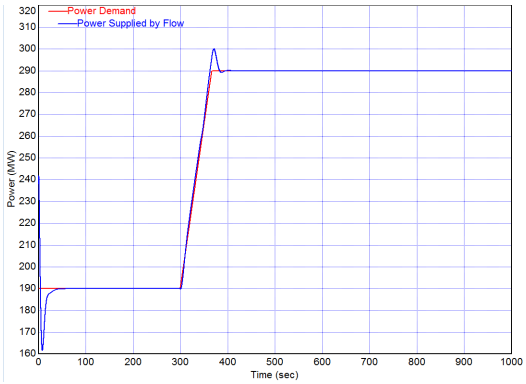

Figure 8: Power Ramp Rate from 190MW to 290 MW at 90MW/min

In the pumping mode with variable speed, the pump easily adjusts to power variations, Fig 10. The adjustments cover the range from 70% to a 100% of full power. Simultaneously, the pump speed changes from 90 to 100 % of design, Fig 11.

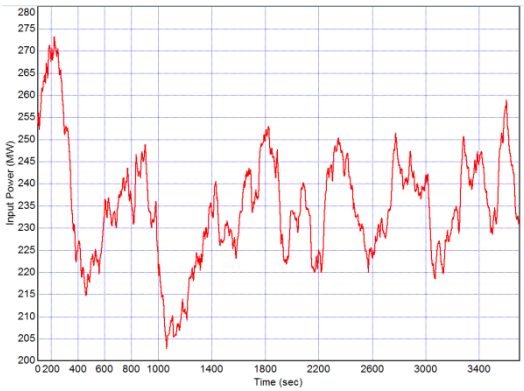

Figure 10: Pump Input Power vs. Time for Hour 1

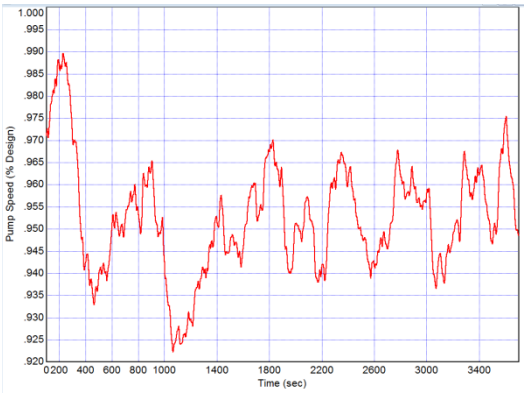

Figure 11: % Pump Speed vs. Time for Hour 1

The gross revenue was computed for a month of each of the four seasons, assuming the plant offered regulation within the limits deemed feasible from our model, and also assuming that the plant operated according to constant capacity during both pumping and generating, namely in arbitrage mode. In either case, the operating hours were chosen so as to maximize the revenue while returning the upper reservoir to its original level. In all cases, for the plant to realize positive revenue, initial (single) pumping and generating hours are chosen at the maximum price differential, and each period is expanded both forward and backward in time until the revenue ceases to increase or the water supply cannot meet the constraints of the model. Figure 13 summarizing our findings is discussed below.

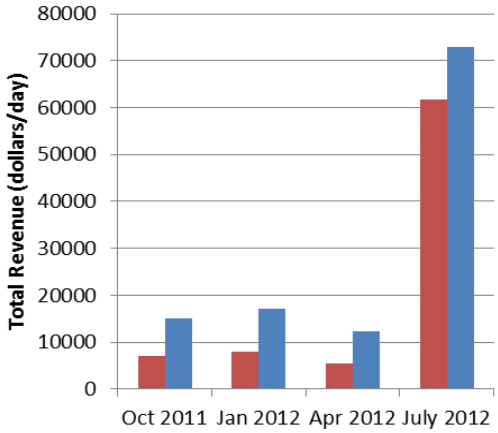

- **No regulation**
- **Regulation**

Figure 13: Total Revenue for One Day

Figure 13 shows the gross revenue for a month in each season. For both cases studied, it is clear that summer operation is much more attractive for pumped storage. This is the case, because peak loads take place in the summer due to the use of air conditioning, and hence the price differential between day and night also increases, and so do the cost effective pumping hours. In Fall, Winter and Spring, offering regulation nearly doubles the revenue. Clearly, the capability of storing energy while simultaneously regulating has a value in PJM. If a preferential rate for storing renewable energy were enacted, the revenue would increase. In the summer months, the additional revenue for offering regulation tends to be small, with regulation increasing the approximately $60,000 to $70,000. If the balancing/storing renewables carried a higher value, the difference in revenue would increase. In all seasons, regulation results in enhanced revenue.

A dynamic model of a large PHS plant using Francis pump/turbine runners was implemented. The model incorporates a variable speed motor/generator, as to allow regulation during pumping. This feature would allow the pumping of renewable (variable) resources during the low-price hours.

Our results show that a 300 MW plant in relative isolation could easily balance up to 60 MW of uncertainty in renewable supply while generating, and about 40 MW during pumping. The plant can meet steep ramps of 90 MW/min to firm up renewable supplies in case of drastic variations. While flexible, this type of plant cannot easily switch from pumping to generating, and hence it is confined to provide regulation only when operating during arbitrage.

Revenue considerations highlight how hard the PHS business can be. The revenues are considerable only during summer months. Whereas regulation does boost revenues, tariffs reflecting the ability to store renewable kW-hrs would go a long way towards increasing revenues. The rationale for such preferential tariff could be that the energy stored carries lesser penalties in terms of environmental effects than other types do.

References

[1] Krasil'nikov, M. F. "Experience in the Start-Up and Full-Scale Tests of the Equipment of the Bajina Basta Pumped-Storage Station in Yugoslavia." *Power Technology and Engineering*. 23.1 (1989): 59-63. Web. <http://www.springerlink.com/content/q430165552vm2335/>.

[2] Horikawa, Kohsuke, and Nozumo Watanabe. "Application of Extra-High Tensile Strength Steel for Hydropower Plants in Japan."1. Web. 29 Jun. 2012. http://www-it.jwes.or.jp/proceedings/en/3-03.pdf

[3] Pejovic, Stanislav, Qin Fen Zhang, Bryan Karney, and Aleksandar Gajic. "Analysis of Pump-Turbine "S" Instability and Reverse Waterhammer Incidents in Hydropower Systems." Belgrade: 2011. Web. 29 Jun. 2012. <http://info.ornl.gov/sites/publications/files/Pub31381.pdf>.

[4] Quinzan-Singer, T. 2012. Analysis And Model Of A Pumped Storage Hydro Plant For Simulating Ramp Rates And Financial Viability. Report to PSU Advisor, H. Perez-Blanco.

[5] Hannett, Louis. "Feild Tests to Validate Hydro Turbine-Governor Model Structure and Parameters." *IEEE Transactions on Power Systems*. 9.4 (1994): 1744-1751. Print.

[6] Roger, Arndt. *Hydraulic Turbines*. Taylor and Francis Group, 2007. 1-19. eBook.

[7] Smith, Cameron, Geargios Kokogiannakis, Sabri Serif'Ilias Tsagas, and Stravridis Konstantinos. "Transmission of Renewable Energy." *The University of Strathclyde in Glasgow*. N.p., 2002. Web. 2 Jul 2012. <http://www.esru.strath.ac.uk/EandE/Web_sites/01-02/RE_transmission/TECHNICAL ISSUES(under construction).htm>.

[8] "Regulation Hydro Lost Opportunity Cost Calculation Examples." Web. 4 Sept 2012. <http://www.pjm.com/markets-and-operations/ancillary-services/~/media/markets-ops/ancillary/20090915-regulation-hydro-lost-opportunity-cost-calc-examples.ashx>.

Girish Kumar Rajan, PhD 2014. Advisor: John M. Cimbala
Stability Analysis and CFD Modeling of the Vortex Rope in Draft Tubes

Introduction: Prior studies (Nishi & Liu (2013)) on draft tube surge have shown that turbines operating away from the best efficiency point (BEP) are laden with undesirable effects in the form of violent pressure fluctuations caused by a helical vortex formed in the draft tube. This helical vortex, called the vortex rope, is described as a 'precessing' fluid structure with high vorticity. The vortex rope manifests itself by means of low frequency, high amplitude pressure fluctuations that are nearly periodic in nature due to the precession of the vortex rope. These fluctuations are extremely intense and induce severe vibrations and noise in the draft tube, thereupon disrupting the functioning of the turbine and reducing its efficiency, and increasing maintenance. Therefore, it is worthwhile to study and analyze the vortex rope extensively, with the notion of mitigating it and minimizing its harmful effects on the turbine.

Susan-Resiga *et al*. (2006) and Susan-Resiga *et al*. (2010) conducted a parametric experimental investigation of the effects of the discharge coefficient and the energy coefficient on the draft tube inlet velocity profiles. Based on their experimental measurements, they also modeled the inlet velocity field as the superposition of two Batchelor's vortices on a base flow in the form of a solid body rotation. The velocity field may be described as a sum of three components:

$$U_\theta = \Omega_0 R + \Omega_1 \frac{R_1^2}{R}\left[1 - \exp\left(\frac{R^2}{R_1^2}\right)\right] + \Omega_2 \frac{R_2^2}{R}\left[1 - \exp\left(\frac{R^2}{R_2^2}\right)\right], \quad (1A)$$

$$U_z = U_0 R + U_1 \exp\left(\frac{R^2}{R_1^2}\right) + U_2 \exp\left(\frac{R^2}{R_2^2}\right), \quad (1B)$$

where R is the radial coordinate, U_θ and U_z are the circumferential and axial velocities respectively, and Ω_i, U_i and R_i are coefficients that are functions of φ. Under these conditions, the discharge coefficient at BEP is roughly 0.37. In this work, we analyze swirling flows in discharge cones of a Francis turbine operating at partial load, and consider flow rates for which $0.34 \leq \varphi \leq 0.37$. We use the FLINDT (Avellan (2000)) draft tube for our analysis. Several researchers (Susan-Resiga *et al*. (2010), Foroutan & Yavuzkurt (2012b)) have used the simplified FLINDT draft tube for their analyses. The simplified draft tube is typically a conical diffuser of angle 17° and a length-to-inlet diameter ratio of 1.685, followed by a discharge section of constant diameter.

The Present Work: We present our results in two sections: a numerical analysis of the swirling flow over a range of discharge coefficients, and a stability analysis that can provide a first estimate of the onset of instability. Results from the numerical analysis yield a qualitative picture of the stability of the swirling flow. In our study, we use the geometry and mesh from Foroutan & Yavuzkurt (2012a), shown in figure 1. Full three-dimensional, unsteady numerical simulations are performed in ANSYS-FLUENT® (ANSYS® (2011b)), using the DES model, for discharge coefficients varying between 0.34 and 0.37, and the results are post-processed in ANSYS-CFX® (ANSYS® (2011a)). The inlet conditions are taken from Susan-Resiga *et al*. (2010). In our stability analysis, we use an axisymmetric

model as suggested by Susan-Resiga *et al*. (2009), and follow Susan-Resiga *et al*. (2006) to formulate a Sturm-Luioville system that can determine the stable and unstable regions in the flow, in a Lyapunov sense. The evolution of the vortex rope may be assessed via such an analysis, with the base flow obtained from the steady axisymmetric model.

Pressure Fluctuations: The range of pressure fluctuations varies only with the discharge coefficient, and this variation may be obtained from numerical simulations, the results of which are presented here. For the purpose of analyzing the pressure fluctuations, we consider a point on the draft tube wall, not far from the inlet, where the effects of the vortex rope are expected to be maximum. To be precise, we present the pressure history at a point on the draft tube wall that is axially at a distance of 10 cm from the inlet cross-section (indicated as 'P' in figure 1). After eliminating the initial unsteady variations, we show the results after the flow becomes stationary and may be described using periodic conditions. Figure 2 shows the variation of pressure with time for four different discharge coefficients close to the BEP. The pressure data are extremely peaky, and indicative of a fluctuating, almost-periodic effect, which may be correlated to the precession of the vortex rope. As expected, the periodicity becomes more pronounced as we move closer to the BEP. Lower discharge coefficients indicate a higher mean pressure and range of pressure fluctuations, suggesting that the vortex rope is much stronger at low discharge coefficients and decreases in strength as we move closer to the BEP. In addition, the rate of change in the pressure values appears to be much smaller near the BEP, and increases as we move farther away from it. The figures also indicate that the amplitude of pressure fluctuations increases by an order of magnitude as we move from the BEP to φ = 0.34, and likewise, the mean pressure increases roughly by a factor of 2. These numbers indicate the strength of the vortex rope at φ = 0.34, relative to that at the BEP, and the relative magnitudes of their effects on the draft tube, exemplified by means of the pressure fluctuations. An actual estimate of the strength of the vortex rope may be obtained by visualizing the vortex rope via isocontours of a few derived variables.

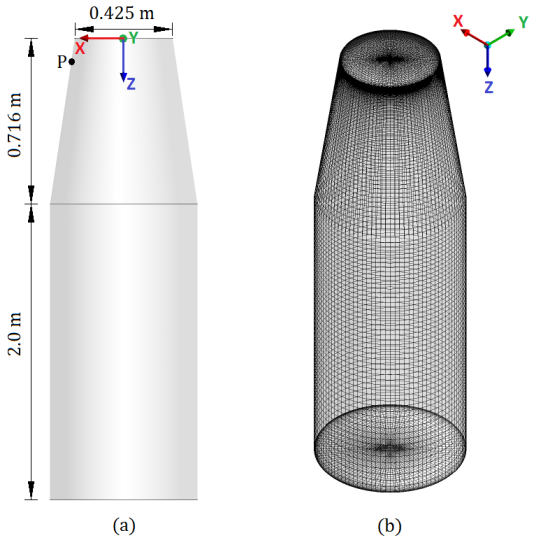

Figure 1 (a) The simplified draft tube and (b) meshed geometry.

Vortex Rope Visualization: Figure 3 shows the vortex rope formed in the draft tube at t = 10 s, for φ = 0.34. It is observed that the isopressure contour does not provide an adequate estimate of the vortex rope structure, and results in a premature cut-off of the rope tail. In other words, even though the rope is defined as a region of low pressure, the structure of the rope cannot be fully pictured by means of an isopressure surface. The remaining variables, on the other hand, are more effective in depicting the vortex rope. It is also worth mentioning that the large scale and small scale features of the vortex rope are ideally illustrated when it is visualized via these variables, and the quantitative structure of the rope is nearly the same in all cases. The vortex rope visualized via isocontours of 'q' is shown in figure 4, for four different discharge coefficients. All the results are shown for the same contour level (q = 1345 1/s^2). A qualitative observation reveals that the strength of the vortex rope increases as φ decreases. While the rope at φ = 0.37 (BEP) is very thin and restricted to a relatively small region around the axis of the draft tube, the vortex rope at φ = 0.34 spreads out in the radial and axial directions and occupies a larger portion of the draft tube. These results are supportive of the variation in the mean pressure and the range of pressure fluctuations.

Stability Analysis: Though numerical simulations may provide accurate results, they prove costly in terms of time and effort. Hence, a simple but rigorous mathematical analysis is worth pursuing, to obtain a first estimate of the onset of instability. In this section, we use the axisymmetric model described by Susan-Resiga *et al*. (2009) and follow Susan-Resiga *et al*. (2006) in analyzing the Squire-Long equation obtained for such flows. In this analysis, we use a steady, axisymmetric, incompressible, and inviscid model to describe the mean flow in the vortex core region of the draft tube. Tsai & Widnall (1980) show that the bulk flow could be considered locally parallel for diverging ducts of angle less than 2°. Susan-Resiga *et al*. (2006) use the fact that the radial velocity in the discharge cone is nearly one order of magnitude smaller than the axial velocity (U_R/U_Z < tan(8.5°) ≈ 0.15) to argue that the local parallel flow approximation could be extended to this case as well. Using the standard Navier-Stokes equations and the continuity equation as the governing equations (with simplifications based on the conditions listed above), defining a two-dimensional stream function $\Psi(R,Z)$, and using a transformation $Y - R^2/2$, we obtain the Squire-Long equation (SLE) (see Bragg & Hawthorne (1950), Squire (1960), and Long (1961)):

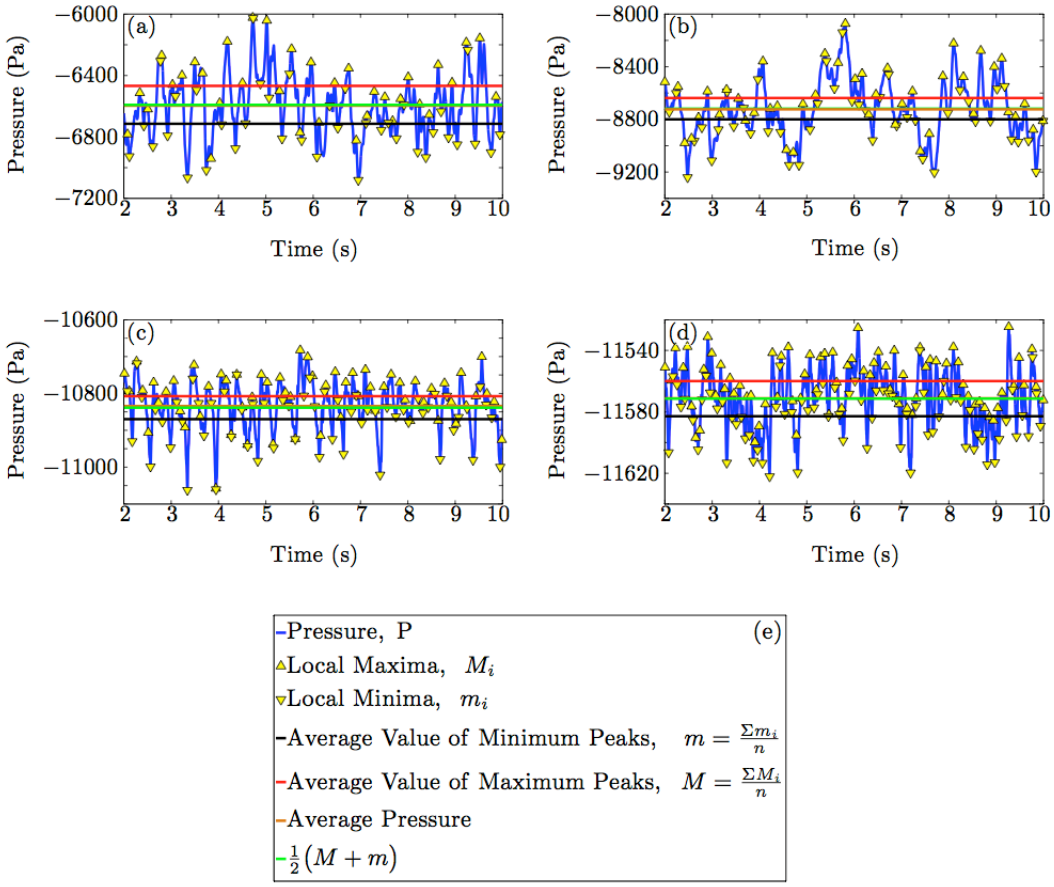

Figure 2. Pressure history at a point on the draft tube wall for (a) $\varphi = 0.34$, (b) $\varphi = 0.35$, (c) $\varphi = 0.36$, and (d) $\varphi = 0.37$ (BEP). The legend is shown in (e).

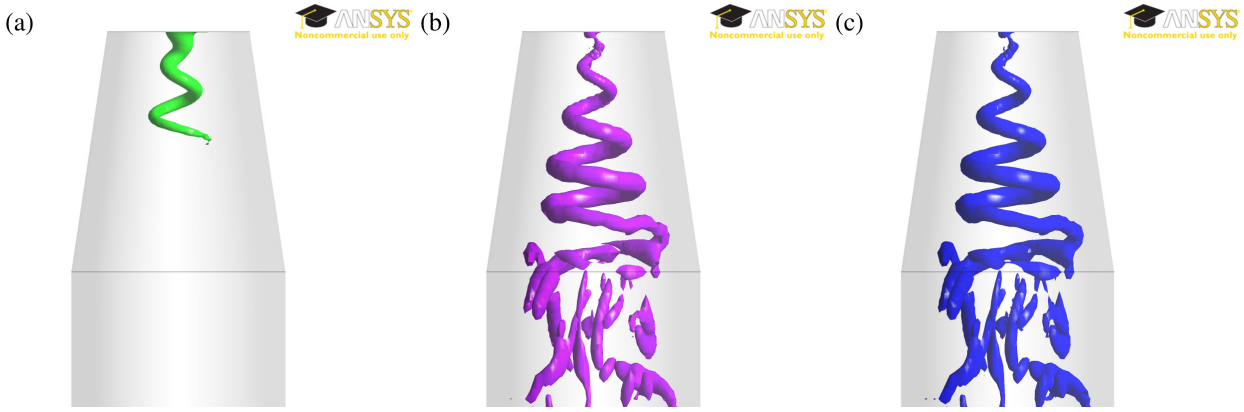

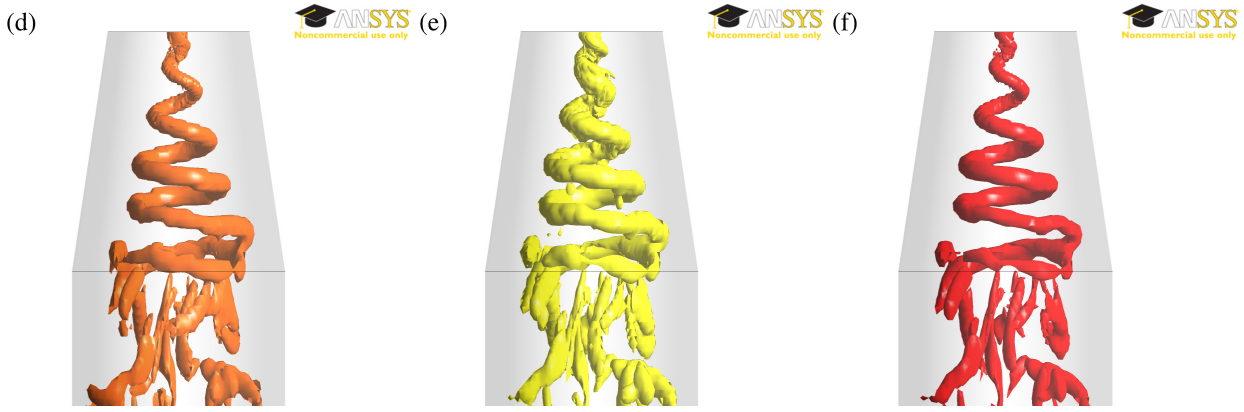

Figure 3. Visualizing the vortex rope. Isosurface countours of (a) pressure (-16600 Pa), (b) λ_2 (-1345 1/s^2), (c) q (1345 1/s^2), (d) real eigen helicity (80 1/s), (e) swirling discriminant (9×10^7 1/s^6), and (f) swirling strength (35 1/s). All results are at t = 10 s, and $\varphi = 0.34$.

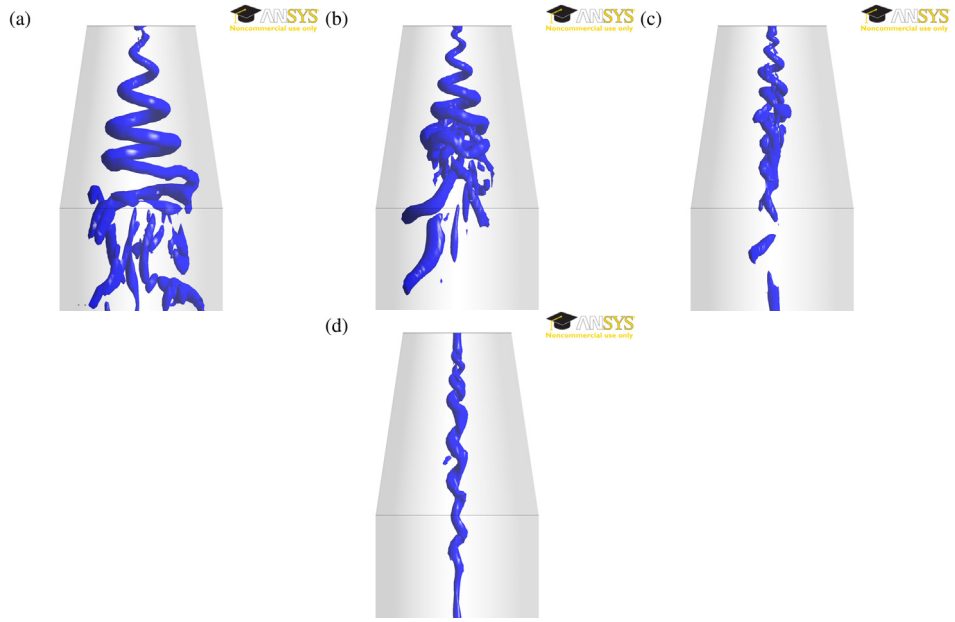

Figure 4. The vortex rope visualized via isocontours of q (1345 1/s^2) for (a) $\varphi = 0.34$, (b) $\varphi = 0.35$, (c) $\varphi = 0.36$, and (d) $\varphi = 0.37$ (BEP). All results are at t = 10 s.

$$\frac{1}{2Y}\left[\frac{\partial^2\Psi}{\partial Z^2}\right] + \frac{\partial^2\Psi}{\partial Y^2} = \frac{dE}{d\Psi} - \frac{I(\Psi)}{2Y}\left(\frac{dI}{d\Psi}\right), \tag{2}$$

where E is the total specific energy and I is the circulation function. The SLE has been used extensively in the analysis of swirling flows and flows involving vortex tubes. Susan-Resiga *et al.* (2006) use the SLE to perform an eigenvalue analysis of the swirling flow in draft tubes, and relate the critical swirl to the drop in the pressure coefficient observed in the scaled model of the Francis hydroturbine. We use the SLE to obtain a Sturm-Luioville (SL) system. Following the

usual procedure for linear stability analyses, we add a perturbation to the base flow and obtain an ordinary differential equation (ODE) for the perturbation amplitude. Then, based on Sturmian theory for stability, we can compute the critical discharge coefficient at which a change is expected in the stability characteristics of the flow. Adding a perturbation to the base flow, we obtain

$$\Psi(Y) = \Psi 0(Y) + \varepsilon \Phi(Y) \exp(iKZ), \tag{3}$$

where $\Phi(Y)$ is the amplitude of the perturbation to the base flow, K is the axial wavenumber of this perturbation, and $\varepsilon \ll 1$ is a small parameter. Substituting (3) in (2) and linearizing, we obtain a second order ODE for $\Phi(Y)$,

$$\frac{\partial^2 \Phi}{\partial Y^2} - \left[C(Y) + \frac{K^2}{2Y} \right] \Phi = 0, \tag{4}$$

where $C(Y) - (d^2U_Z/dY^2)/U_Z + U_\theta[U_\theta + 2Y(dU_\theta/dY)]/2Y^2U_Z^2$, and U_θ and U_Z are defined in (1). Equation (4) represents a Sturm-Luioville system for Φ in the domain $0 \leq Y \leq Y_{max}$ (Y_{max} is chosen here to correspond to the edge of the wall boundary layer), and the solution of the system depends on the sign of the term in brackets, namely, $C(Y) + (K^2/2Y)$. Using Sturmian theory (cf. Ince (1958), Ch 10), we obtain two predominant cases. Case (1): $C(Y) + (K^2/2Y) > 0$ – For this case, there are no zeroes of the SL system in $Y \in [0, Y_{max}]$. Hence the solutions of (4) are exponential, and do not have a bound. The amplitude of the perturbation keeps growing, and we term this an unstable solution of the SL system. Case (2): $C(Y) + (K^2/2Y) < 0$ – For this case, there are one or more zeroes of the SL system in $Y \in [0, Y_{max}]$. The solutions of (4) are oscillatory, but remain bounded. The amplitude of the perturbation varies sinusoidally within fixed limits, and we term this a stable solution of the SL system. It is possible to show that the oscillatory solutions obtained in the second case are bounded, and the solution of the system is linearly stable in a Lyapunov sense (cf. Nemytskii & Stepanov (1960)). In other words, it is possible to find an upper bound δ, such that $|\Phi| < \delta \; \forall \; Y \in [0, Ymax]$. The condition $C(Y) + (K^2/2Y) = 0$ represents an inflection point. However, it is very rare that this condition holds for the entire domain; it may occur locally at a finite number of points. The coefficients ($Ut, Rt, \Omega t$) in the velocity components defined in (1) are functions of φ, which implies that the function $C(Y) + (K^2/2Y)$ depends on φ. To obtain the regions of stability and instability, we plot the function $C(Y) + (K^2/2Y)$ for various discharge coefficients, φ. The parameter K is the eigenvalue of the system, and may be obtained numerically, after discretizing (4) through a suitable scheme, such as finite differences. Thus, we obtain as many eigenvalues as the size of the system. The largest of these eigenvalues is the most influential; hence we use it in our computations. Figure 5 shows the dimensionless quantity $c(y) + (k^2/2y)$ as a function of y over a range of discharge coefficients, where we have used the length scale R_{ref} and the time scale Ω^{-1} to nondimensionalize all quantities (all lowercase letters denote dimensionless parameters corresponding to the respective uppercase letters). It is observed from figure 5 that the function $c(y) + (k^2/2y) < 0 \; \forall \; y \in [0, y_{max}]$ *for* $\varphi \geq 0.3635$. Thus, the region described by $\varphi \geq 0.3635$ is defined as an unconditionally stable region, and the effects of the vortex rope are relatively insignificant in this region, and therefore could be neglected. On the other hand, the flow is destabilized for $\varphi \leq 0.3635$, and the effects of the vortex rope are amplified in this region. This is a first estimate of the critical discharge coefficient at which the stability characteristics of the flow change. This result is supportive of the trend observed in the vortex rope strength. From the visualizations, we see that the vortex rope is thin and small for

$\varphi - 0.37$, and relatively much larger for $\varphi \leq 0.36$, which falls in the unstable regime. It is also observed from figure 5 that there are no inflection points for $\varphi \geq 0.3635$. On the contrary, there is at least one inflection point for $\varphi \leq 0.3629$, and at least two for $0.3629 \leq \varphi \leq 0.3635$. Thus, the function $c(y) + (k^2/2y)$ changes sign in $y \in [0, y_{max}]$ once or twice accordingly for these discharge coefficients, and there are subregions where it is positive and negative. As a result, for $\varphi \leq 0.3635$, we obtain conditional instability. For $\varphi \leq 0.3629$, most of the domain falls in the unstable zone, except for a small finite region around the axis. The magnitude $|c(y) + (k^2/2y)|$ gives an estimate of how large the exponentials are in the unstable zone, since $\Psi \sim \exp(mr)$, where $m \propto |c(y) + (k^2/2y)|$. The inflection points are locally neutral points, and slight deviations at these points may result in the flow being pushed into a stable or unstable zone.

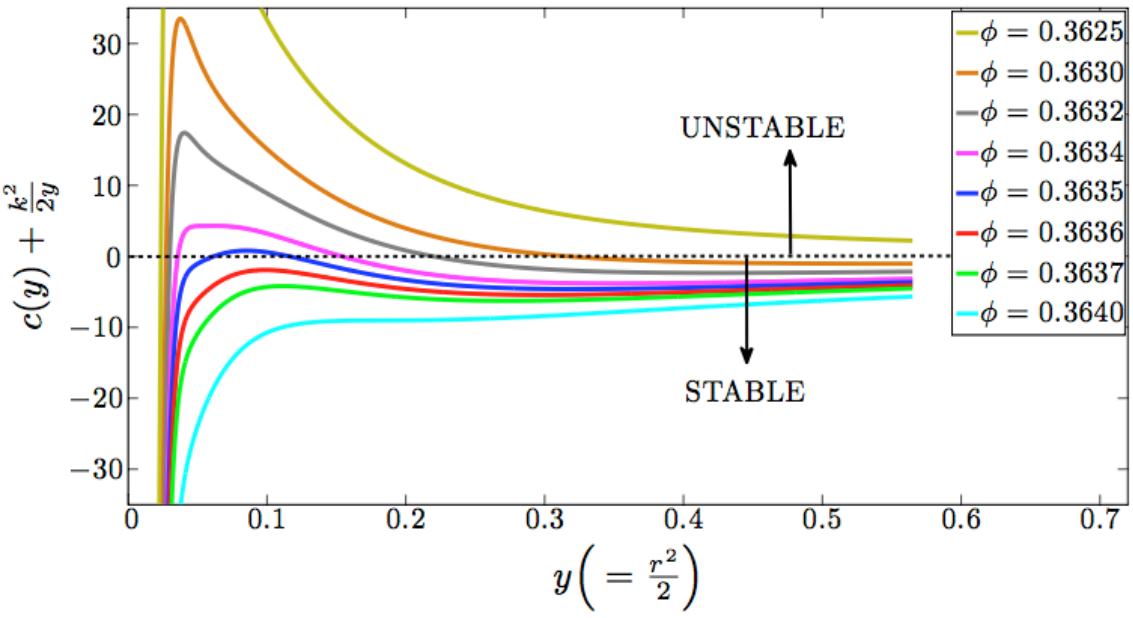

Figure 5. The stability characteristics of the flow at different discharge coefficients.

Figure 6 shows the efficiency and the pressure recovery coefficient of the draft tube of a scaled model of a Francis hydroturbine. It is observed that both of these quantities have maxima at $\varphi \approx 0.37$. This peak in efficiency and pressure recovery at $\varphi \approx 0.37$ is an experimentally observed phenomenon, and the critical discharge coefficient obtained through the stability analysis, i.e., $\varphi \approx 0.3635$, is very close to this value, differing by only approximately 1.76%. For this reason, it is customary to expect that the stability characteristics of the swirling flow in the draft tube affect its efficiency and pressure recovery. Therefore, the results from the stability analysis also provide insight here, and may be used in deciding the optimum point of operation of the turbine for maximum efficiency. Susan-Resiga *et al*. (2006) also observe this effect, and they characterize the flow as subcritical and supercritical for discharge coefficients less than and greater than 0.365, respectively. Our critical discharge coefficient differs from their value by 0.4%. Our mathematical analysis provides a first estimate of the stability characteristics of the swirling flow in draft tubes, which helps to better understand the effects caused by the vortex

rope. In addition, it also helps explain the relation between the experimentally observed variations in efficiency and the stability characteristics. Consequently, it is worthwhile to use mathematical analyses in combination with CFD to enable us to get a good perception of such flows. For future work, it is of interest to expand this analysis to a full three-dimensional, unsteady model, without the axisymmetric approximation, to get more accurate results.

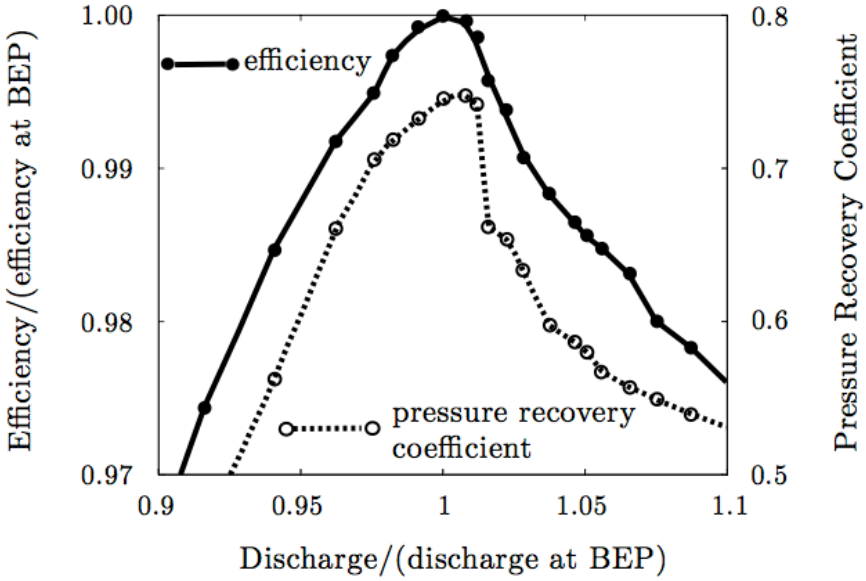

Figure 6. The draft tube efficiency and pressure recovery coefficient for a model test of a Francis turbine operating at a specific speed of 0.56. Courtesy: Susan-Resiga *et al*. (2006)

Closure: In this work, we have investigated swirling flow in the draft tube of a scaled model of a Francis turbine operating at a specific speed of 0.56. Four discharge coefficients are considered for the numerical analysis, and the amplitudes of the pressure fluctuations and the vortex rope structure are obtained for these cases. The variations in the range of the pressure fluctuations indicate that the vortex rope formed at $\varphi = 0.34$ is roughly an order of magnitude stronger than the one formed at $\varphi = 0.37$. This gives a rough idea about how strong the rope gets as the turbine operates away from the BEP. It is also observed that the trends in the range of pressure fluctuations, the average pressure, and the length of the rope obtained from the visualizations, are all identical to one another. The pressure fluctuations and the vortex rope visualizations provide a good qualitative picture of the effects of the rope and its structure, respectively. Results from both these analyses complement one another. The vortex rope visualizations also reveal that pressure is not a suitable parameter for picturing the rope. Nevertheless, the other chosen parameters depict the rope completely, and are nearly identical to one another when comparing the large scale and small-scale features. The results produced from the numerical simulations are further confirmed by the mathematical analysis, which helps in explaining the experimental observations in the efficiency of the draft tube and its pressure recovery. The mathematical analysis provides an insight into the stability characteristics of the swirling flow, and indicates that the onset of instability occurs at $\varphi = 0.3635$. For larger discharge coefficients (closer to BEP) the flow is stable in a Lyapunov sense to axial perturbations, and it corresponds to a weaker rope. The other

side of the critical discharge coefficient corresponds to stronger vortex ropes. This is in good agreement with the visually observed structure of the ropes at the four discharge coefficients considered. The mathematical analysis also shows that the axisymmetric approximation can provide results comparable to those from the full three-dimensional unsteady CFD simulations. In summary, both numerical and mathematical analyses have been used to provide compatibility and to ensure a greater degree of certainty in the results. It is therefore appropriate to mention that such combinations aid in a better understanding of such complicated flows, and help to acquire good acumen in terms of classifying observed phenomena.

References

[1] Avellan, F. 2000 Flow investigation in a Francis draft tube: the FLINDT project. *In Proceedings of the 20th IAHR Symposium, Charlotte, North Carolina, USA*.

[2] Bragg, S. L. & Hawthorne, W. R. 1950. Some exact solutions of the flow through annular cascade actuator disks. *Journal of the Aeronautical Sciences* **17** (4).

[3] Foroutan, H. & Yavuzkurt, S. 2012a Analysis and prevention of vortex rope formation in the draft tube cone of a hydraulic turbine. *In Proceedings of the ASME 2012 International Mechanical Engineering Congress and Exposition IMECE2012, Fluids and Heat Transfer, Parts A, B, C, and D*, vol. 7. Houston, Texas.

[4] Foroutan, H. & Yavuzkurt, S. 2012b Simulation of flow in a simplified draft tube: turbulence closure considerations. *IOP Conference Series: Earth and Environmental Science* **15** (2), 022020.

[5] Ince, E. L. 1958 *Ordinary Differential Equations*.. Dover.

[6] Long, R. R. 1961 A vortex in an infinite viscous fluid. *Journal of Fluid Mechanics* **11** (4).

[7] Nemytskii, V. V. & Stepanov, V. V. 1960 *Qualitative Theory of Differential Equations*. Princeton U. Press, Princeton NJ.

[8] Nishi, Michihiro & Liu, Shuhong 2013 An outlook on the draft-tube-surge study. *International Journal of Fluid Machinery and Systems* **6** (1), 33–48.

[9] Squire, H. B. 1960 Analysis of the vortex breakdown phenomenon. *Miszellaneen der Angewandten Mechanik*.

[10] Susan-Resiga, R., Dan Ciocan, G., Anton, I. & Avellan, F. 2006 Analysis of the Swirling Flow Downstream a Francis Turbine Runner. *Journal of Fluids Engineering* **128**, 177.

[11] Susan-Resiga, R., Muntean, S., Hasmatuchi, V., Anton, I. & Avellan, F. 2010 Analysis and prevention of vortex breakdown in the simplified discharge cone of a Francis turbine. *Journal of Fluids Engineering* **132** (5).

[12] Susan-Resiga, R., Muntean, S., Stein, P. & Avellan, F. 2009 Axisymmetric swirling flowsimulation of the draft tube vortex in francis turbines at partial discharge. *International*

Journal of Fluid Machinery and Systems **2** (4), 295–302.

Publications Resulting from this Project:

1. Rajan, G. and Cimbala J., Stability Analysis of the Vortex Rope Formed in Draft Tubes, Bulletin of the American Physical Society, Vol. 58, No. 18, p. 109, November 2013.

2. Rajan, G. and Cimbala, J. M. Computational and Stability Analyses of the Precessing Vortex Rope in a Hydroturbine Draft Tube, to be submitted to J. Fluid Mechanics, 19 pp., Jan. 2014.

Scott Richards, M.S. 2011. Advisor: H. Perez-Blanco

TECHNOECONOMIC ANALYSIS OF PUMPED HYDROELECTRIC STORAGE AS A MEANS TO MITIGATE THE VARIABILITY OF RENEWABLE GENERATION

Abridged by: H. Perez-Blanco

Introduction

Electrical power that is generated from renewable sources, such as the wind and the sun, is inherently variable and difficult to forecast. In many locations, the current penetration of renewable energy is small enough that the fluctuations can be managed using the same methods adopted to manage the variability in the load. As the amount of renewable generation increases, it will be more and more difficult to match electricity generation with electricity consumption because of the additional supply-side variability. This fact causes concerns regarding the reliability of electric grids with a high penetration of renewable generation [1].

Pumped Hydroelectric Storage (PHS) is a mature energy storage technology that can be used to mitigate the variability of renewable generators. It also has the ability to store energy generated from renewable sources so that it can be sold when the electricity prices are high. PHS is one option for providing the additional generation flexibility that Kirby believes to be necessary [2] for accommodating significant amounts of renewable generation but is limited by the availability of water and the local topography. Denholm stresses the importance of examining the technical impacts of renewable energy before considering the use of energy storage technologies [1].

A variety of computer models have been created to study things like the economics of energy arbitrage in PJM [3], the performance of photovoltaic generation [4], and the technical limits of variable renewable generation as a function of system flexibility [5].

Due to the limitations of these models, a computer model of a PHS facility, wind and solar power generation, and the PJM electricity market was programmed in Mathcad 14. The PJM electricity market, which encompasses 13 mid-Atlantic states and the District of Columbia, was chosen because historical wind generation and electricity market data are readily available from its website. The Mathcad model is capable of simulating PJM wind power generation, solar power generation, and the operation of a fixed speed pump-turbine PHS facility in the PJM interconnection at one-minute resolution, for an entire year. The novelty of the model is a result of its ability to simulate the complex interaction between energy storage and wind and solar generators with sub hourly resolution.

In addition to analyzing the technical aspects of using PHS as a means of mitigating the variability of renewable generation, the model is capable of analyzing PHS from an economic perspective. The technical aspects include, but are not limited to, the maximum ramp rates of renewable generators over various time scales, and the economic aspects include matters such as the financial penalties that result from a renewable generator incorrectly forecasting its power production. The most interesting results are those that quantify how the PHS facility's revenue stream changes as a result of varying technical parameters of the facility. For example, how changes in round trip efficiency of the PHS facility affect the utilization of the plant and ultimately its energy arbitrage revenue. Even though the model is based on pumped hydroelectric storage and renewable generators, the results obtained from the model are pertinent to conventional power generators as well as other types of energy storage technologies.

Variability of Load, Wind and Solar

The PJM service area has a considerable amount of variation in temperature throughout the year. Since the load is significantly affected by temperature, it should be expected that the load profile gradually changes over the course of a year. Figure 1 is a collection of weekday load profiles for PJM, one for each season of the year. The shape of the summer load profile, such as August 2, is dictated by the electricity requirements for air conditioning which peak in the late afternoon [6].

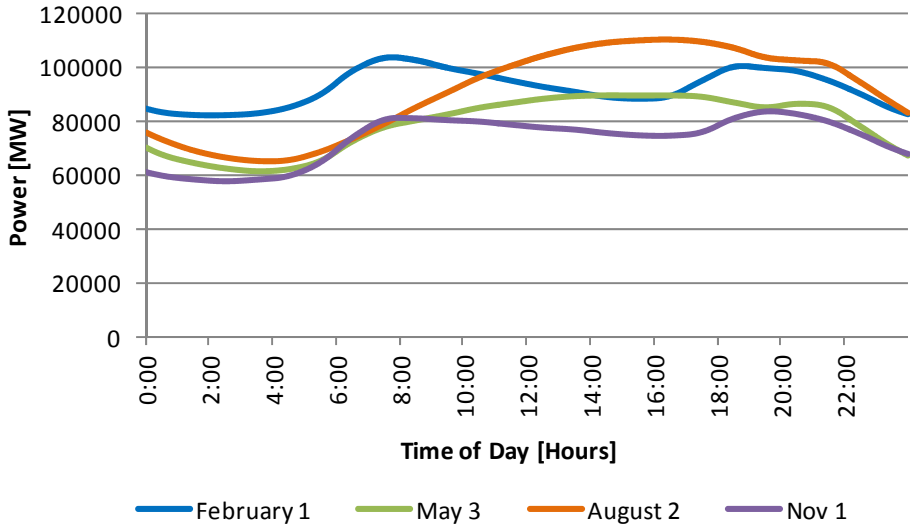

Figure 1: Seasonal Variations of the PJM Weekday Load Profile During 2010.

The aggregate variability of wind generators in the PJM service area is difficult to convey with a single figure. One of the characteristics of wind generators in PJM is that, on average, their power production is higher at night than it is during the day. Figure 2 shows the average hourly wind generation for January dates, as given by the data-driven wind simulation embedded in the model.

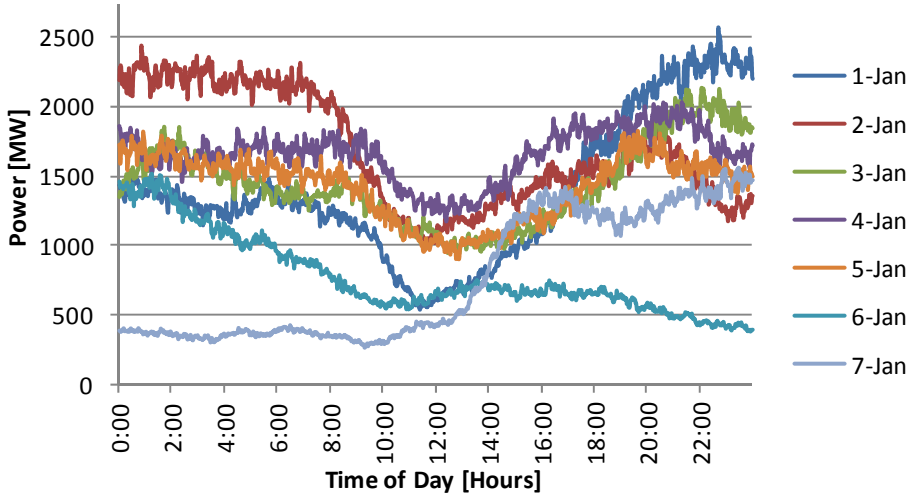

Figure 2: Synthetic Wind Power Generation in PJM During the First Week of 2010.

Figure 3 shows the synthetic solar power generation profiles during the first week of August 2010. Unlike the wind power generation profiles in Figure , the solar power generation profiles exhibit a fair amount of similarity from day to day.

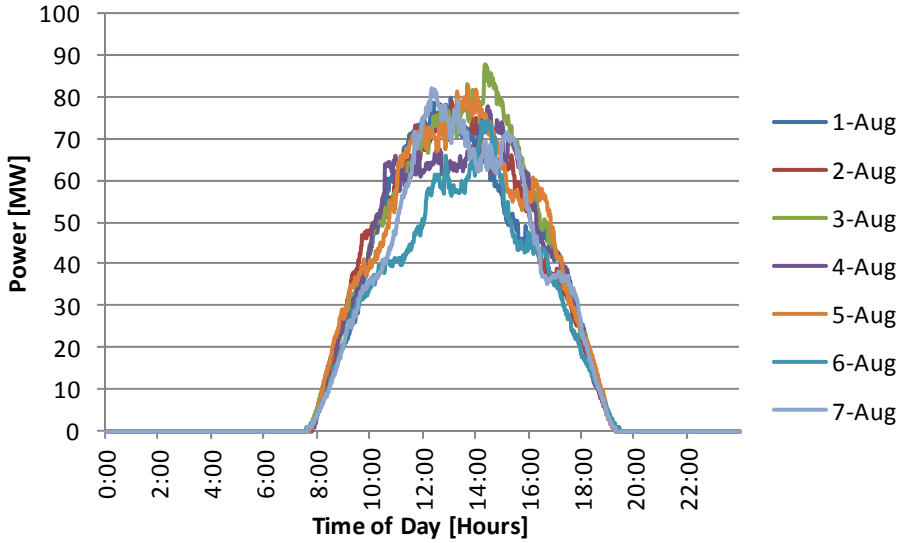

Figure 3: Synthetic Solar Power Generation in PJM During the First Week of August 2010.

In simulating wind and solar, it became apparent that each energy source has a different value in terms of availability. Capacity factors (CF) are used to characterize the availability of the energy source to provide energy say throughout a quarter, and CF values for each quarter are shown in Table 1. Clearly, wind tends to be more available in the winter/fall months, and least available in the summer months.

Table 1: Capacity Factors by Quarter of the Year.

	Wind	Solar
Q1 Capacity Factor	0.304	0.143
Q2 Capacity Factor	0.252	0.177
Q3 Capacity Factor	0.158	0.171
Q4 Capacity Factor	0.337	0.120
Annual Capacity Factor	0.263	0.153

Another figure of merit is the capacity value (CV), which measures how much energy is provided by the source during peak hours, namely during periods of the year and within that period hours of the day when demand occurs. For PJM, the CVs are much more significant in the summer for solar than for wind. As of 2010, existing wind generators inside PJM had an average CV of 13% and existing solar generators had an average CV of 38% [7].

Model Features and Results

Renewable Generation Technical Results

The amount of renewable generation being simulated in this thesis is capable of exhibiting significant power ramp rates. Large, unanticipated negative ramp rates (decreasing renewable generation) can be problematic for system operators because dispatchable generators are often required to provide fill-in energy on short notice. Large, unexpected positive ramp rates are much more manageable because they can be counteracted by curtailing some or all of the additional renewable generation. However, managing positive ramps by curtailing renewable generation wastes low marginal cost energy and increases the average cost of renewable generation, as was discussed in [8].

Comparing the variation in net load to the variation in load provides a way to assess whether the renewable power ramps help or hinder the system operator's efforts to balance the supply of electricity with demand. In general, renewable generation that decreases the variability of the net load by reducing its ramp rates and/or the difference between the intraday maximum and minimum is beneficial. Figure 4 illustrates the variability of the net load compared to that of the load. In this figure, the renewable power production ramps down between 7:00 and 11:00, as the demand for electricity experiences its morning ramp up. The result is a net load with a positive ramp rate that is greater than the ramp rate of the load during the same time period. Between 21:00 and 23:00 hrs the renewable power production ramps down again, but this time it decreases the relative ramp rate of the net load because the demand for electricity is also decreasing. As the net load ramp rates increase as a result of increased renewable penetration, generation fleets with a high degree of flexibility will be needed to accommodate the renewable generation as efficiently as possible.

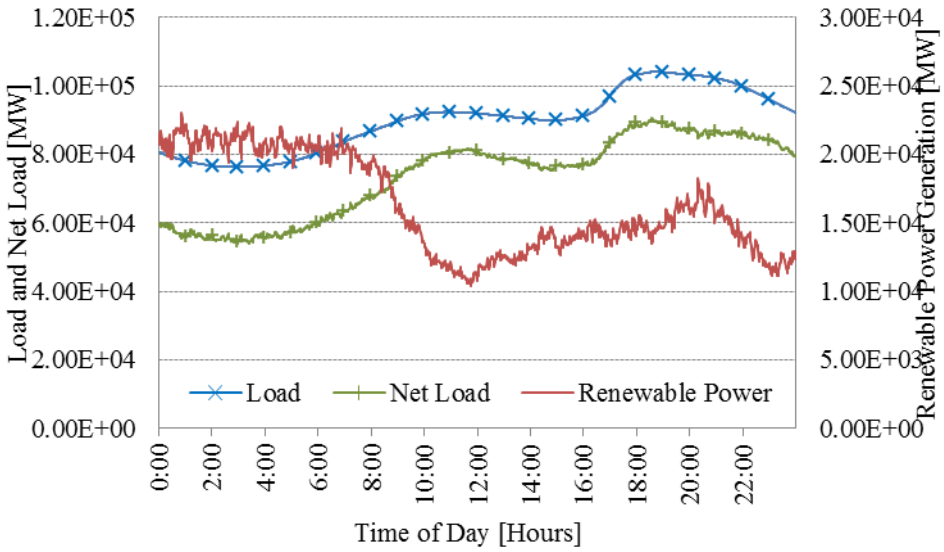

Figure 4: Comparison of Net Load Ramp Rates to the Ramp Rates of the Original Load.

Pumped Hydroelectric Storage Technoeconomic Results

The economics of PHS are very closely related to, and sometimes dependent on, the facility's technical parameters. Modern PHS facilities have a round trip efficiency, η_{RT}, that is typically between 65% and 85% [3]. The effects of changes in pumping efficiency, η_{Pump}, as well as generating efficiency, η_{Gen}, for constant energy stored (4444 MWh) as unearthed by the model, are shown in Fig 5. In this figure, pink denotes pumping and blue denotes generation. The values

for η_{Pump} and η_{Gen} are set to either 0.8 or 0.9. The hourly LMP is shown by the black trace and corresponds to the right hand axis of the figure.

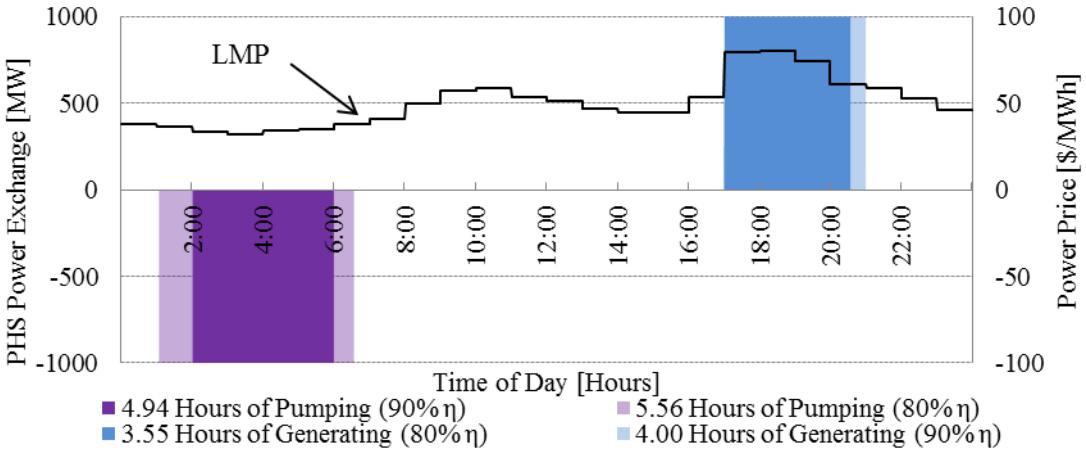

Figure 5: The Operational Schedule of Pumped Hydroelectric Storage as a Function of Pumping and Generating Efficiency.

As either of the efficiencies decreases, the η_{RT} decreases and more energy is lost for each MWh that is stored and discharged from the PHS facility. When the PHS facility is storing energy at its rated capacity, the number of hours of pumping is inversely proportional to its η_{Pump}. This means that a decrease in η_{Pump} results in more time being required to store the same amount of energy in the upper reservoir. The cost of the increased pumping is compounded by energy prices that are typically more expensive during the additional hours. In generation mode, the number of hours that a PHS facility can generate at its rated capacity is proportional to its η_{Gen}. For the example shown in Fig 5, a generator with a η_{Gen} of 0.90 is able to generate 26 minutes longer than a generator with a η_{Gen} of 0.80. The revenue perceived increases with η_{Gen} on two counts: first, generation proceeds in a period of most favorable energy prices, and second, more energy is delivered to the grid.

The Effects Of Changes In Round Trip Efficiency

Instead of looking at changes in pumping and generating efficiency individually, it is now assumed that they are equal to one another and we focus on the effects of changing η_{RT}. A decrease in η_{RT} translates into fewer hours of profitable intraday arbitrage. This can be seen in Fig 6, which compares the operating schedules for two 1000 MW PHS facilities, one with a η_{RT} of 81% and the other with a η_{RT} of 56.3%.

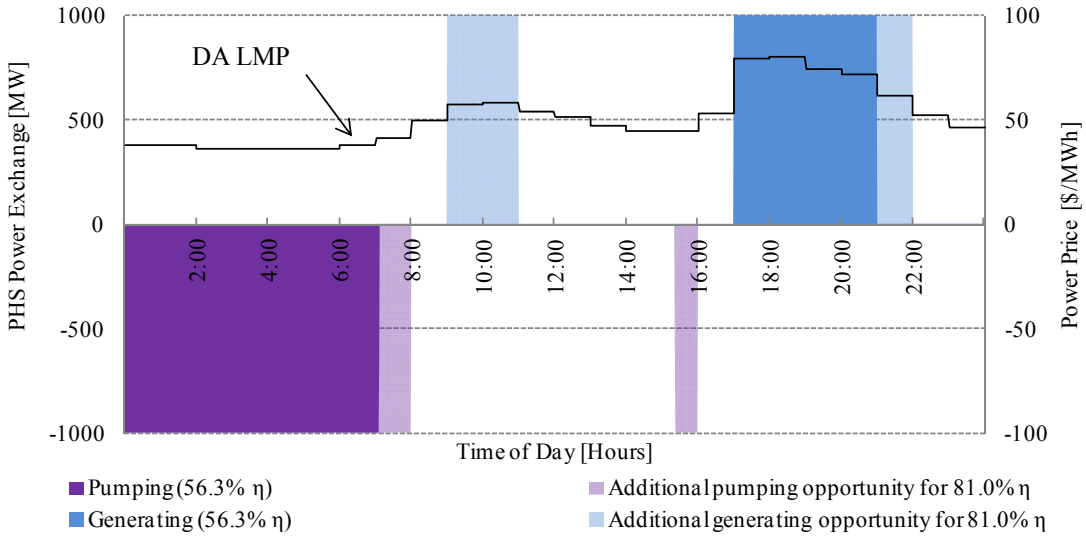

Figure 6: Operational Schedules for Two Pumped Hydroelectric Storage Facilities With Different Round Trip Efficiencies.

Based on the LMPs shown in the figure, a PHS facility with a η_{RT} of 81% would generate power for 7 hours based on 8.64 hours of pumping, whereas a facility with a η_{RT} of 56.3% would generate for 4 hours based on 7.11 hours of pumping. The average profit per MWh is sensitive to changes in η_{RT}, storage capacity of the upper reservoir and the variability in power prices. [8]

Power Capacity

The last aspect analyzed in [8] is now summarized. If a large renewable penetration is assumed, the variability of supply increases. The economic implications of changes in power capacity for PHS facilities performing arbitrage are fairly straightforward, since intraday profits scale linearly with power capacity. The technical implications of changes in power capacity are much more complex, e.g., how the power capacity relates to the PHS facility's ability to provide firming power for renewable generation.

The operational schedule for the 81% η_{RT} PHS facility from Fig 6 and the projected generation/offer necessary to stabilize to firm up simulated 20 GW of renewable supply are used to establish the PHS availability and power requirements seen in Fig 7. The colored trace represents the firming power required to counteract the variability of the renewable generation. When the trace is green, the PHS facility is available to provide the required firming power but when the trace is red, the PHS facility is unable to provide the power due to arbitrage obligations or the firming power exceeding its 1000 MW power capacity.

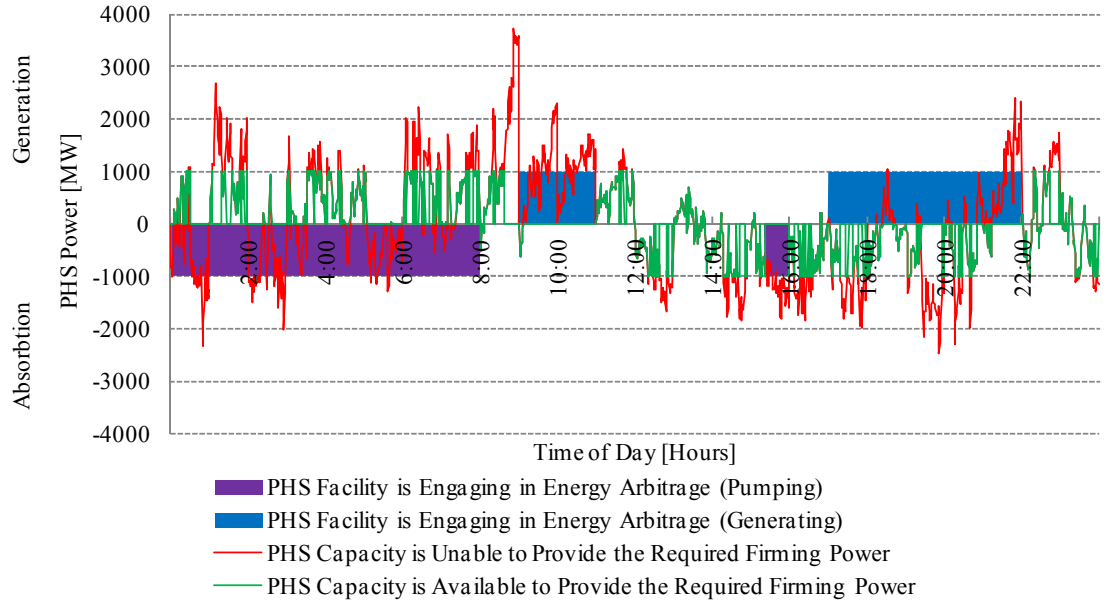

Figure 7: The Power Required to Firm Renewable Generation Superimposed on Top of the PHS Facility's Operational Schedule [8].

Figure 7 presents a puzzle, since technology to meet the green firming trace using reversible Francis impellers does not currently exist. If a PHS facility is to operate continuously and produce an accelerated ROI, it becomes necessary to study other technologies. It was determined at the time of the completion of this study that increased PHS flexibility is a must in order to balance renewable supply.

Finally, this study unearthed two more worrisome conclusions. PHS plants operate only a limited amount the time, and to balance renewables, they would have to be active continuously, which in arbitrage they are not. Second, when Francis constant speed runners are employed, the capacity ranges indicated by Figure 7 may not be available. Even if they were, the green trace calls for inversion from generation to pumping instantaneously, an impossibility for reversible runners. Evidently, technologies other than conventional PHS will be necessary to effectively firm-up renewables.

References

[1] Denholm, P., Ela, E., Kirby, B., and Milligan, M., 2010, "The Role of Energy Storage with Renewable Electricity Generation," National Renewable Energy Laboratory. http://www.nrel.gov/docs/fy10osti/47187.pdf

[2] Kirby, B., 2008, "Examination of capacity and ramping impacts of wind energy on power systems," No. NREL/TP-500-42872, National Renewable Energy Laboratory, Golden, Colorado. http://www.nrel.gov/docs/fy08osti/42872.pdf

[3] Sioshansi, R., Denholm, P., Jenkin, T., and Weiss, J., 2009, "Estimating the value of electricity storage in PJM: Arbitrage and some welfare effects," Energy Economics, 31(2), pp. 269-277. http://ideas.repec.org/a/eee/eneeco/v31y2009i2p269-277.html

[4] NREL's Electricity Resources and Building Systems Integration Center, "PVWatts v. 1," National Renewable Energy Laboratory. http://rredc.nrel.gov/solar/calculators/PVWATTS/version1/

[5] Denholm, P., 2006, "REFlex Model," National Renewable Energy Laboratory. http://www.nrel.gov/analysis/analysis_tools_tech_sol.html

[6] Denholm, P., and Margolis, R. M., 2007, "Evaluating the limits of solar photovoltaics (PV) in traditional electric power systems," Energy Policy, 35(5), pp. 2852-2861. http://www.sciencedirect.com/science/article/pii/S0301421506003740

[7] 2010, "PJM Manual 21: Rules and Procedures for Determination of Generating Capability," http://pjm.com/~/media/documents/manuals/m21.ashx

[8] Richards S., 2012. "Technoeconomic Analysis Of Pumped Hydroelectric Storage As A Means To Mitigate The Variability Of Renewable Generation". MS Thesis, Penn State.

Publications:

Richards, S. and H. Perez-Blanco, "Mitigating the Variability of Wind and Solar Energy Through Pumped Hydroelectric Storage, GT2012-68121, 2012 Turbo Expo.

Richards, S. and H. Perez-Blanco, "The Price Suppression Effects of Wind Power Generation in PJM are Likely to Decrease the Profits of Pumped Hydroelectric Storage Facilities that Engage in Energy Arbitrage", 2012 HydroVision Conference.

Richards, S. and H. Perez-Blanco, "Financial Considerations of Using Pumped Hydroelectric Storage to Increase the Penetration of Wind and Solar Generation", GT2012-68147, 2012 Turbo Expo.

Perez-Blanco H. , S. Richards, B. Leyde 2013. " When intermittent power production serves transient loads" , Applied Thermal Engineering 50 (2013) 1549-1556.

Benjamin Rittenhouse, MS 2013. Advisor: Alok Sinha
Optimal Sliding Mode Gaussian Control of Hydro Power Plants

The goal of this work is to examine modern control techniques that could increase the operating range of a hydro turbine and decrease system transients associated with load disturbances. In order to test new controllers the hydropower plant is simulated in the modeling program SIMSEN. SIMSEN is a modular software package for the analysis of power networks, electrical machines, and hydraulic circuits [1], and is used in industry for system studies.

The power generated by the hydroelectric plant can be divided into two groups, active and reactive power [2]. Active power control is analogous to frequency control and reactive power control is analogous to voltage control. The control of these two types of power is separated. In addition, the control of isolated systems and network connected systems is different. Isolated system active power control is concerned only with the rotor frequency since the grid frequency of a small isolated system will be identical to machine frequency. Network system active power control is concerned with both the grid frequency and machine frequency since the two will be different.

This work focuses on active power / load frequency control of both isolated power systems with no grid dynamics and network power systems with grid dynamics. Proportional integral controllers (PI), linear quadratic Gaussian controllers (LQG), and optimal sliding mode Gaussian controllers (OSG) are designed for each system and simulated in SIMSEN.

The first step in simulating a hydropower station in these situations is to develop models to represent the different components of the system. Hydropower stations generally consist of a reservoir, penstock, wicket gate servo system, turbine, generator, draft tube and downstream reservoir. In addition the dynamics of the connected load need to be considered. In our studies we developed analytical models for the wicket gate servo system and grid network while the models for the other system components were derived via system identification. The analytical model for the wicket gate servo system is represented by a cascaded system of first order transfer functions while the analytical model for the grid network is more involved. The block diagram for the gird network is given in figure 1 and is based on the work in [25]. In simple terms the mechanical power produced by the turbine , P_m, is transmitted to the grid, P_g, to satisfy the grid demand power, P_{md}. Grid frequency and machine frequency are also monitored by this model, F_g, and F_m respectively.

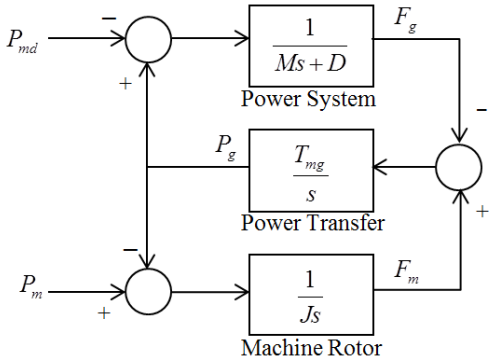

Figure 1. Grid system layout.

The remaining system component models were derived via system identification methods. In order to do this random, Gaussian, zero mean signals of different standard deviations as seen were generated and given as inputs to the system to be modeled and the corresponding output signals were recorded and evaluated to produce state space models of the respective system. In the case of the isolated hydroelectric system the penstock, turbine and rotor system was modeled. In the case of the network connected system only the penstock and turbine were modeled since the machine rotor is taken in to account in the grid model. After a model for each system component was obtained a complete system model could be built to model the behavior of the system in SIMSEN.

Before the design of the controller can be undertaken the system states must be measured. Since the system model uses estimated states they are impossible to measure. To overcome this problem, a system observer is developed with the gains chosen via the Kalmin Filter technique. This allows us to estimate the system states from only the input and output data. Next, the design of the different controllers could be undertaken. The design of PI and LQG controllers is well known and is carried out according to the literature on the subject. The design of the OSG controller is outline for each type of system in references [4] and [5]. Sliding mode controllers offer robust performance under varying loads and off design conditions and operate by forcing the system to slide along a hyperplane in state space representing the system's normal behavior. For a system with measured states this implies a discontinuous control signal but in the case where an observer is employed, the control signal is linear and simple to implement.

The performance of the OSG, LQG and PI controllers for the isolated system with no grid dynamics to a 0.1 *p.u.* step decrease in generator torque is given in figure 2. From the figure, OSG control provides the smallest deviation in rotational speed at 0.964 *p.u.* with LQG and PI control still providing good performance with deviations of 0.966 *p.u.* and 0.97 *p.u.* respectively. The settling time for the system is very similar for both OSG and LQG control at about 15 seconds with PI control settling in about 20 seconds.

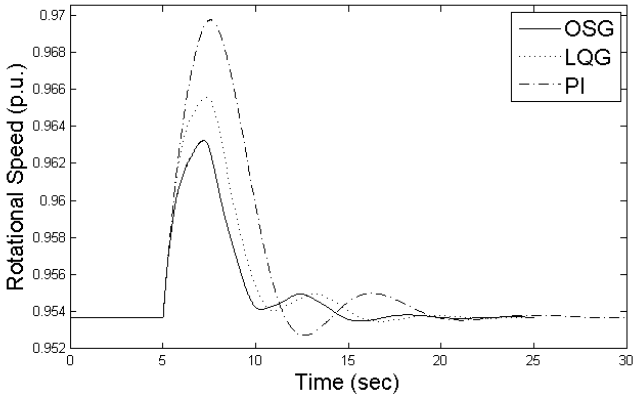

Figure 2. Rotational speed versus time with 10% decrease in torque.

The performance of the OSG, LQG and PI controllers for the isolated system with no grid dynamics to a 0.1 *p.u.* step decrease in generator torque is given in figure 3. From the figure, OSG and LQG control provide the similar deviations in grid frequency of 0.0106 *p.u.* and 0.0123 *p.u* respectively. PI control provides much slower performance with a maximum deviation of 0.019 *p.u.* The settling time for the system is very similar for both OSG and LQG control at about 5 seconds with PI control settling in about 25 seconds.

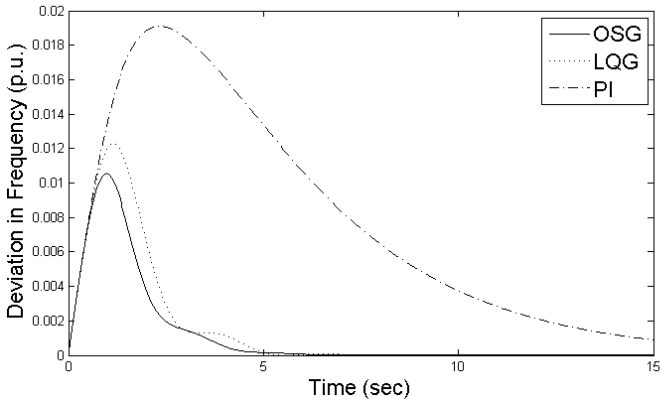

Figure 3.. Grid frequency versus time with 10% decrease in demand power.

References:

1. Swiss Federal Institute of Technology, (2002). SIMSEN: Modular SimulationSoftware for the Analysis of Energy Conversion Systems (Version 2.3). [Software]. Available from http://www.simsen.epfl.ch/.
2. P. Kundur, Power System Stability and Control, McGraw-Hill, 1994.
3. S. Mansoor, D. Jones, D. Bradley, F. Aris and G. Jones, "Reproducing Oscillatory Behaviour of a Hydroelectric Power Station by Computer Simulation," *Control Engineering Practice,* vol. 8, no. 11, pp. 1261-1272, 2000.
4. Rittenhouse, B. and Sinha, A., 2013. "Optimal Sliding Mode Gaussian Controller for a Hydropower Plant". American Control Conference (ACC), 17-June 19, 2013. Accepted.
5. Rittenhouse, B. and Sinha, A., 2013. "Optimal Sliding Mode Gaussian Controller for Hydropower Plant with Grid Dynamics". ASME Dynamic Systems and Control Conference (DSCC), October 21-October 23, 2013. Accepted.

Publications Resulting from this Project:

1. Benjamin D. Rittenhouse, "Optimal Sliding Mode Gaussian Control of Hydro Power Plants," Master's Thesis, The Pennsylvania State University, April 2013.
2. Rittenhouse, B. and Sinha, A., 2013. "Optimal Sliding Mode Gaussian Controller for a Hydropower Plant". American Control Conference (ACC), 17-June 19, 2013. Accepted.
3. Rittenhouse, B. and Sinha, A., 2013. "Optimal Sliding Mode Gaussian Controller for Hydropower Plant with Grid Dynamics". ASME Dynamic Systems and Control Conference (DSCC), October 21-October 23, 2013. Accepted.

Vinod Vishwakarma, PhD 2014. Advisor: Alok Sinha
Modal characteristics of GAMM hydro turbine

Introduction

The ever increasing and variable demand on the energy market, coupled with limited energy storage capabilities, requires flexibility in operating condition of hydraulic turbines. Thus the head, fluid velocity and hydraulic force on the hydro turbine blades increase considerably. Consequently, severe vibrations can occur due to geometrical defects in runner or changes in operating conditions. This can cause stress and fatigue in the rotor. These variations of surface geometry is called geometric mistuning. These variation are usually small and random and can be due to manufacturing process variation or wear and tear in operation. Though intentional mistuning has been used to modify the vibration characteristics of turbomachinery rotors [1], useful properties such as cyclic symmetry for tuned rotors (geometry of all sectors is identical) is lost.

Numerical study of the vibrational characteristics such as mode shapes and natural frequency for mistuned rotor requires time consuming process of full 360° rotor FEM analysis. To overcome this problem a high fidelity reduced order modeling method Modified Modal Domain Analysis (MMDA) was developed by Sinha [2], which had been tested on an industrial scale gas compressor [3]. In this work the use of MMDA on GAMM hydro turbine a model is proposed to test the accuracy of reduced order modeling in presence of strong coupling provided by band.

Following steps are required to achieve the objective. First, a solid model of full tuned rotor and a sector of a GAMM francis rotor is created. Second, cyclic symmetry analysis of the solid model of sector is performed properties such as natural frequencies are observed via Campbell diagram. Third, intentional geometric mistuning is added to runner surface's of FEM model to simulate mistuning, then MMDA method is tested on the mistuned rotor so that results from MMDA and full rotor FEM analysis can be compared. The fluid mass added effect is not studied in this work, it has been studied experimentally in [4] and numerically in [5].

Modeling

GAMM runner models are a class of Francis turbine models designed for academic study. The turbine runner, crown and band surface model was provided by Bryan Lewis[1], as shown in Figure 9.

The CAD model is generated from the surface profile of crown, band and runner using SolidWorks 2014. The crown and band solid models are generated by thickening their respective surfaces by 5mm. Hub attachments and nose cap are created separately. A solid hexahedral block is created around the runner surface. The intersection of this solid block, runner, crown, band, hub and nose cap solid models resulted in the solid model of the hydroturbine with only one runner and given surfaces, as shown in Figure 10.

The sector model of the hydroturbine is obtained from this model by creating two construction surfaces such that copying and rotating them by appropriate angle for 13 sector rotor model cuts out a sector as shown in Figure 10. The intersection of these surfaces and the solid model gives the sector solid model as shown in Figure 11.

[1] Ph.D. student at Penn State

A full 360° rotor model is generated by regenerating these sectors and rotating them along the axis of symmetry. These sectors are then merged to form a full tuned rotor as shown in Figure 12.

Meshing

The FE mesh for the sector model is generated in Pointwise by Bryan Lewis with tetrahedral mesh shown in Figure 13. The full 360° rotor model can be created by replicating and rotating this FE model of the sector. The periodic surfaces on crown and band have matching mesh, so that these surface are superimposed on each other when replicating the sector. The mesh on these surfaces will be merged when creating full rotor. The degree of freedom (DOF) of nodes at the surface nodes of hub contact is constrained in all directions. Few properties of the FE model are given in Table 1.

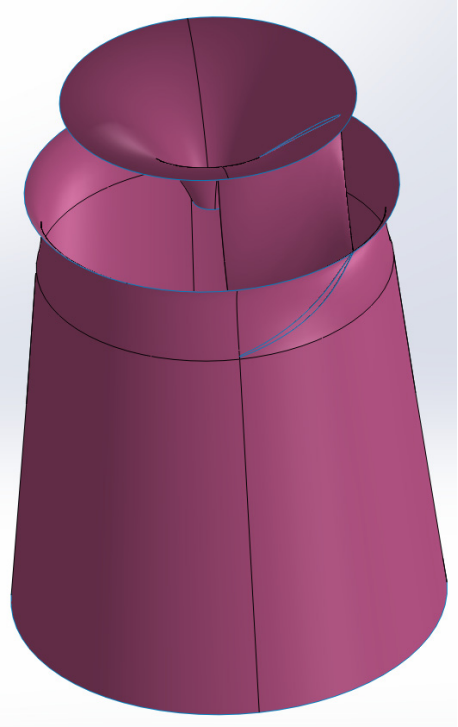

Figure 9: GAMM runner surface model

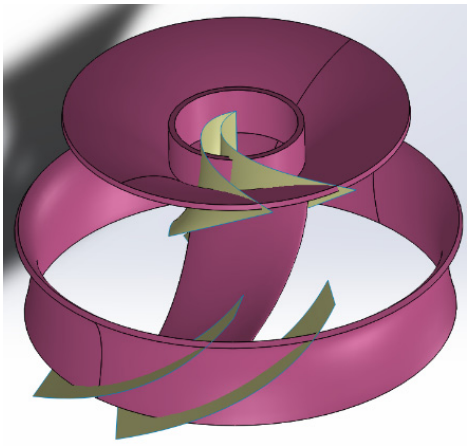

Figure 10: Solid model with one runner

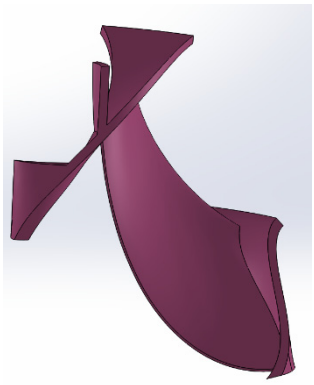

Figure 11: Solid model of a sector

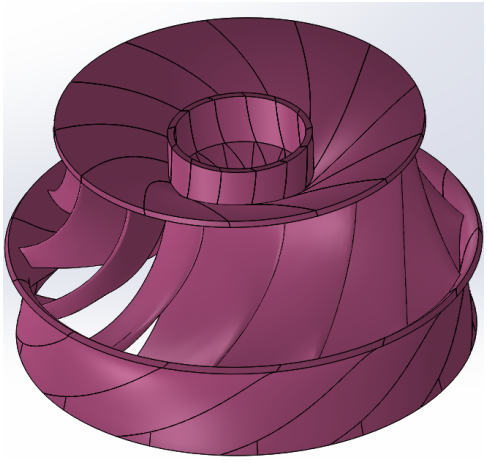

Figure 12: Solid model of full 360º GAMM hydro turbine

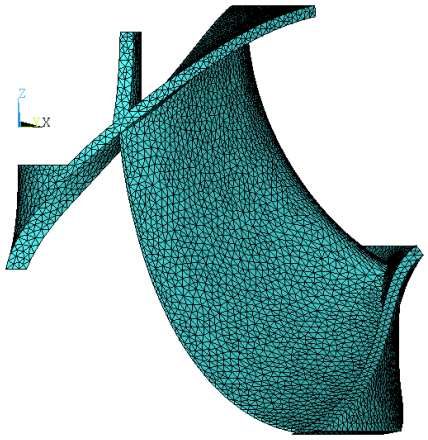

Figure 13: Meshed sector model

Table 1: FEM model properties

Number of sectors	13
Sector Angle	360/13
Number of nodes	13973
Number of elements per sector	Tetrahedral – 56346
DOF of nodes at hub constrained	2370
Young's Modulus	28x10^6 psi
Density	0.289 lbm/in^3
Possion ratio	0.3

Analysis

The equation of motion for mistuned hydroturbine is given by

$$M\ddot{\mathbf{x}} + C\dot{\mathbf{x}} + K\mathbf{x} = \mathbf{f}(t) \tag{1}$$

$$M = M_t + \delta M, \quad K = K_t + \delta K \tag{2}$$

Where M, C and K are mass, damping and stiffness matrices respectively. M_t and K_t are tuned mass and stiffness matrices, δM and δK are deviation in mass and stiffness matrices. $\mathbf{x}$ is the displacement vectors for nodal degree of freedom. $\mathbf{f}(t)$ is the force being applied to the system. The mode shapes and natural frequencies are obtained by solving following eigenvalue problem.

$$K\boldsymbol{\psi} = \omega^2 M\boldsymbol{\psi} \tag{3}$$

Where $\boldsymbol{\psi}$ is the mode shape and ω is the natural angular frequency. For tuned rotor, these properties are obtained from ANSYS cyclic symmetry analysis. Natural frequencies of first five family of modes are shown in the nodal diameter map Figure 14. The first family of modes is predominantly bending modes, second family is torsion modes and towards higher family of

modes mixed modal behavior is observed. Mode shapes for few harmonic indices corresponding to first family of modes is shown in Figure 15-Figure 17.

MMDA method requires only mass and stiffness matrices from ANSYS (which is faster to compute) and mode shapes of tuned rotor perturbed along the POD features. Details of MMDA are given in [2]. The POD feature consists of deviations in x,y and z DOF of the nodes of runner such that the linear combinations of POD features results in the perturbation of the geometry of the runner. A mistuned rotor is created by perturbing the nodes of runner of each sector randomly along two artificially created POD features. The POD mistuning parameters are chosen randomly. Though the mistuned full rotor modal characteristics are obtained from ANSYS but the results did not match with MMDA. The reasons for this mismatch is attributed to mesh type and it is currently being investigated.

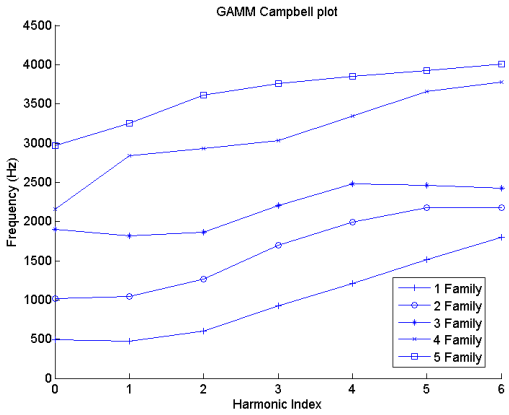

Figure 14: Nodal diameter map

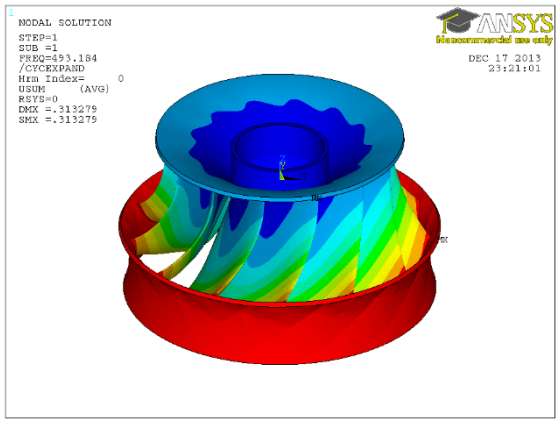

Figure 15:Tuned rotor mode shape for 1st family and 0th harmonic index

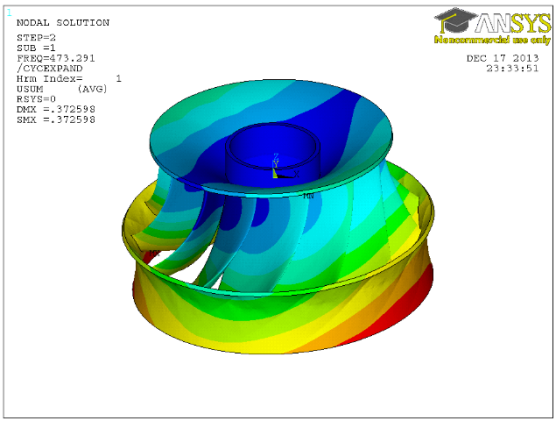

Figure 16:Tuned rotor mode shape for 1st family and 1th harmonic index

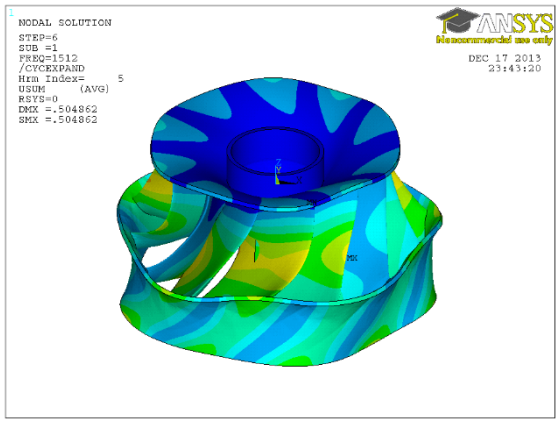

Figure 17:Tuned rotor mode shape for 1st family and 6th harmonic index

Conclusion

FE model of a sector meshed with tetrahedral elements has been successfully used to obtain modal characteristics of tuned hydroturbine. From nodal diameter map it is observed that the first family of modes at higher harmonic indices have frequencies close to second family of modes. This can result in mode mixing at slight mistuning. Application of MMDA reduced order modeling to this hydroturbine is still under investigation.

References

[1] M. Castanier and C. Pierre, "Using Intentional Mistuning in the Design of Turbomachinery Rotors," *AIAA,* vol. 40, no. 10, pp. 2077-2086, 2002.

[2] A. Sinha, "Reduced-Order Model of a Bladed Rotor With Geometric Mistuning," *Journal of Turbomachinery,* vol. 131, 2009.

[3] V. Vishwakarma, A. Sinha, Y. Bhartiya and J. Brown, "Modified Modal Domain Analysis of a Bladed Rotor Using Coordinate Measurement Machine Data on Geometric Mistuning," in *ASME Turbo Expo 2013 : Power for Land, Sea and Air*, San Antonio, TX, 2013.

[4] C. Rodriguez, E. Egusquiza, L. Q. Escaler X and F. Avellan, "Experimental investigation of added mass effects on a Francis turbine runner in still water," *Journal of Fluids and Structures,* vol. 22, pp. 699-712, 2006.

[5] Q. Liang, C. Rodriguez, E. Egusquiza, X. Escaler, M. Farhat and F. Avellan, "Numerical simulation of fluid added mass effect on a francis turbine runner," *Computers and Fluids,* vol. 36, pp. 110-1118, 2007.

[6] Y. Bhartiya and A. Sinha, "Reduced Order Modeling of a Bladed Rotor with Geometric Mistuning via Estimated Deviations in Mass and Stiffness Matrices," in *DETC*, 2011.

Alex Wouden, PhD Student. Advisor: John Cimbala
Develop/Expand CFD Capabilities to Study the Unsteady Interaction between Hydroturbine Wicket Gates and Runner

The blade cascade of hydroturbines, most particularly of the Francis-type configuration, typically consist of three blade rows: the stator, wicket gate, and rotor. Each blade row has an essential purpose. The stator maintains the structural integrity of the unit; the wicket gates control the flow rate; and the rotor extracts mechanical energy. During the design process, the designated blade counts of the wicket gate row and the rotor are specified to avoid destructive harmonic forces that arise through rotor-stator interaction. For example, one Francis turbine was designed with 20 wicket gates and 13 runner blades. This specification prevents synchronous blade passing which could trigger and propagate harmonic resonance and noise within the machine.

For industrial applications, computational fluid dynamics (CFD) is used to simulate and predict the performance characteristics of turbomachinery components. However, the usefulness of the calculations is limited by the lack of a common periodicity between the blade rows. Typical methods that reduce the cost of a simulation, e.g., defining periodic boundaries on a subset of the flow passage, miscalculate the realistic interaction between the blade rows. Without the aid of such methods, a high fidelity model requires a computational domain spanning a sufficient subset of blade passages – assuming a least common multiple exists between sequential blade rows – or spanning the entire turbine geometry. The simulation becomes expensive in computer time, data storage, and resource overhead.

Various methods have been implemented to decrease the computational cost of coupled rotor/stator simulations [Tucker, 2011]. Figure 1 identifies the hierarchy of modeling methods ranging from a *mixing-plane* method, which produces a fast simulation lacking a predictive capacity for unsteady behavior, to the time-consuming, high-fidelity *unsteady full 360°* method. Between these, each method is a compromise between simulation accuracy and resource conservation.

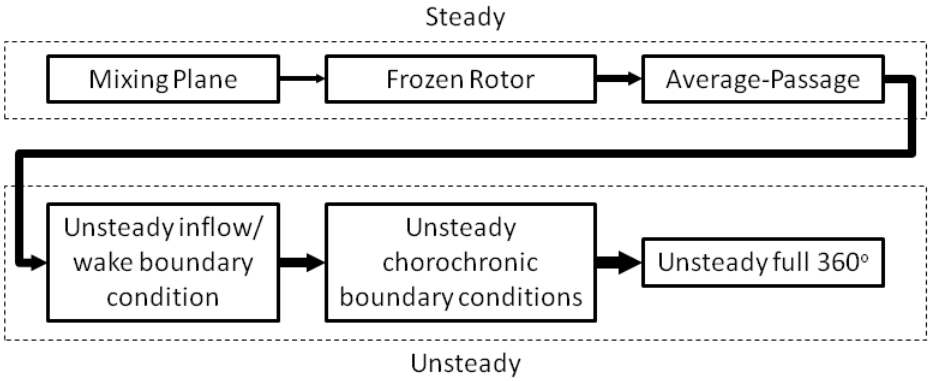

Figure 1. Hierarchy of turbomachine cascade modeling methods [Tucker, 2011].

The *unsteady chorochronic boundary condition*, also known in various literature as a phase-lag boundary condition, produces an accurate transient simulation from a computational domain containing only one blade passage per blade row regardless of its periodicity. The boundary condition assumes that the spatial (choro) periodic relation between a set of coupled faces is delayed by a time-dependent (chronic) component proportional to the fundamental blade passing periods. Thus, an economic analysis of the unsteady rotor-stator interaction is realizable by imposing chorochronic boundary conditions on the coupled faces.

Erdos et al. [Erdos, 1977] introduced the theory behind the chorochronic boundary condition and applied it using a "direct-storage" technique. For each iteration, data from a previous time step different by a quantity proportional to the blade passing period are retrieved in lieu of the data generated by the current time step at the coupled boundaries. Figure 2 illustrates the storage and retrieval process of the corresponding data. The direct-storage method was refined by Gerolymos [Gerolymos, 1991] to include arbitrary angular velocities and pitch ratios. Further, Wang and Chen [Wang, 2004] extended the phase-lag boundary condition to three-dimensional flows.

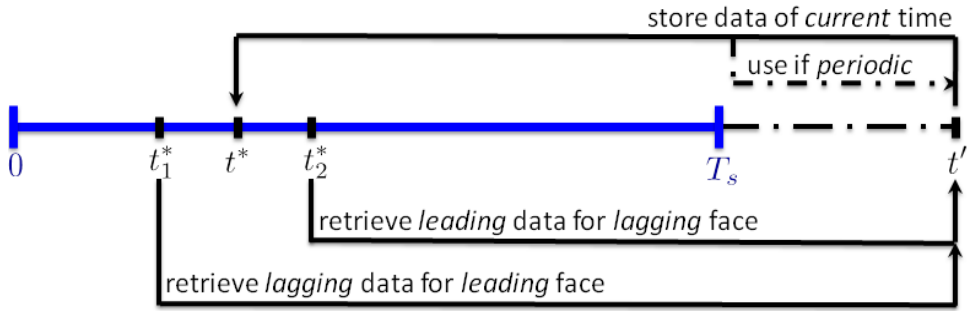

Figure 2. Storage and retrieval of the historical data at the coupled faces of a phase-lag boundary.

In the publications marking the development of the phase-lag boundary condition as well as many supporting publications over the past thirty years, the problem of interest has focused on compressible fluid flow in gas turbine applications. As a result of the compressible assumption, the velocity and energy variables are included in the solution space whereas the pressure is determined through an equation of state. In accordance with preliminary observations, the implementation of a phase-lagged boundary condition for pressure-based methods introduces a challenge to stability in the pressure field that must be handled sufficiently. In line with the objectives of this research project to develop and expand CFD capabilities with the intent of studying the unsteady interaction of the wicket gate and runner, The direct-storage method is developed for use with the pressure-based solvers of OpenFOAM®. Results thus far obtained through this project reflect the potential of a phase-lagged boundary condition for the incompressible flow through hydroturbines.

As a benchmark case for evaluating the implementation of a phase-lagged boundary condition in OpenFOAM®, a two-dimensional wake field was simulated. The computational domain encompasses a quiescent region downstream of a sinusoidal velocity fluctuation consisting of five peaks through the full domain height. The grid is shown in Figure 3. A quarter of the domain was isolated to demonstrate the capability of the phase-lag boundary condition; the configuration imposes a 5:4 periodicity ratio. Data were monitored at the locations shown on the phase-lag

computational domain and compared with corresponding locations from the full wheel simulation. In addition, a phase-lagged simulation covering two passages was also initiated.

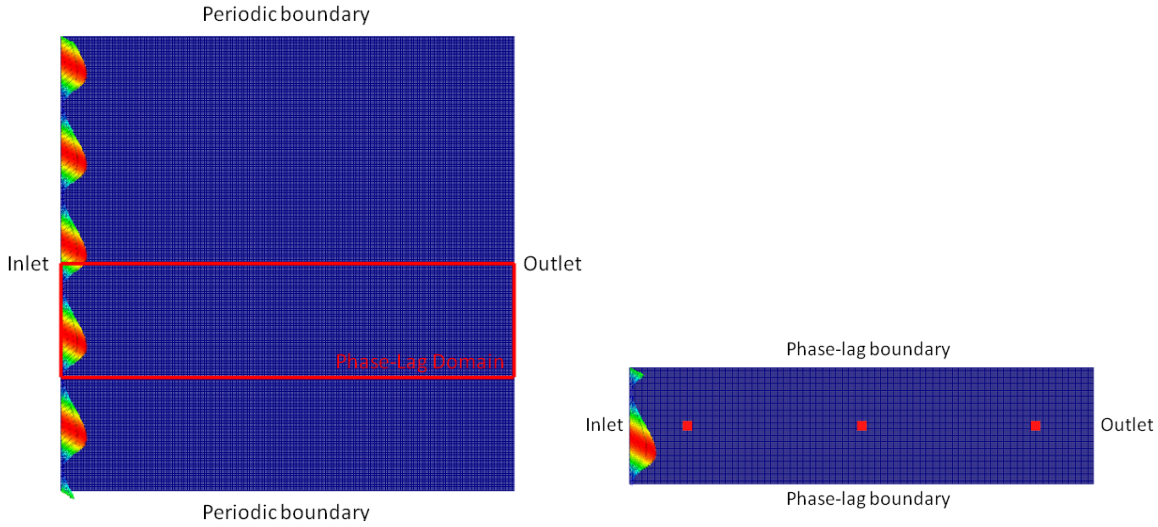

Figure 3. Two-dimensional wake field geometry, prescribed with a 5:4 periodicity ratio. (Right) Full wheel computational domain with indication of the blade passage used for the phase-lagged simulation. (Left) Phase-lag computational domain.

After 1400 time steps, the phase-lag simulations were compared to the full domain simulation. Figure 4 displays the velocity profiles for the three simulations at the final time step when the profiles have become nearly indistinguishable. However, as shown in figure 5, there is a unrealistic disturbance inclusive of the transient data of the pressure field; data is shown for the central probing location. As previously mentioned, span of publications describing results of chorochronic boundary conditions employed a compressible solver that calculated pressure explicitly through an equation of state as a function of the variable density. By using a pressure-based method, the implicit computations become sensitive to small perturbations. Further, because the simulation represents the discharge from an upstream velocity fluctuation into a region subject to an outlet of fixed relative pressure, the phase-lag simulations display a sensitivity to deviations during the iteration process.

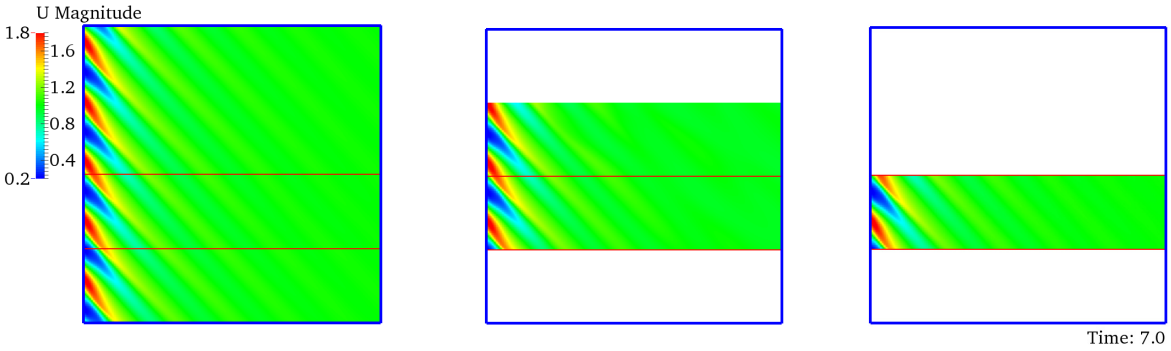

Figure 4. Comparison of the velocity profiles after 1400 time steps.

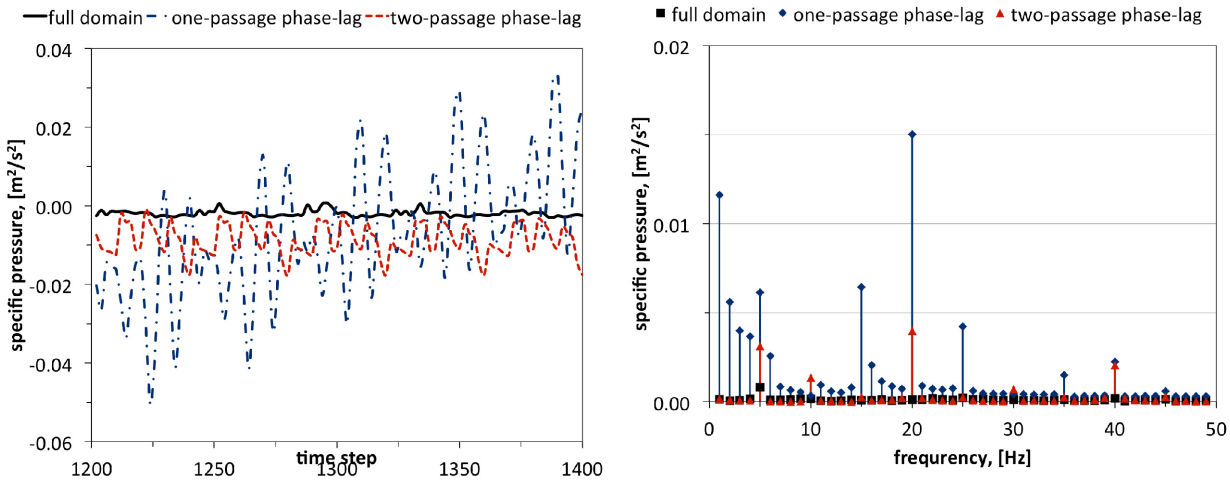

Figure 5. Time-periodic profile and frequency spectrum of the pressure at the central probe of the two-dimensional quiescent case.

Nonetheless, this simple demonstration illustrates the impact of a reduced domain on the economy of the simulation. Table 1 summarizes the computational cost of the three simulations. The percentages are based on the memory usage and run times of the full domain simulation. The memory usage reduces favorably as the computational domain is reduced. Although the full-domain simulation outperformed the phase-lagged simulation in reaching a converged time-periodic solution more efficiently, the phase-lagged simulation demonstrates an overall reduction in necessary run time to complete a fixed number of time steps. Thus, a reduced computational cost is achieved by the phase-lagged simulations provided the analysis of the unsteady interaction exceeds a threshold for the number of time steps included in the simulation.

	Hard drive memory usage	Req'd time to time-periodic solution	Req'd time for 1400 time steps
Full domain	6.06 GB	36.8 min	198.5 min
One-passage phase-lag	1.58 GB (26.1%)	46.3 min (125.8%)	61.2 min (30.8%)
Two-passage phase-lag	3.07 GB (50.7%)	62.4 min (169.6%)	112.0 min (56.4%)

Table 1. File storage utilization and run time acquisition for a two-dimensional quiescent case; percentages based on the full-domain simulation.

To more fully evaluate the effectiveness of the phase-lag boundary condition, a more complex two-dimensional coupled rotor-stator problem was modeled. The computational domain is shown in figure 6. The model is a representation of a typical Francis turbine configuration with a prescribed wicket gate to runner blade ratio of 20:17. The blades are comprised of scale NACA

2312 airfoils to maintain simplicity in the blade design. A mesh was constructed separately on each blade passage and a general grid interface was configured at the adjoining surfaces. The rotor rotates dynamically during run time at 60 rpm. The outlet is constrained with a fixed uniform relative pressure of zero and the inlet supplies a fixed sinusoidal velocity profile that is aligned with the chord of the wicket gate.

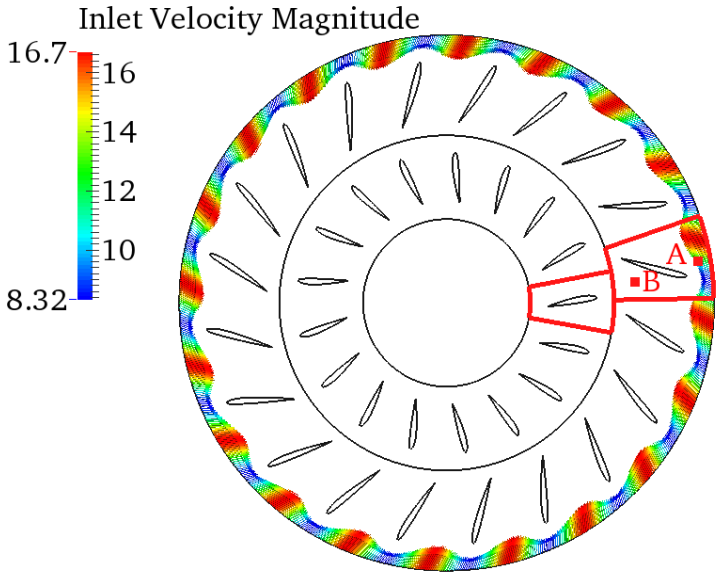

Figure 6. Two-dimensional coupled simulation of the wicket gate and runner passages similar to those found in Francis turbine configurations.

A simulation was conducted for on single-passage phase-lagged domains of the rotor and stator with interface communication during run time. The results were compared with the a simulation of the full passage. Consistent with a reduction of blade passages included in the computational domain (37 passages reduced to 2 passages), the phase-lag simulation required only 2.2% of the time needed to complete 10,000 time steps. From an industrial perspective to integrate high-fidelity CFD into the design process, this reduction reflects the potential for phase-lag simulations.

The velocity profile of the phase-lag simulation is compared with that of the full-domain simulation in figure 7 and the transient pressure fluctuations monitored at location B (see figure 6) are shown in figure 8. The phase-lag simulation provides a poor representation of the flow through both blade passages. It is suspected that the present construction of the phase-lag boundary condition may be amplifying early numerical perturbations in the later iterations.

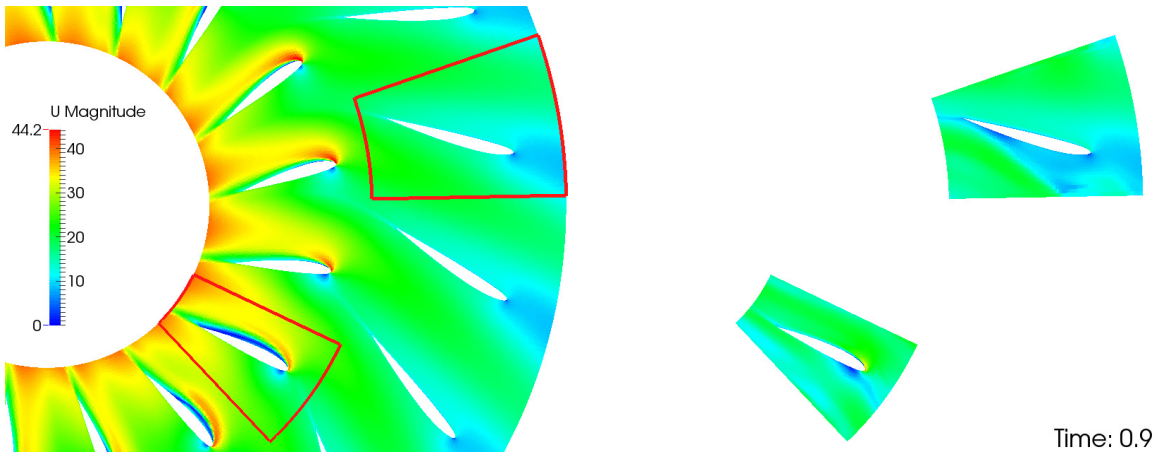

Figure 7. Comparison of the velocity profiles after 9,000 time steps for the two-dimensional rotor-stator case.

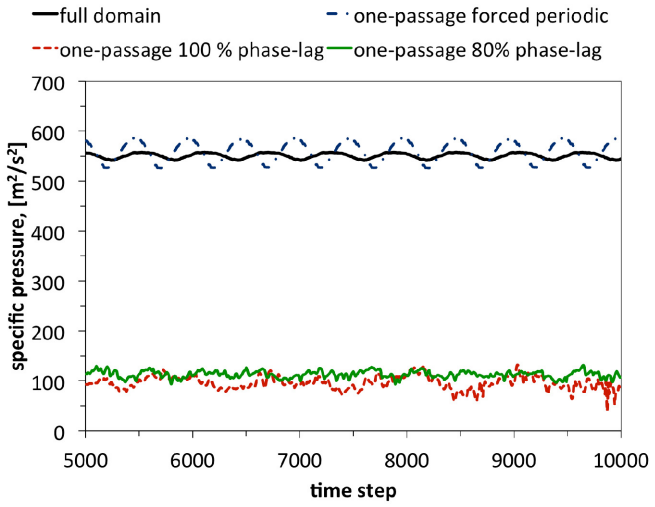

Figure 8. Time-periodic profile of the pressure at location B for the two-dimensional rotor-stator case.

In summary, the phase-lag boundary condition is presently being reviewed to understand the unrealistic perturbations that arise in the pressure field. Ongoing work is focused in understanding the origin of the perturbations and sufficiently diminishing them to provide a more impactful estimation of the unsteady flow behavior resulting from the interaction of the blade cascade typical of hydroturbines.

References:

1. P.G. Tucker (2011), Computation of unsteady turbomachinery: Part 1 – progress and challenges, *Progress in Aerospace Sciences*, Vol. 47(7)
2. J.I. Erdos, E. Alzner, and W. McNally (1977), Numerical solution of periodic transonic flow through a fan stage, *AIAA Journal*, Vol. 15(11)

3. G.A. Gerolymos and V. Chapin (1991), Generalized expression of chorochronic periodicity in turbomachinery blade-row interaction, *La Recharche Aerospatiale*, Vol. 5
4. X. Wang and J.P. Chen (2004), A post-processor to render turbomachinery flows using phase-lag simulations, *43rd AIAA Aerospace Sciences Meeting and Exhibit*

Publications Resulting from this Project:

1. A. Wouden, J. Cimbala, and B. Lewis, Detecting Unsteady Blade Row Interaction in a Francis Turbine using a Phase-Lag Boundary Condition, *Bulletin of the American Physical Society*, Vol. 58(18), Nov. 2013
2. A. Wouden, J. Cimbala, and B. Lewis, An Evaluation of the Phase-Lagged Boundary Condition using Open-source Software, *28th Annual Graduate Exhibition*, Penn State, poster, March 2013
3. A. Wouden, J. Cimbala, and B. Lewis, A Phase-Lag Boundary for Unsteady Flows in Turbomachinery Applications, *College of Engineering Research Symposium*, Penn State, March 2013
4. A. Wouden, J. Cimbala, and B. Lewis, Implementation of a Phase-Lagged Boundary Condition for Turbomachinery, *Bulletin of the American Physical Society*, Vol. 57(17), Nov. 2012
5. A. Wouden, J. Cimbala, and B. Lewis, Implementation of a Phase-Lagged Scheme on Hydroturbine Type Geometries Using CFD, *27th Annual Graduate Exhibition*, Penn State, Poster, March 2012
6. A. Wouden, J. Cimbala, and B. Lewis, A Parametric Study of Unsteady Rotor-Stator Interaction in a Simplified Francis Turbine, *APS 64th Annual DFD Meeting*, Nov 2011
7. A. Wouden, B. Lewis, J. Cimbala, and E. Paterson, OpenFOAM and Turbomachinery: A Demonstration of a Simplified Francis Turbine Geometry, *6th OpenFOAM Workshop*, June 2011

PARTICIPANTS & OTHER COLLABORATING ORGANIZATIONS

Individuals:

Faculty:

Name	**John M. Cimbala**
Project Role	PI, advisor for 4 grad students
Nearest Person Month worked	Approx. 25% time (approximately 12 person months since start of the project; 48 calendar months since Jan. 2010)
Contribution to Project	Overall coordinator, budget administration, write quarterly reports, supervise 4 grad students, help to supervise the other grad students
Funding Support	This DOE project
Collaborated w/ individual in foreign country	
Country(ies) of foreign collaborator	
Traveled to foreign country	Slovenia (for model turbine testing)
If traveled to foreign country, duration of stay	1 week (April 2011)

Name	**Jules (Jay) W. Lindau**
Project Role	Advisor for 1 grad student
Nearest Person Month worked	Approx. 12.5% time (approximately 5.25 person months since he started on the project; 42 calendar months since July 2010)
Contribution to Project	Supervise 1 grad student
Funding Support	This DOE project
Collaborated w/ individual in foreign country	
Country(ies) of foreign collaborator	
Traveled to foreign country	
If traveled to foreign country, duration of stay	

Name	**Jeffrey S. Mayer**
Project Role	Co-PI, advisor for 1 grad student
Nearest Person Month worked	Approx. 12.5% time (approximately 4.9 person months since start of the project; 39 calendar months since Jan. 2010) – Jeff stopped serving as advisor to David Beever in January 2013.
Contribution to Project	Supervise 1 grad student
Funding Support	This DOE project
Collaborated w/ individual in foreign country	

Country(ies) of foreign collaborator	
Traveled to foreign country	
If traveled to foreign country, duration of stay	

Name	**Eric G. Paterson**
Project Role	Co-PI, advisor for 1 grad student
Nearest Person Month worked	Approx. 12.5% time (approximately 3.8 person months since start of the project; 30 calendar months since Jan. 2010) – Eric left PSU in August of 2012, but still serves as advisor for David Boger until his graduation
Contribution to Project	Supervise 1 grad student, serve as grid generation and CFD expert to assist other grad students
Funding Support	This DOE project
Collaborated w/ individual in foreign country	
Country(ies) of foreign collaborator	
Traveled to foreign country	Gothenburg, Sweden (OpenFoam workshop), Darmstadt, Germany (OpenFoam workship)
If traveled to foreign country, duration of stay	Four days

Name	**Horacio Perez-Blanco**
Project Role	Advisor for 1 grad student
Nearest Person Month worked	Approx. 12.5% time (approximately 5.25 person months since he started on the project; 42 calendar months since July 2010)
Contribution to Project	Supervise 1 grad student
Funding Support	This DOE project
Collaborated w/ individual in foreign country	
Country(ies) of foreign collaborator	
Traveled to foreign country	Copenhagen, Denmark (ASME conference)
If traveled to foreign country, duration of stay	

Name	**Alok Sinha**
Project Role	Co-PI, advisor for 1 grad student
Nearest Person Month worked	Approx. 17% time (approximately 8.16 person months since start of the project; 48 calendar months since Jan. 2010)
Contribution to Project	Supervise 1 grad student
Funding Support	This DOE project
Collaborated w/ individual in foreign country	

Country(ies) of foreign collaborator	
Traveled to foreign country	
If traveled to foreign country, duration of stay	

Name	**Savas Yavuzkurt**
Project Role	Advisor for 1 grad student
Nearest Person Month worked	Approx. 12.5% time (approximately 5.25 person months since he started on the project; 42 calendar months since July 2010)
Contribution to Project	Supervise 1 grad student
Funding Support	This DOE project
Collaborated w/ individual in foreign country	
Country(ies) of foreign collaborator	
Traveled to foreign country	Shizuoka, Japan (ASME conference)
If traveled to foreign country, duration of stay	One week

Graduate Students:

Name	**David B. Beevers**
Project Role	PhD graduate student
Nearest Person Month worked	Approx. 50% time (approximately 21 person months since he started on the project; 42 calendar months since July 2010).
Contribution to Project	Perform research towards a graduate degree
Funding Support	This DOE project
Collaborated w/ individual in foreign country	
Country(ies) of foreign collaborator	
Traveled to foreign country	
If traveled to foreign country, duration of stay	

Name	**David A. Boger**
Project Role	PhD graduate student
Nearest Person Month worked	Approx. 50% time (approximately 20.0 person months since start of the project; 40 calendar months from Jan. 2010 to May 2013– David graduated in May 2013)
Contribution to Project	Perform research towards a graduate degree
Funding Support	This DOE project
Collaborated w/ individual in foreign country	
Country(ies) of foreign collaborator	
Traveled to foreign country	Gothenburg, Sweden (OpenFoam workshop)
If traveled to foreign country, duration of stay	Four days

Name	**Andrew Byers**
Project Role	MS graduate student
Nearest Person Month worked	Approx. 50% time (approximately 2.5 person months from Aug. 2010 to Dec. 2010; 5 calendar months) – Andrew stopped his graduate studies after one semester.
Contribution to Project	Perform research towards a graduate degree
Funding Support	This DOE project
Collaborated w/ individual in foreign country	
Country(ies) of foreign collaborator	
Traveled to foreign country	
If traveled to foreign country, duration of stay	

Name	**Sushant Dhiman**
Project Role	MS graduate student
Nearest Person Month worked	Approx. 50% time (approximately 4 person months from Jan 2010 to August 2010; 8 calendar months) – Sushant graduated and left PSU in the fall of 2010
Contribution to Project	Perform research
Funding Support	This DOE project
Collaborated w/ individual in foreign country	
Country(ies) of foreign collaborator	
Traveled to foreign country	
If traveled to foreign country, duration of stay	

Name	**Xibei Ding**
Project Role	MS graduate student
Nearest Person Month worked	Approx. 50% time (approximately 9 person months since start of the project; 18 calendar months from Jan 2010 to June 2011) – Xibei graduated in May 2011 and is no longer at Penn State
Contribution to Project	Perform research towards a graduate degree
Funding Support	This DOE project
Collaborated w/ individual in foreign country	
Country(ies) of foreign collaborator	
Traveled to foreign country	
If traveled to foreign country, duration of stay	

Name	**Hosein Foroutan**
Project Role	PhD graduate student
Nearest Person Month worked	Approx. 50% time (approximately 18 person months since he started on the project; 36 calendar months since Jan. 2011)
Contribution to Project	Perform research towards a graduate degree
Funding Support	This DOE project and an HRF Fellowship
Collaborated w/ individual in foreign country	
Country(ies) of foreign collaborator	
Traveled to foreign country	
If traveled to foreign country, duration of stay	

Name	**Daniel J. Leonard**
Project Role	PhD graduate student
Nearest Person Month worked	Approx. 50% time (approximately 24 person months since start of the project; 48 calendar months since Jan. 2010)
Contribution to Project	Perform research towards a graduate degree
Funding Support	This DOE project and an HRF Fellowship
Collaborated w/ individual in foreign country	
Country(ies) of foreign collaborator	
Traveled to foreign country	
If traveled to foreign country, duration of stay	

Name	**Bryan J. Lewis**
Project Role	PhD graduate student
Nearest Person Month worked	Approx. 50% time (approximately 21 person months since he started on the project; 42 calendar months since July 2010)
Contribution to Project	Perform research towards a graduate degree
Funding Support	NDSEG Graduate Fellowship (DOD) and this DOE project
Collaborated w/ individual in foreign country	
Country(ies) of foreign collaborator	
Traveled to foreign country	China
If traveled to foreign country, duration of stay	One week to give a presentation

Name	**Keith A. Martin**
Project Role	MS graduate student

Nearest Person Month worked	Approx. 50% time (approximately 16 person months since he started on the project, 32 calendar months since May 2011); Keith started on the project as an undergraduate in the summer of 2010.
Contribution to Project	Perform research towards a graduate degree
Funding Support	Hydro Research Foundation Fellowship
Collaborated w/ individual in foreign country	
Country(ies) of foreign collaborator	
Traveled to foreign country	
If traveled to foreign country, duration of stay	

Name	**Girish Kumar Rajan**
Project Role	PhD graduate student
Nearest Person Month worked	Approx. 50% time (approximately 12 person months since he started on the project, 24 calendar months since Jan., 2012)
Contribution to Project	Perform research towards a graduate degree
Funding Support	This DOE project
Collaborated w/ individual in foreign country	
Country(ies) of foreign collaborator	
Traveled to foreign country	
If traveled to foreign country, duration of stay	

Name	**Scott A. Richards**
Project Role	MS graduate student
Nearest Person Month worked	Approx. 50% time (approximately 12 person months since start of the project; 24 calendar months from May 2010 to May 2012) – Scott graduated in May 2012 and is no longer at Penn State
Contribution to Project	Perform research towards a graduate degree
Funding Support	This DOE project
Collaborated w/ individual in foreign country	
Country(ies) of foreign collaborator	
Traveled to foreign country	
If traveled to foreign country, duration of stay	

Name	**Benjamin D. Rittenhouse**
Project Role	MS graduate student

Nearest Person Month worked	Approx. 50% time (approximately 11.0 person months since he started on the project, 22 calendar months from July 2011to May 2013 – Ben graduated in May 2013 and is no longer at PSU)
Contribution to Project	Perform research towards a graduate degree
Funding Support	This DOE project
Collaborated w/ individual in foreign country	
Country(ies) of foreign collaborator	
Traveled to foreign country	
If traveled to foreign country, duration of stay	

Name	**Vinod Vishwakarma**
Project Role	PhD graduate student
Nearest Person Month worked	Approx. 50% time (approximately 1 person months since he started on the project; 1 calendar months since August 2013)
Contribution to Project	Perform research towards a graduate degree
Funding Support	This DOE project
Collaborated w/ individual in foreign country	
Country(ies) of foreign collaborator	
Traveled to foreign country	
If traveled to foreign country, duration of stay	

Name	**Alex M. Wouden**
Project Role	PhD graduate student
Nearest Person Month worked	Approx. 50% time (approximately 21 person months since he started on the project; 42 calendar months since July 2010)
Contribution to Project	Perform research towards a graduate degree
Funding Support	This DOE project
Collaborated w/ individual in foreign country	
Country(ies) of foreign collaborator	
Traveled to foreign country	
If traveled to foreign country, duration of stay	

Undergraduate Students:

Name	**Lisa Branchini**
Project Role	Visiting student from U. of Bologna
Nearest Person Month worked	100% time (approximately 6 person months

	from Jan 2011 to June 2011; 6 calendar months)
Contribution to Project	Perform research to assist Prof. Perez-Blanco
Funding Support	Not supported by this DOE project
Collaborated w/ individual in foreign country	
Country(ies) of foreign collaborator	
Traveled to foreign country	
If traveled to foreign country, duration of stay	

Name	**Zack Francis**
Project Role	Undergraduate student
Nearest Person Month worked	Approx. 40% time (approximately 4.8 person months since he started on the project; 12 calendar months from May 2012 to May 2013 – Zack graduated in May 2013 and is no longer at PSU)
Contribution to Project	Perform research towards a senior thesis
Funding Support	This DOE project
Collaborated w/ individual in foreign country	
Country(ies) of foreign collaborator	
Traveled to foreign country	Copenhagen, Denmark (ASME conference)
If traveled to foreign country, duration of stay	

Name	**Peter Hiebert**
Project Role	Undergraduate student
Nearest Person Month worked	Approx. 40% time (approximately 3.6 person months total on the project; 9 calendar months from May 2012 to May 2013 – Peter graduated in May 2013 and is no longer at PSU)
Contribution to Project	Perform research towards a senior thesis
Funding Support	This DOE project
Collaborated w/ individual in foreign country	
Country(ies) of foreign collaborator	
Traveled to foreign country	
If traveled to foreign country, duration of stay	

Name	**Scott Hromisin**
Project Role	Undergraduate student
Nearest Person Month worked	Approx. 40% time (approximately 1.6 person months since he started on the project; 4

	calendar months from January 2013 to April 2013 – Scott finished working on this project)
Contribution to Project	Perform research towards a senior thesis
Funding Support	This DOE project
Collaborated w/ individual in foreign country	
Country(ies) of foreign collaborator	
Traveled to foreign country	
If traveled to foreign country, duration of stay	

Name	**Jeremy Ogorzalek**
Project Role	Undergraduate student
Nearest Person Month worked	Approx. 40% time (approximately 2.4 person months since he started on the project; 6 calendar months since January 2013) Jeremy is no longer working on this project.
Contribution to Project	Perform research towards a senior thesis
Funding Support	This DOE project
Collaborated w/ individual in foreign country	
Country(ies) of foreign collaborator	
Traveled to foreign country	
If traveled to foreign country, duration of stay	

Name	**Tyler Quinzan-Singer**
Project Role	Undergraduate student
Nearest Person Month worked	Approx. 40% time (approximately 3.6 person months total on the project; 9 calendar months from May 2012 to May 2013 – Tyler graduated in May 2013 and is no longer at PSU)
Contribution to Project	Perform research towards a senior thesis
Funding Support	This DOE project
Collaborated w/ individual in foreign country	
Country(ies) of foreign collaborator	
Traveled to foreign country	
If traveled to foreign country, duration of stay	

Name	**Greg Vater**
Project Role	Undergraduate student
Nearest Person Month worked	Approx. 20% time (approximately 0.2 person months since he started on the project; 1 calendar months since September 2013)
Contribution to Project	Perform research towards a senior thesis

Funding Support	This DOE project
Collaborated w/ individual in foreign country	
Country(ies) of foreign collaborator	
Traveled to foreign country	
If traveled to foreign country, duration of stay	

Organizations:

Weir American Hydro (WAH) / a branch of Weir Power and Industrial, York, PA
Contributions: In-kind support and technical advice. Also, Professor Cimbala spent his sabbatical year (2010-2011) there. One of the graduate students, Keith Martin, worked at WAH full time in the summer of 2012 as an intern. Several students have visited for short times (typically a day) to discuss their research. On alternative semesters (twice a year), our entire group meets for a review session either at Penn State or at WAH.
Contact: Robert A. Rittase, Chief Hydraulic Engineer, Robert.Rittase@weirgroup.com

IMPACT [OPTIONAL]

Discuss the impact of this project relative to:

- The development of the principal discipline(s) of the project

The principal discipline(s) of the project are computational fluid dynamics (CFD) of turbomachinery, control systems for hydroelectric plants, integration of hydro power with other renewable power sources such as wind and solar, and economic analysis of hydroelectric plants for maximum efficiency or profit. It is anticipated that all of these disciplines will benefit from the present research.

- Other disciplines
- The development of human resources
- Physical, institutional, and information resources that form infrastructure
- Technology transfer (include transfer of results to entities in government or industry, adoption of new practices, or instances where research has led to the initiation of a startup company)

We were in close contact with our industry partner, Weir American Hydro (WAH). Professor Cimbala spent his sabbatical year (2010–2011) working at WAH. Several students have made trips to WAH to discuss their research and share data. One of the graduate students, Keith Martin, worked at WAH full time in the summer of 2012 as an intern.

- Society beyond science and technology.

CHANGES / PROBLEMS

Discuss the following if applicable:

- Changes in approach and reasons for change.

Because of HRF Fellowships received by two of our students, we are able to continue some of the research beyond the project end date, into 2014. The other students will need to be Teaching Assistants while they finish their degrees.

- Actual or anticipated problems or delays and actions or plans to resolve them.

As anticipated, we spent the first several months of the project recruiting excellent graduate students. Thus, the project was delayed for several months before all the projects were started.

- Changes that have a significant impact on expenditures.

Because of the delay due to graduate student recruitment, our expenditures were below what might be expected for linear spending during the duration of the project. We requested and received two no-cost extensions of six months each so that our project now ends on December 31, 2013 rather than on December 31, 2012.

- Significant changes in use or care of animals, human subjects, and/or biohazards.

N/A